CENTRE FOR ORE DEPOSIT AND EXPLORATION STUDIES

STRUCTURE AND MINERALISATION OF WESTERN TASMANIA

AMIRA PROJECT P.291A

Fifth Report

May 1996

UNIVERSITY OF TASMANIA

CENTRE FOR ORE DEPOSIT AND EXPLORATION STUDIES

STRUCTURE AND MINERALISATION OF WESTERN TASMANIA

AMIRA PROJECT P.291A
Fifth Report
May 1996

UNIVERSITY OF TASMANIA

Contents

P291A - Meeting 5
Executive Summary

Ron Berry

The project is now getting into the latter stages. The original proposal included nine tests of the structural model proposed in project P291. Three sections have been completed in previous years. The report here gives progress on five other sections. The only section not begun is the investigation of sedimentological evidence for Middle Cambrian movement on the Firewood Siding Fault/Linda Zone.

Additional whole rock chemistry of sedimentary rocks from western Tasmania were obtained to confirm the trends identified in the previous report. The Tyndall Group has a distinctive source composition which has contributed to the magnetic susceptibility of this unit. This composition is best reflected in the Lynchford Member and reflects an andesitic character with a tholeiitic incompatible element pattern. The closest match to this pattern in western Tasmania is the Henty dykes and the basalts of the Henty Fault wedge. The White Spur Formation is not easily distinguished from the CVC on volcanic chemistry. Further work on the Sticht Range Formation confirmed its similarity to the Stitt Quartzite.

Chromite in Dundas Group sandstones is largely from a MUC (ophiolite) source. The MUC are very rich in chromite and even a small contribution from this source leads to a dominance of low-TiO2 chromite in the heavy mineral assemblage. Chromite composition is the clearest indicator of a MUC contribution to the provenance of sandstones in western Tasmania. The whole rock chemistry usually reflects more enriched sources such as the Crimson Creek Formation. The Animal Creek Greywacke has a contribution from the MUC. The metamorphic basement signature associated with the Stitt Quartzite and Sticht Range Formation was not recognised in the whole rock chemistry of Animal Creek Greywacke despite the clear component of basement source in the heavy mineral assemblage. This probably reflects the effect of mixing in a significant additional component from the MUC source.

A new geological cross-section was drawn along the northing 5350000mN, from west of the Professor Range to the Tyndall Range. This section matches the style of sections to the south (Queenstown and Mt. Jukes), with only moderate total shortening of 14 km. No dominant transport direction was recognised. A possible position for a major low angle Devonian thrust is west of the section under Permian cover. The level of erosion is such that a very good separation of this shortening between Cambrian and Devonian deformation is possible. The section emphasized the importance of late Cambrian folding in the structure of the Mt. Read Volcanics. The section drawn at Rosebery continues to be anomalous compared to other sections drawn in this project.

The Mt. Cripps Fault was identified as a major Cambrian transfer largely based on differences between structure and stratigraphy north and south of this fault. We proposed a major Cambrian normal fault roughly in the position of the Henty Fault was offset along this structure and this offset was not entirely a result of Late Cambrian and Devonian compressional tectonics. New cross-sections were drawn north (5396000nM) and south (5392000mN) of the Mt. Cripps Fault. Detailed investigations along the Mt. Cripps Fault have provided supporting evidence that the fault was present during the deposition of the Southwell Subgroup. No additional evidence has been found for the existence of this structure during the earlier part of the Mt. Read depositional cycle.

A structural cross-section of the Mt Read Volcanics at 535000N

Ron Berry

Centre for Ore Deposit and Exploration Studies, Geology Department, University of Tasmania

Introduction

The large differences between previous sections at Zeehan and at Mt Lyell required a major change in the structure across this break. In order to better constrain the nature of these changes, a new section was drawn between these two positions. This section was drawn along the northing 535000. This section starts west of the Professor Range passes close to the Henty River bridge on the Murchison Highway and along the southern section of the Anthony Road before crossing the southern section of the Tyndall range.

The section lies on the newly printed Zeehan 1:50,000 sheet (Brown et al. 1994), also on the Mt Read Project maps 3 and 5 (Corbett 1986, Corbett & Jackson 1987), and the Queenstown 1:25,000 scale map (Corbett et al. 1989). There is additional information relevant to this section on the Strahan and Lyell 1:50,000 maps (Baillie et al. 1978, Calver et al. 1987) and the Mt Read 1:100,000 compilation (Map 6, Corbett & McNeill 1988). In addition, I had access to the original field notes of Dr K Corbett from the Strahan sheet mapping, and extensive discussions with him about the geology on the section. The mapping of Poltock (1992) is largely to the north of this section but has some implications for the interpretation.

Mesoscopic data

The mesoscopic structural data collected along this section is shown in Figure 1. The structural data is separated into three sectors. The western sector is from the Professor Range to the Henty Bridge. Measurements from the Ordovician have been excluded. The cleavage in this sector averages 88°/061°. There is a small spread from 320°–350° in strike. The bedding has a complex distribution. The average strikes is about 340° with a preponderance of west dips but there are two great circle distributions. One about a near horizontal axis and the other about a steep fold axis. This complexity is interpreted as the result of interference between a Cambrian fold trend of 350° with a Devonian fold trend of 330° as represented by the widespread cleavage. In contrast the Ordovician and Silurian bedding data (Fig. 2) have a simpler distribution with a calculated fold axis of 46°/332°.

The eastern sector has a very similar history. The measured cleavage has an average value of 84°/064°which is identical to that measured in the western sector. The bedding is dominated by steep W- and NW-dipping orientations, with poles to bedding defining a great circle distribution about a steep NW-trending fold axis. The east dipping orientations have a broader spread and may partly support a south-plunging fold axis. This interpretation is supported by the measured bedding cleavage intersection (Fig. 3). On the west-dipping limbs the bedding cleavage intersection plunges towards the NW while on east-dipping limbs some bedding cleavage intersections plunge towards the SE. Along this sector there are several folds exposed on road cutting which are transected by the regional cleavage. These data are consistent with a Devonian cleavage transecting a north-trending Cambrian anticline.

The small central sector along the Zeehan Highway has the cleavage and bedding orientations rotated 20° clockwise. This syn- or post-Devonian cleavage rotation is probably due to the complex interaction of faults in this area.

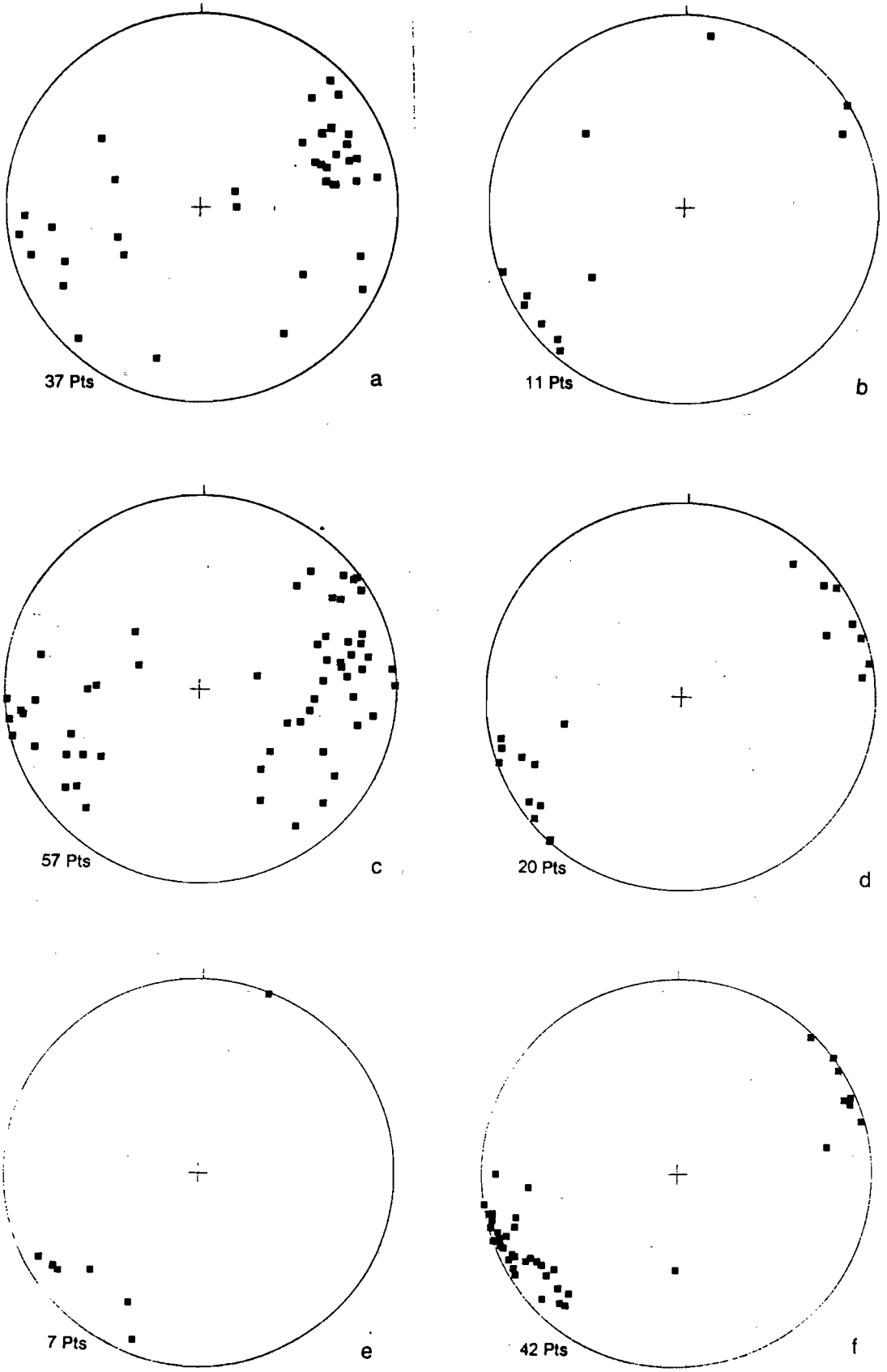

Figure 1—Equal area stereographic projection of structural data(a) Poles to bedding in western area; (b) Poles to bedding in central area; (c) Poles to bedding in eastern area; (d) Poles to cleavage in western area; (e) Poles to cleavage in central area; (f) Poles to cleavage in eastern area.

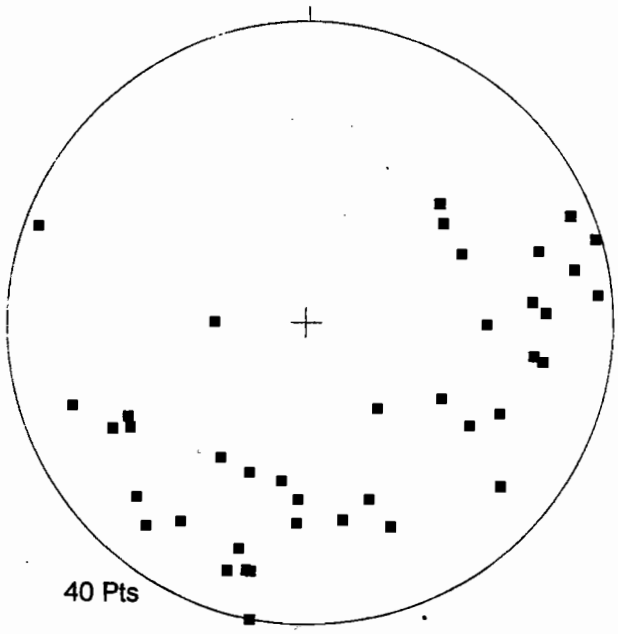

Figure 2—Equal area stereographic projection of poles to bedding in Ordovician and Silurian rocks of the western area. Most of data from Brown et al (1994).

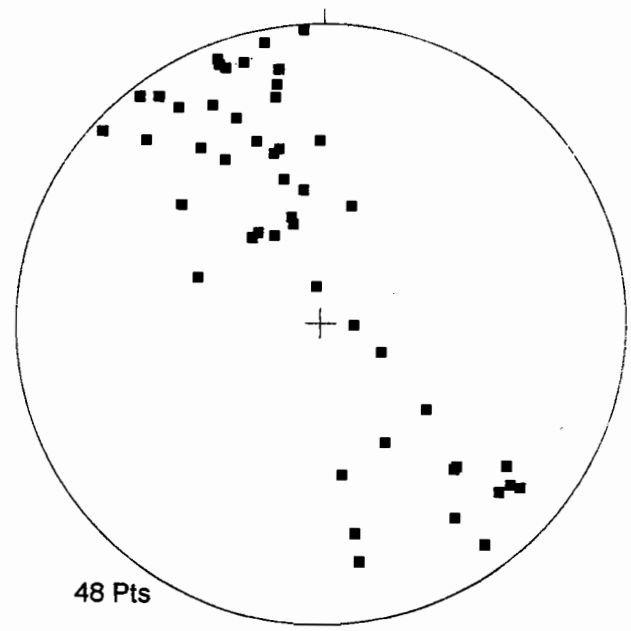

Figure 3—Equal area stereographic projection of bedding cleavage intersection.

Geology

The section (Fig. 4) is drawn from 35600E to 40000E, The first 10 km to 36600E are based entirely on geology from the Strahan and Zeehan map sheets. There are no Cambrian rocks exposed in this area. The structure is simple except for the strongly overturned limb exposed south of the highway (36100E 534700N) on Strahan map sheet. This structure suggests a major thrust lies just west of the section and under the Permian cover. A possible interpretation is that this is the southern extension of the Rosebery Fault and much of the shortening in the Rosebery section lies west of the present exposure.

The next part of the cross-section from the Professor Range to Ewarts Creek (36600E to 37250E) has received a lot of attention in the western part around the Professor Range but very little work has been done in the eastern part. The Ordovician sequence here sits unconformably on a wide range of rock-types. The unconformity northeast of the Professor Range (36740E 535030N) was recognised by Corbett (1984). A similar unconformity was reported south of the section in the Henty Valley by Baillie & Corbett (1985). This unconformity surface was also found exposed in the small creek at 37097E 535146N during field work for this project. The 10 m section of Pioneer correlate at this locality sits unconformably on steeply dipping micaceous sandstone. The next creek to the west has Westcott Argillite lithology against this contact but the overlying stratigraphy is not exposed. New structural data along this section is shown in Figure 5. There is a strong contrast in orientation of structure between the Cambrian and Ordovician–Devonian section. The structure unambiguously requires a N–S folding event which predates the Ordovician. The anticlinal position is eroded and the Ordovician rocks lap across the entire section. The Professor Range sequence is interpreted as a syn-orogenic facies accumulating in the synclinal keel as the anticline was eroded (Fig. 6a). The thickness of stratigraphy truncated across this section is consistent with a 20°–30° W dip of the Cambrian sediments during the formation of the Ordovician unconformity.

The section has been drawn below the unconformity by an interpolation from data collected in this project, Corbett (unpublished), and the new Zeehan map sheet, to the data on the Strahan sheet. The western part of the section is a conglomerate

section (Owen correlate) which overlies a fossiliferous Late Cambrian unit that has been correlated on biostratigraphic grounds with the Newton Creek Sandstone (Corbett pers. comm.). To the north it is very similar lithologically to the Westcott Argillite. The zone from 36800E to 37000E is poorly exposed as deeply weathered sandstones, sometimes pebbly but there are several outcrops of cherty conglomerate in this sector. The next outcrop in the creek at 37070E 535130N is again thin sandstone beds in green siltstones which I correlate with the younger section of the Dundas Group. Within the area of sandstones and siltstones a fold pair is exposed to the north of the section at 36930E 535190N and this is correlated with to the fold shown on the Strahan map sheet. There is one magnetic unit within the Westcott correlate which crosses the section at 36830E.

East of 37000E, the sequence is dominated by a micaceous sandstone unit which is most similar to the Stitt Quartzite. This unit is along strike from outcrops of Stitt correlate at the Farrell Rivulet, 3 km to the north. Some further work is required on the composition of this unit to confirm this correlation.

The section shows a projected position of the Ordovician unconformity. This unconformity is projected from 2 km north of the section. The fold plunge inferred from bedding in this region (46°/332°) would place this surface 500 m higher than shown on the section but the recognition of Ordovician units south of the section requires that the folds shallow in dip and finally plunge to the south near the Firewood Siding Fault. The position shown is not well constrained but is plausible based on the existing dataset.

The sector from Ewarts Creek (37250E) to the South Henty Fault (37500E) is complicated by a number of faults with out-of-section movement. In addition, the structural data indicates that, the structures strike obliquely to the section. The synclinal structure in the Ordovician stratigraphy is projected from data south of the section on the Strahan sheet. A major fault is inferred at 37360E (Fig. 5) based on (a) the intense strain in the rocks exposed along the highway and (b) the sharp truncation of magnetic anomalies associated with the Ewarts Track sequence (of Poltock 1992). The intense disruption in this zone produces strong shears that are oblique to the section. The orientation of these structures is consistent with the rotated fabric recorded in this sector. The southern unit is correlated with the Yolande River Group to the south. The northern unit is part of the Henty Fault wedge stratigraphy. The best available interpretation is that this "Ewart Track" sequence correlates with the Lynchford member of the Tyndall Group. [Poltock (1992) argued that correlation with Tyndall Group was most likely. A magnetic unit along strike to the south has been flagged as a probable Tyndall correlate in unpublished Tasmanian Mines Dept reports. Whole rock geochemistry of basaltic andesites in this area and the related Henty Dykes are the best available source for the mafic component of the Lynchford member — see lithostratigraphy section. This scenario suggests a volcanic centre in the Henty Fault Wedge contributes a mafic component to the Lynchford Member. The process of spreading this material over a wide area is poorly constrained, it may be partly due to explosive volcanism.]

The section from the South Henty Fault (37360E) to the Great Lyell Fault (38080E) has been well mapped by many previous workers. It is especially well known along the Anthony Road. The structural data measured for this project emphasized the relatively consistent west dipping and facing structure as far as 37760E along the Anthony Road and then a change to east facing and dipping east of this point. Unfortunately the road here is well north of the section. The structure has been projected onto the section assuming the Cambrian fold trend defines the structure here rather than the 330° trend of Devonian structures. This is required by structures shown south of the section on the Queenstown 1:25,000 map (Corbett et al. 1989). The structure has also been projected assuming a subhorizontal fold axis trend in contrast to the measured bedding cleavage intersection. With these constraints the Yolande River Group on the section line is shown as a lateral facies equivalent of the CVC. This is required by the absence of CVC between Yolande River Group and Tyndall Group north of the section and given the absence of convincing evidence for structural complications in this area. The interfingering relationship between these units in the upper Yolande River was recognised during the mapping in this area (Corbett pers. comm.) The structure in this sector indicates the difficulty of distinguishing Cambrian structural trends through the Devonian overprint.

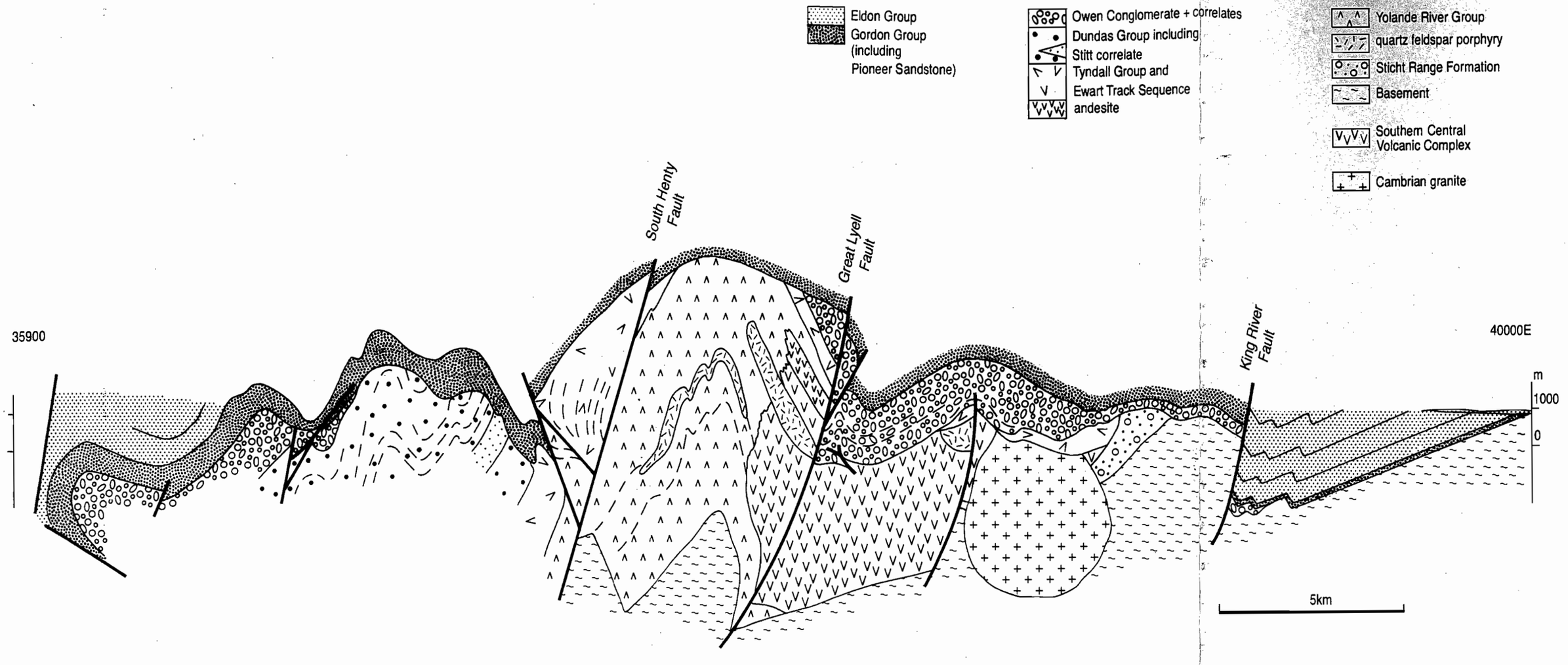

Figure 4—Geological cross-section of the Mount Read Volcanics at 535000N

The deeper structure in this area is poorly constrained. The Ewarts Track sequence in the Henty Fault wedge appears to sit directly on basement (gabbro block correlated with the ophiolite). To the east there is a thicker stratigraphy. This structure is analogous to the Concert Schist block to the north and suggests a normal fault east of the gabbro acting as a basin bounding fault for the older stratigraphy (Yolande cycle) but overlapped by Tyndall cycle sediments in the sag phase. There is no evidence whether this structure continues to the south but its projected position is shown on the section as a western boundary for most of the Yolande Group section. The unconformity surface in this zone is based on inferred Late Cambrian dips of 40∞E and 25∞W in the restored section. It is subject to large error.

The section east of the Mt Lyell Fault is based on existing maps (Lyell 1:50,000, Queenstown 1:25,000). The only added features are the King River Fault (Berry 1991). East of the King River some folds are required to produce the observed distribution of Bell Shale although there is not enough structural data to properly constrain the geometry. The folds shown are compatible with existing data. The Owen Conglomerate, on the Tyndall Range, marks the synclinal position where no stratigraphy is removed during early Ordovician erosion. The next limb of Cambrian folding is marked by Marble Bluff where the Cambrian stratigraphy is again cut off at a 40° angle.

The deeper structure under the Tyndall Range has been largely projected from the south. The position of Cambrian Granite is based on magnetics (Payne 1991). A weakly inverted Cambrian growth fault is shown just west of the granite. This structure is based on variations in Jukes Conglomerate and Tyndall Group thickness on the range. The thickness of CVC here is entirely speculative but compatible with dips in the Sticht Range Formation and west of the Great Lyell Fault. The presence of Tyndall Group west of the Great Lyell Fault has been used to infer a Cambrian normal movement on this structure which is partly inverted in the Late Cambrian. Most of the inversion occurred in the Devonian. The dips at the end of the Cambrian are inferred from work on the Haulage unconformity to the south. The geometry of the Great Lyell Fault is necessary for a line balance at the basement interface.

Restored section

The history described above indicates the structure needs to be considered as a two stage process. The restored section has been drawn here for a horizontal Ordovician stratigraphy. The strong out-of-section movement at the Henty Bridge prevents a meaningful reconstruction across this zone, so the restoration is in two sections. The western section (Fig. 6a) is straight forward but includes a component of flattening in the Cambrian section as required by the cleavage development. The cutoff angle for Cambrian stratigraphy is accurate to ±10°. This section has a Devonian shortening of 5 km excluding any movement on the proposed hidden thrust. The section as drawn also requires 2 km of Cambrian shortening.

The eastern sector has been restored to a horizontal base of the Ordovician as well. The Tyndall Range and further east is straight forward with the main ambiguity being the dip on the King River Fault. West of the Great Lyell Fault the anticline has been drawn with an east limb dipping at 40° based on the Haulage unconformity to the south. The west limb has been drawn parallel to the restored Cambrian section west of the Henty Bridge. The restoration has assumed all the hinge thickening occurred during the Devonian. The geometry of the Great Lyell Fault was adjusted to line balance the base of the Mount Read section. This section implies 5 km of Devonian shortening mainly west of the Great Lyell Fault, and 2 km of Cambrian shortening.

This section matches the style of sections to the south, with only moderate total shortening of 14 km. The level of erosion is such that a very good separation of this shortening between Cambrian and Devonian deformation is possible. No obvious dominant transport direction was recognised. A possible position for a major low angle Devonian thrust is west of the section under Permian cover. At first appearance this could be thought of as a continuation of the Rosebery Fault, with the Little Henty Fault acting as a transfer structure. This requires a dextral sense of movement across the structure. In contrast, the outcrop pattern south of the Little Henty Fault fits a sinistral transfer model extremely well and there are no features known which fit a dextral sense of shear on this fault zone.

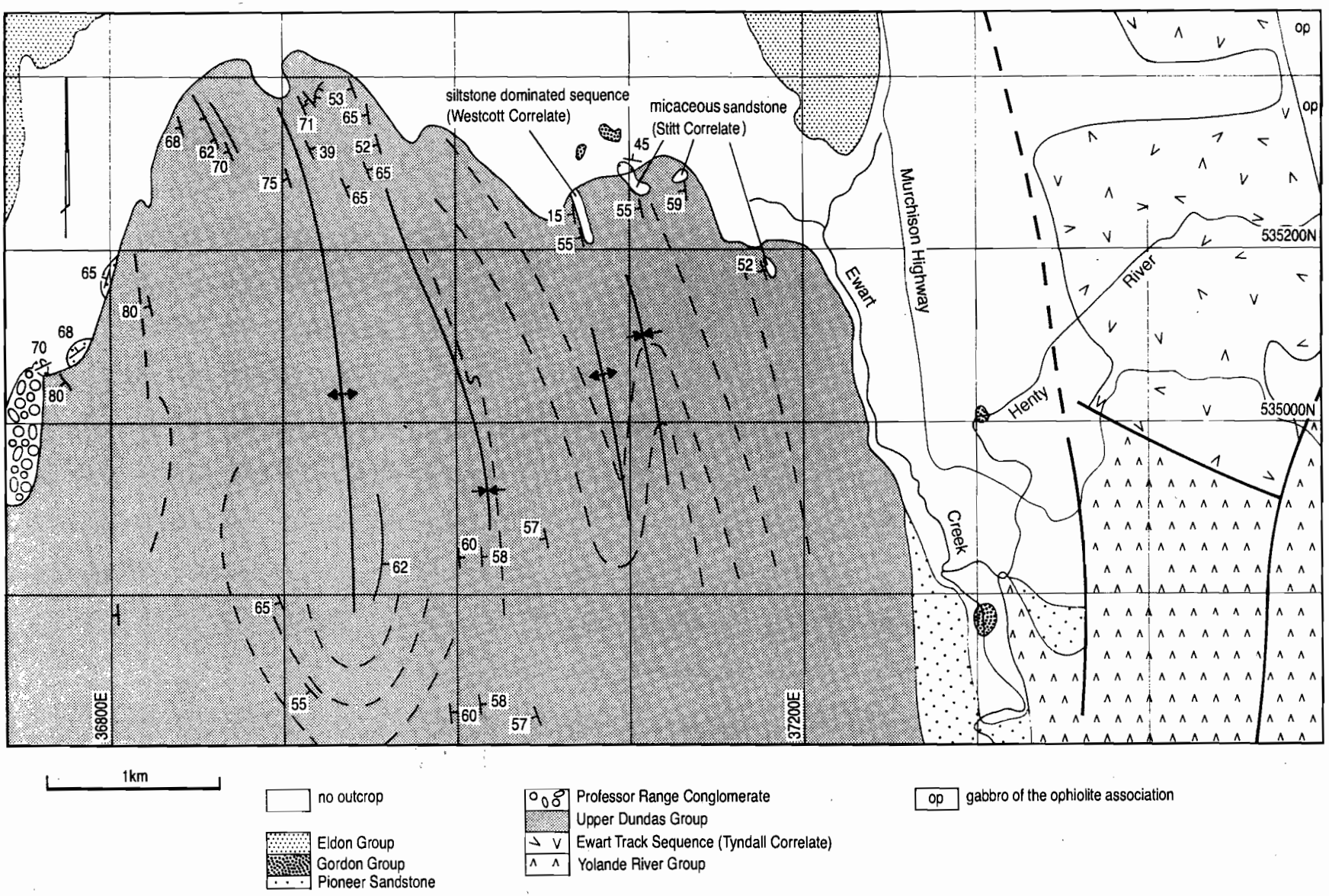

Figure 5—Geology along the transect of the Mount Read Volcanics modified from Brown et al (1994), Corbett (1986), Corbett & Jackson (1987), Corbett et al (1989), Baillie et al (1978), Calver et al (1987), Corbett & McNeill (1988) and Poltock (1992).

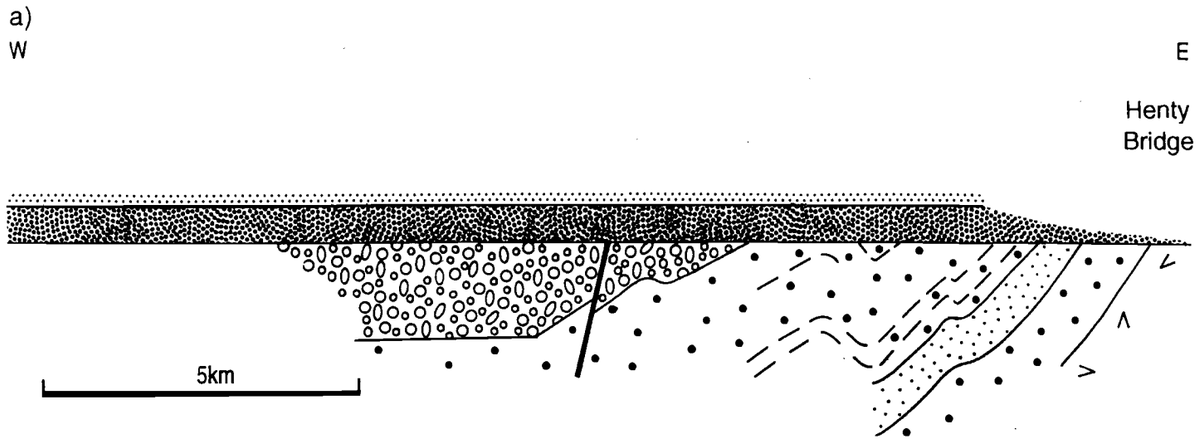

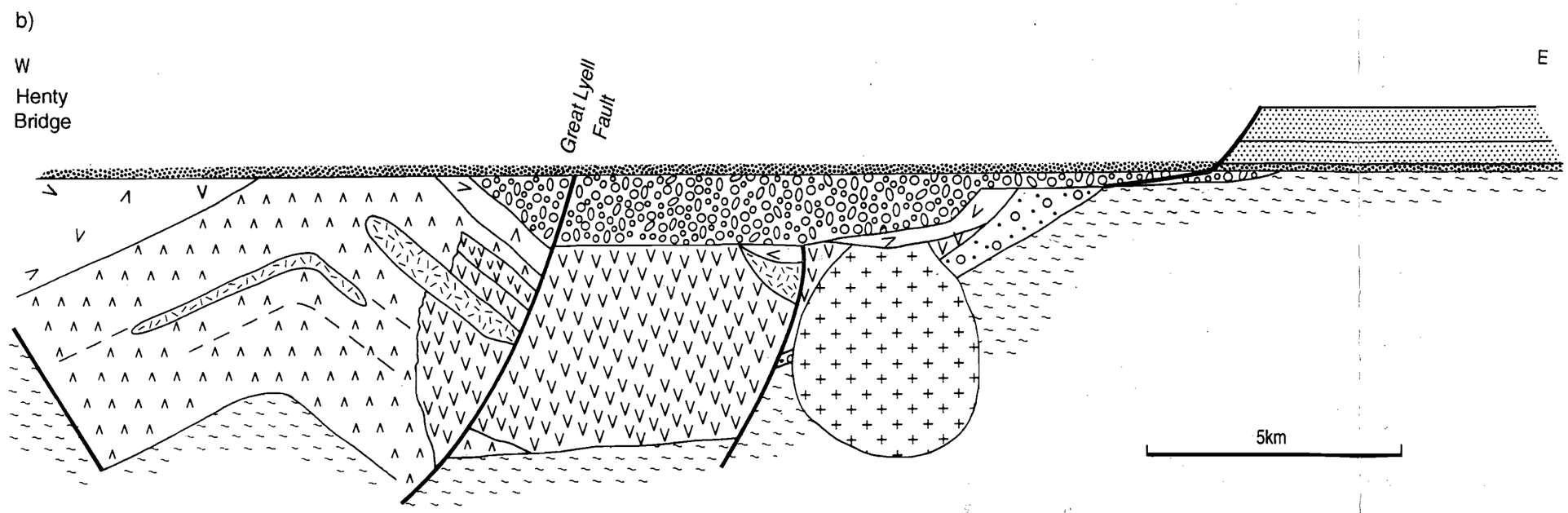

Figure 6—Cross-section restored to a horizontal basal Ordovician stratigraphy assuming a small component of homogeneous flattening (a) west of the Henty Bridge, (b) east of the Henty Bridge.

References

Baillie PW & Corbett KD 1985. Strahan Tasmania: explanatory report. Geological atlas, 1:50,000 series, Tasmanian Dept Mines

Baillie PW, Corbett KD, Cox SF, Corbett EB, Bravo AP, Gee RD, Gulline AB, Legge PJ, Pike GP, Turner NJ, Williams PR, McClenaghan MP & Brown AV 1978. Strahan geological atlas, 1:50,000 series, Tasmanian Dept Mines.

Berry RF 1991. Victoria Pass to Queenstown regional section. AMIRA P291 Report 3 , 22–30.

Brown AV, Findlay RH, Goscombe BD, McClenaghan MP & Seymour DB 1994. Zeehan geological atlas, 1:50,000 series, Tasmanian Dept Mines.

Calver CR, Baillie PW, Everard JL, Seymour DB, Williams PR, Forsyth SM, Turner NJ, & Williams E 1987. Lyell geological atlas, 1:50,000 series, Tasmanian Dept Mines.

Corbett KD 1984. Geological maps and summary of Cambrian stratigraphic units and relationships in the Henty River–Williamsford area. Tasmanian Dept Mines unpubl. report 1984/84.

Corbett KD 1986. Mount Read Volcanics project: map 3. Geology of the Henty River–Mt Read area. Tasmanian Dept Mines

Corbett KD & Jackson JC 1987. Mount Read Volcanics project: map 5. Geology of the Tyndall Range area. Tasmanian Dept Mines

Corbett KD & McNeill AW 1988. Geological compilation map of the Mount Read volcanics and associated rocks, Hellyer to South Darwin Peak. 1:100,000. Tasmanian Dept Mines.

Corbett KD, Calver CR, Everard JL & Seymour DB 1989. Queenstown 1:25,000 sheet. Tasmanian Dept Mines.

Payne B 1991. Geophysical interpretations of the Mt Sedgwick – Red Hills area, western Tasmania. Hons thesis Univ Tasm (unpubl.) 107pp.

Poltock R 1992. Geology of the Henty Fault wedge, western Tasmania. M Econ Geol Thesis, Univ Tasm (unpubl.) 76pp.

Lithogeochemistry: report 2

R.F. Berry, D. Selley and M.J. White
Centre for Ore Deposit and Exploration Studies, Geology Department, University of Tasmania

Abstract

Additional whole rock chemistry of sedimentary rocks from western Tasmania were obtained to confirm the trends identified in the previous report. The geochemical signature of the Tyndall Group was confirmed and a possible source from the Henty dykes was noted. The White Spur Formation is not easily distinguished from the CVC on volcanic chemistry. Further work on the Sticht Range Formation confirmed its similarity to the Stitt Quartzite.

Chromite in Dundas Group sandstones is largely from a MUC (ophiolite) source. The composition of chromite is a major aid in the recognition of blocks of Crimson Creek Formation in contentious positions within the Mt Read volcanics.

Introduction

A major aim of the combined ARC–AMIRA project is to define the basin geometry for the Mount Read Volcanics. A structural model was put forward in P291 which is being used as a template for this analysis. The project has looked at the heavy mineral suite and whole rock chemistry as a guide to what sources are available to the basin at each stage in its genesis.

The results put forward in the last report suggested that whole rock chemistry was most useful for distinguishing between volcaniclastic units and especially pointed out that the Tyndall Group formed a discreet compositional set. At the meeting there was some discussion about the significance of the distinction of the Tyndall group and more analyses have been carried out as a result. Other volcaniclastic units are more difficult to distinguish and as a result more work on the White Spur Formation and related rocks is included here. In addition the question of the Sticht Range Formation requires some more attention. Six more samples were analysed for this report.

Heavy minerals and especially chromite are important in determining the distinction between Crimson Creek Formation and other lithologies. Another batch of 40 samples has been prepared from a range of lithologies but only a few have been analysed so far. These initial results are discussed below.

The results discussed below are dependent on work that is formally outside the AMIRA project but made available to the AMIRA sponsors in a pre-publication form. Most of the geochemistry of the Tyndall Group reported here is within the PhD program of Matt White and outside the AMIRA project. The Dundas area, Stitt Quartzite and Oonah Formation samples, and arguments about the distinction of Crimson Creek from Dundas Group, and Concert Schist from Dundas form part of the PhD program of Dave Selley which is formally outside the AMIRA project. The Sticht Range Formation samples analysed here were made available by the Tasmania Department of Mines and the analyses carried out on them will be released to them when it is completed as part of the arrangement under which they were made available. In the following discussion, the Moores sandstones are from presumed Precambrian exposed on Moores Pinnacles, and the Tyndall Group includes the samples from the Mt Cripps Formation and Jukes conglomerate.

Geochemistry

The whole rock compositions of the samples analysed since the last meeting are shown in Table 1.

Chemical characteristics of the Tyndall Group

In the last report is was noted that the small group of available samples suggested that the the Tyndall Group included a contribution from a distinct mafic source not recognised in other parts of the Mt Read stratigraphy. This component was most easily recognised in the Ti/Th ratio which was much higher than in any other unit. This component was best reflected in the Lynchford Member from the base of the Tyndall Group. At the meeting some questions arose over whether this was too heavily based on a single analysis. Since then we have analysed four other Lynchford member volcaniclastic rocks and the unit which has been correlated with them from NW of the Pinnacles. The position of these samples reinforces the information from the previous meeting with four of the samples showing extreme values in Ti/Th (Fig. 1). All analyses of Tyndall Group samples are shown on a normalised (to PAAS) diagram in Figure 2 . The Lynchford Member samples show an overall incompatible element depleted signature (slope to the left) indicating a mafic signature. There is no Nb, P or Ti anomaly in contrast to most volcaniclastic rocks in the Mt Read Volcanics. In addition there are two other unusual features. The Th is very low, less than Nb in normalised terms and the Sc is extremely high. These features overall form a very distinctive signature for lower Tyndall Group rocks. The extreme Ti/Th values reported for Lynchford Member in the previous report reflects the very low Th combined with the lack of a negative Ti anomaly. The pattern revealed here is typical of a tholeiitic to weakly calc-alkaline basaltic source. The sample 78300, from the magnetic sandstone package north andwest of Pinnacles, fits very closely with the Lynchford Member samples supporting the correlation of this package with the Tyndall Group (McKibben 1993).

This signature is not as strong in other Tyndall Group rocks where there is a dilution by felsic volcanic material. These rocks still have a distinctive slope to the left in the PAAS normalised spidergram (Fig. 2b) and lack a Nb depletion. Some of the samples, 4 of 15, have a low Th (<Nb in normalised terms) and the Sc/Y is fairly high for felsic rocks. However the signature is not as distinctive as the Lynchford Member.

The distinctive composition of the Lynchford Member indicates a discrete new source of basaltic material with a tholeiitic signature. This could be similar to Crimson Creek Formation. On a PAAS normalised diagram (Fig. 3a) a Crimson Creek Formation correlate from Montgomery (Brown and Stolz unpublised data) has a very strong slope to the left with very low Th/Nb. These rocks have a positive Ti,P and Nb anomaly on a PAAS normalised spidergram. This pattern would need very strong mixing with a felsic source with calc-alkaline composition to form the Lynchford Member compositions. A more likely composition in age terms is the high Ti tholeiitic basaltic andesites from the Henty Fault wedge analysed by Poltock (1991). These are shown in Figure 3b. They are less depleted than the Montgomery basalts However the positive Nb, Ti and P anomalies are still visible. Other Suite 4 volcanics (Henty dykes) have been reported by Crawford et al 1992 (Fig. 3c). The Nb here is below detection limit but does not require a large Nb anomaly as seen in many other units. The Suite 4 Henty dykes and related Henty Fault wedge volcanics are the most likely source for the Lynchford Member.

The alternative signatures found in the Mt Read volcanics include the Suite 3 basalts (Fig. 3d). These are distinctive for there strong negative Nb anomaly combined with high P and REE. They are not a possible source for the Lynchford Member. The source for the Tyndall Group andesitic signature which has often been inferred because of the spatial correlation are the andesites which are exposed just below this stratigraphic position along the Anthony Road and near Queenstown. These Suite 2 andesites (Fig3e) have a strong negative Ti and Nb anomaly and do not look chemically similar to the Lynchford Member.

Other volcaniclastic units

For comparison purposes, other stratigraphic units have been plotted in the same diagram (Fig. 4). The samples shown are limited volcaniclastic rocks except for Eastern Quartz-phyric sequence which is largely coherent volcanics. Samples which in hand specimen appear to be sandstones have been are considered separately.

The volcaniclastic units previously reported from the south are shown in Figure 4a. These include two

DEC05

Ident		Easting	Northing	SiO2	TiO2	Al2O3	Fe2O3	MnO	MgO	CaO	Na2O	K2O	P2O5	Loss	Sum	La	Ce	Nd	Nb	Zr	Sr	Cr	Ba	Sc	V	Y	Rb	Th	Ni	Pb
Dundas area																														
88	Q phyric vcc	373200	5366740	59.2	0.61	24	2.51	0.01	1.22	0.11	3.51	4.85	0.1	3.55	99.66	20	43	22	14	335	139	7	632	9	42	30	180	31	9	3
828	vitric vcc	369303	5362920	77.54	0.32	11.76	2.87	0.01	1.46	0.03	0.44	2.78	0.03	2.68	99.95	65	128	57	14	208	17	29	300	6	23	38	106	24	12	7
883	Vcc - shoshonit	373720	5367780	56.62	0.82	22.31	5.48	1	1.16	0.24	0.32	6.5	0.24	5.46	99.16	107	196	83	25	368	26	329	731	15	94	50	228	44	105	73
D-86	vitric vcc	371920	5366310	76.51	0.31	12.14	2.41	0.24	1.36	0.31	0.59	2.99	0.09	3.06	100.02	61	122	51	13	197	40	109	447	10	50	36	112	25	20	10
H-5	Q phyric vcc	Husskison River		70.04	0.41	15.68	3.15	0.02	1.67	0.08	6.13	0.73	0.05	2.34	100.3	42	78	33	8	186	218	20	208	10	48	27	26	15	17	2
982	F vcc	374460	5367470	54.37	1.04	18.92	9.53	0.08	4.47	0.7	7.11	0.35	0.25	3.31	100.13	52	103	45	11	149	305	51	227	27	309	29	13	11	21	8
D158	QF vcc	372540	5366250	73.77	0.47	13.18	3.48	0.04	1.28	0.27	2.95	1.84	0.09	2.16	99.53	20	46	22	9	154	115	26	282	10	53	22	84	7	13	8
95004	Q phyric vcc	367969	5363066	68.02	0.53	15.41	4.04	0.04	1.57	0.09	6.3	0.45	0.09	2.66	99.2	36	75	37	14	230	200	28	244	11	76	38	19	15	10	4
Boco Road area																														
75740-DB	pum sst	388810	5393370	78.22	0.2	11.97	0.53	0	0.38	0.02	3	3.58	0.02	1.84	99.76	66	117	42	14	125	53	12	1123	2	18	29	115	33	2	5
78289-JM	QF xtal sst	378260	5386505	69.33	0.39	14.9	3.12	0.06	0.91	0.22	4.55	1.09	0.03	5.14	99.74	13	26	11	9	193	195	6	524	8	50	13	35	15	4	6
78291-JM	QF xtal sst	379060	5386030	72.65	0.33	14.85	1.5	0.05	0.52	1.73	3.83	2.42	0.07	1.58	99.53	32	80	28	8	172	568	4	1677	7	42	28	121	14	1	10
Halls Rivulet canal																														
131346	WS vcc	375460	5357870	62.3	0.68	17.54	6.33	0.01	3.56	0.02	1.06	4.14	0.1	4.44	100.18	33	70	29	14	200	33	175	1038	22	159	36	155	13	72	21
131348	WS vcc	375620	5358200	66.47	0.46	16.99	4.28	0.03	1.95	0.26	4.78	2.64	0.09	2.32	100.27	34	65	25	11	235	248	9	1077	12	60	27	100	20	8	3
131357	WS vcc	375880	5358270	70.39	0.4	14.68	3.38	0.03	1.33	0.14	4.59	1.91	0.09	3.91	100.86	33	71	29	10	189	185	20	677	10	50	31	69	17	14	11
131358	WS sst	375880	5358270	74.64	0.23	12.99	1.82	0.01	0.92	0.17	3.77	1.86	0.04	3.13	99.58	45	91	33	11	237	205	4	737	4	11	29	86	26	6	6
131364	WS conglom	376060	5358480	62.72	0.65	15.86	6.49	0.03	6.19	0.06	0.5	2.37	0.05	5.49	100.43	40	77	33	13	231	38	128	1034	21	82	35	72	12	73	4
131365	WS sst	376060	5358480	78.87	0.52	8.77	3.68	0.02	3.76	0.04	0.4	1.28	0.03	2.99	100.35	22	44	21	11	163	13	196	266	12	77	26	49	8	84	13
131376	WS sst	377210	5358420	72.85	1.1	9.9	7.41	0.04	3.45	0.04	0.51	1.28	0.08	3.74	100.39	14	31	15	8	172	28	368	323	29	228					
131377	WS mudst	376720	5358120	57.39	0.69	13.12	8.82	0.05	3.71	3.09	0.88	3.07	0.14	7.67	98.63	51	97	37	13	147	106	117	794	20	155	26	126	14	88	127
131379	WS sst	377320	5358820	69.22	1.03	12.41	6.69	0.02	4.43	0.02	0.61	1.79	0.02	4.25	100.48	32	63	34	15	212	27	183	497	25	188	39	60	10	58	12
131381	WS mudst	377280	5359250	61.83	0.84	12.14	11.96	0.39	3.98	0.55	0.65	2.03	0.25	5.71	100.32	30	55	27	12	120	25	129	500	25	195	37	84	9	68	16
131383	WS vcc	377150	5359830	74.47	0.17	14.99	0.88	0	0.52	0.21	4.38	2.8	0.02	1.32	99.76	62	121	43	17	134	231	10	1157	2	7	33	129	41	3	36
131386	WS hyaloclast	377240	5360200	80.36	0.2	10.93	1.09	<0.01	0.68	0.08	1.8	2.18	0.03	2.19	99.55	46	95	34	11	108	165	20	834	4	23	30	105	26	4	58
131387	WS sst	377210	5360290	68.14	0.31	16.93	2.04	0	1.19	0.01	0.82	7.05	0.04	3.2	99.74	68	134	45	13	174	101	32	2360	5	29	36	271	39	7	24
131388	WS vcc	377330	5360480	57.67	0.66	22.17	4.42	0.02	2.46	0.16	0.67	5.18	0.16	5.61	99.18	45	109	45	13	244	166	25	3079	24	156	38	213	14	12	13
131396	WS sst	377420	5360440	72.81	0.52	14.14	3.41	0.04	1.86	0.13	1.99	1.16	0.02	4.54	100.61	40	83	34	20	230	70	64	473	8	64	28	70	38	24	38
131396	WS sst	377420	5360440	72.64	0.51	13.62	3.26	0.04	1.75	0.14	1.79	1.13	0.02	4.67	99.55	43	89	37	19	229	74	59	473	8	60	29	70	38	24	32
131368	Pink/green vc	376250	5358240	64	0.79	16.91	4.95	0.1	1.41	1.14	5.94	2.98	0.15	1.67	100.04	36	82	39	13	311	377	6	1178	20	59	43	74	14	3	12
131369	Pink/green vc	376340	5358060	66.1	0.72	16.7	5.02	0.04	1.75	0.12	1.28	3.62	0.11	3.8	99.27	52	111	47	15	336	156	5	983	16	50	50	149	21	4	26
131374	Pink/green vc	376300	5357920	69.56	0.52	14.93	3.31	0.05	0.93	0.63	5.79	1.93	0.11	1.5	99.25	41	90	39	13	252	182	5	1074	12	32	37	47	19	2	8
131375	Pink/green vc	376390	5357950	71.59	0.36	14.33	2.25	0.08	0.64	0.86	4.28	3.48	0.05	1.78	99.7	58	122	54	14	282	353	3	1529	9	10	53	96	20	2	5
Possible White Spur correlates at Rosebery																														
Rosebery		R4746	254.3m	69.02	0.39	14.11	5.9	0.16	0.7	0.77	1.89	4.1	0.08	2.45	99.58	32	64	26	8	163	85	4	915	9	34	28	713	10	4	3
Rosebery		R1502	760ft	73.88	0.3	13.86	1.88	0.23	0.61	1.21	3.83	2.12	0.04	2.26	100.22	38	86	31	11	214	210	3	2314	7	15	35	96	19	2	14
96/27	hwvcc	377560	5378440	64.42	0.41	11.89	3.77	0.26	1.75	4.76	3.78	1.56	0.11	7.79	100.51	6	16	6	7	159	148	6	446	12	39	35	67	8	3	34
Lynchford Member																														
131946	Zigzag Hill	381790	5345995	56.94	0.7	18.22	7.47	0.15	4.19	0.96	8.29	0.82	0.13	2.27	100.14	22	45	24	7	129	205	16	154	29	172	25	23	3	4	6
131995	Comstock	383265	5345272	66.83	0.44	15.38	4.38	0.07	2.39	1.35	3.43	2.99	0.12	2.75	100.13	35	77	31	15	293	202	14	1662	11	32	38	71	18	4	12
132084	HentyCanal	380940	5357150	53.19	1.09	17.18	10.99	0.14	6.11	0.33	5.7	1.01	0.16	3.8	99.7	17	33	16	9	142	322	31	697	49	303	18	23	4	6	58
132126	Lynchford	379950	5337495	57.63	0.81	14.47	8.89	0.14	4.86	3.52	5.58	1.72	0.14	1.87	99.62	23	47	22	7	122	191	49	305	32	243	24	44	6	8	6
Lynchford correlates on Silver Falls track																														
78299-JM	lithic xtal sst	378620	388395	58.12	0.78	18.09	5.81	0.06	2.45	0.01	0.1	3.4	0.04	10.92	99.78	100	199	92	17	318	13	23	876	18	130	54	160	19	36	47
78300-JM	px-ilm lithic sst	378620	388425	50.35	1.22	18.17	12.01	0.22	4.83	4	2.89	2.17	0.22	3.83	99.87	22	49	22	9	132	657	51	1396	30	282	28	78	4	21	7
Sticht Range Fm																														
J180-JP	BackPeak	405200	5391700	67.9	0.32	16.46	4.9	0.04	1.17	0.02	0.11	4.94	0.05	3.45	99.34	111	238	112	24	374	4	4	480	16	8	108	258	32	3	7
V109 -JP	BackPeak	405200	5391700	92.89	0.2	3.8	0.9	0	0.22	0.01	0.05	1.2	0.01	0.75	100.03	14	31	14	6	223	10	13	108	2	15	20	49	6	2	5
SR19 -PB	Tyndall Rge	388700	5354000	88.66	0.29	4.93	1.62	0.01	0.84	0.03	0.15	1.4	0.03	1.46	99.41	21	48	23	7	196	7	41	215	6	43	24	61	6	9	14
SR90-PB	Tyndall Rge	388650	5353800	86.76	0.49	5.73	1.95	0.01	1	0.03	0.3	1.68	0.04	1.5	99.49	23	55	26	11	434	11	49	290	6	46	24	75	7	14	9
B272-JB	D'Aguilar Range	387900	5277900	91.66	0.25	4.25	0.94	0	0.26	0.01	0.02	1.6	0.01	0.85	99.85	16	32	15	7	182	3	23	278	3	19	13	93	5	8	2
B275-JB	D'Aguilar Range	387900	5278400	89.2	0.26	4.82	1.81	0.03	0.87	0.01	0.07	1.23	0.01	1.27	99.57	15	34	16	6	126	5	20	201	3	24	15	57	4	6	7
B197-JB	D'Aguilar Range	388300	5275500	94.38	0.08	3.21	0.2	0	0.16	0.01	0.02	1.05	0	0.69	99.8	10	15	8	2	156	4	6	77	<2	8	7	38	3	1	12

Table 1. Whole rock chemistry of sandstones.

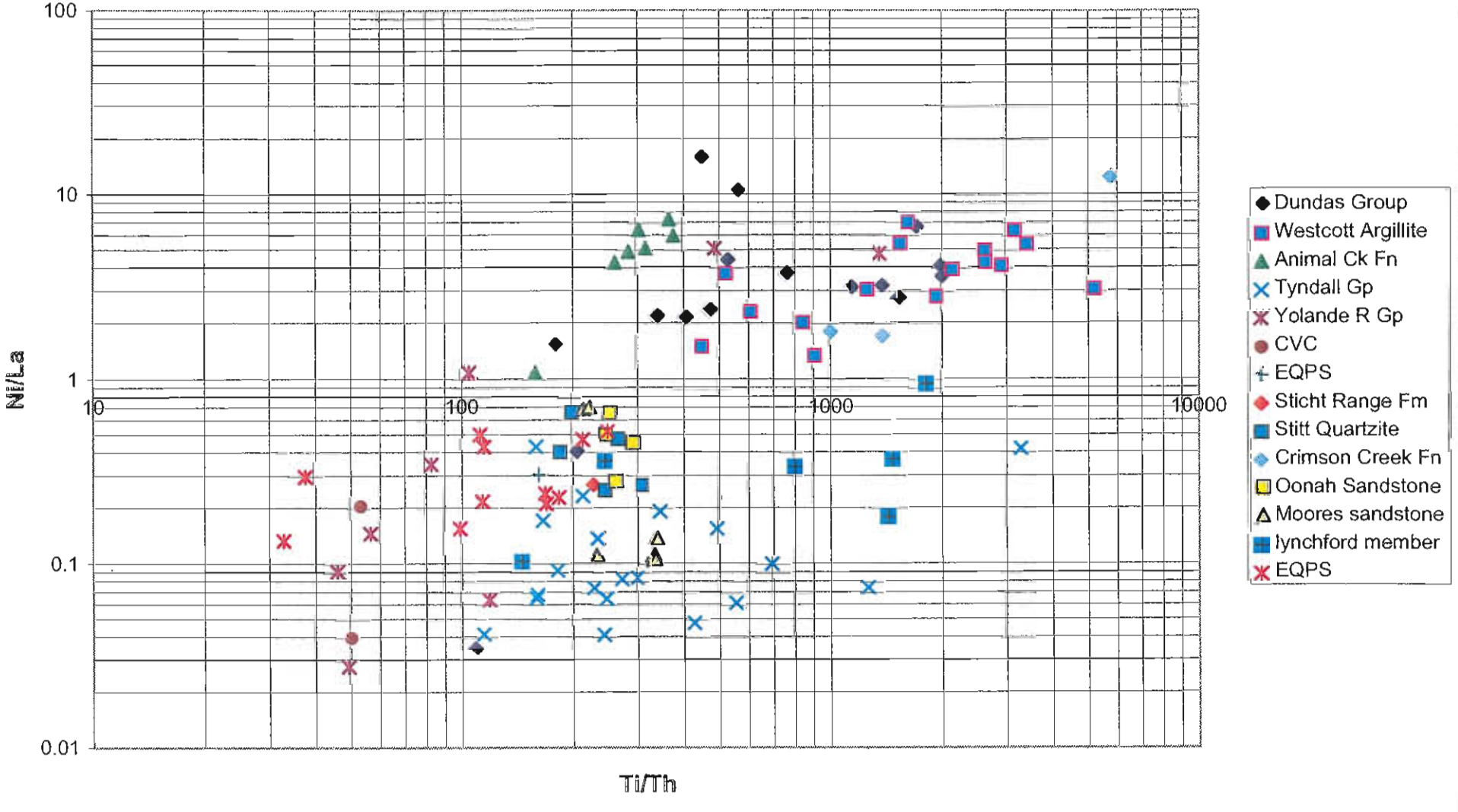

Figure 1—Ni/La vs Ti/Th of samples reported previously with the addition of data from the Lynchford member (this report) and EQPS (data from Mt Read Project physical properties database)

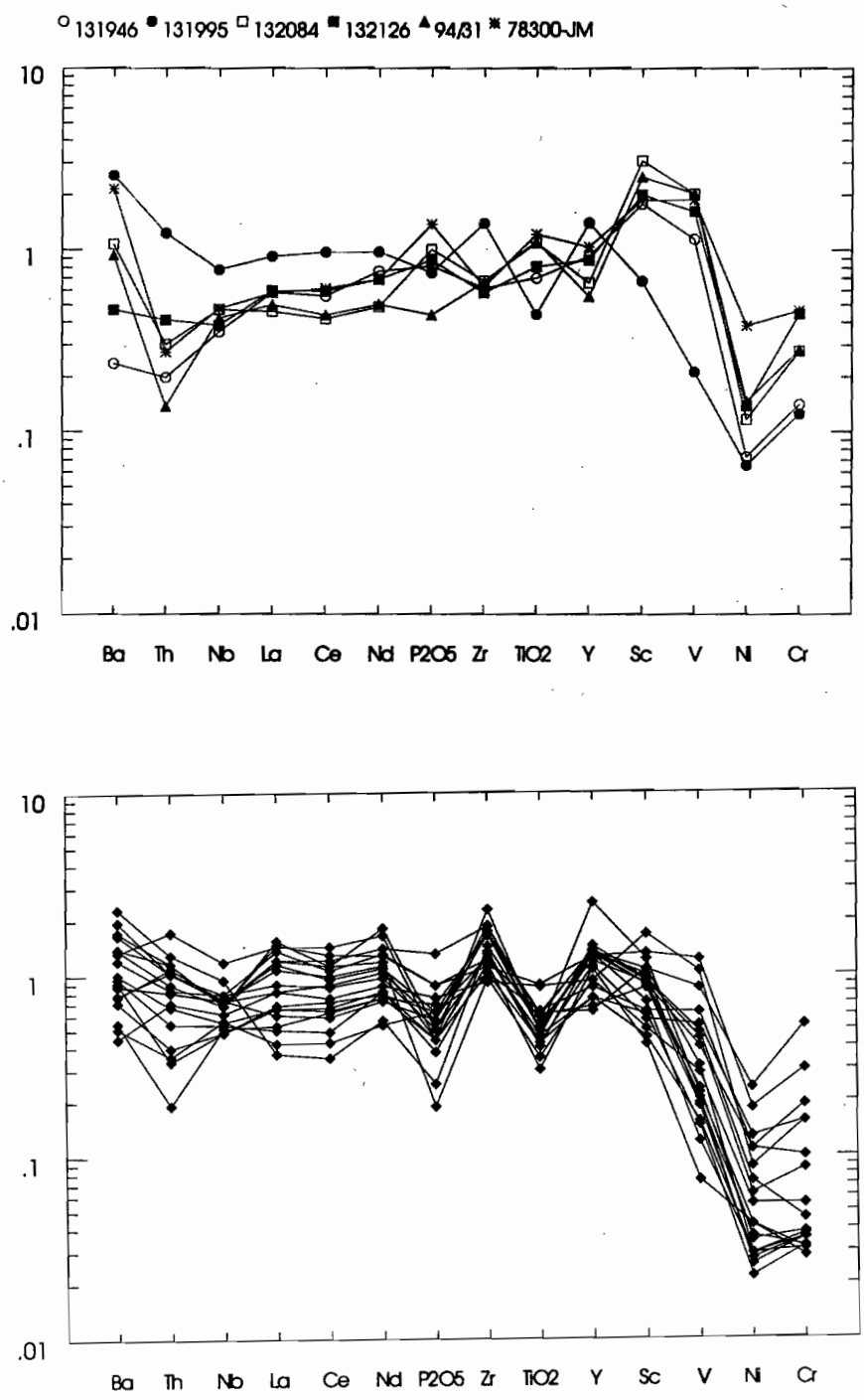

Figure 2—Spidergrams normalised to Post-Archean Australia shales (PAAS, Taylor & McClennan 1985). (a) Lynchford Member; (b) Other Tyndall Group

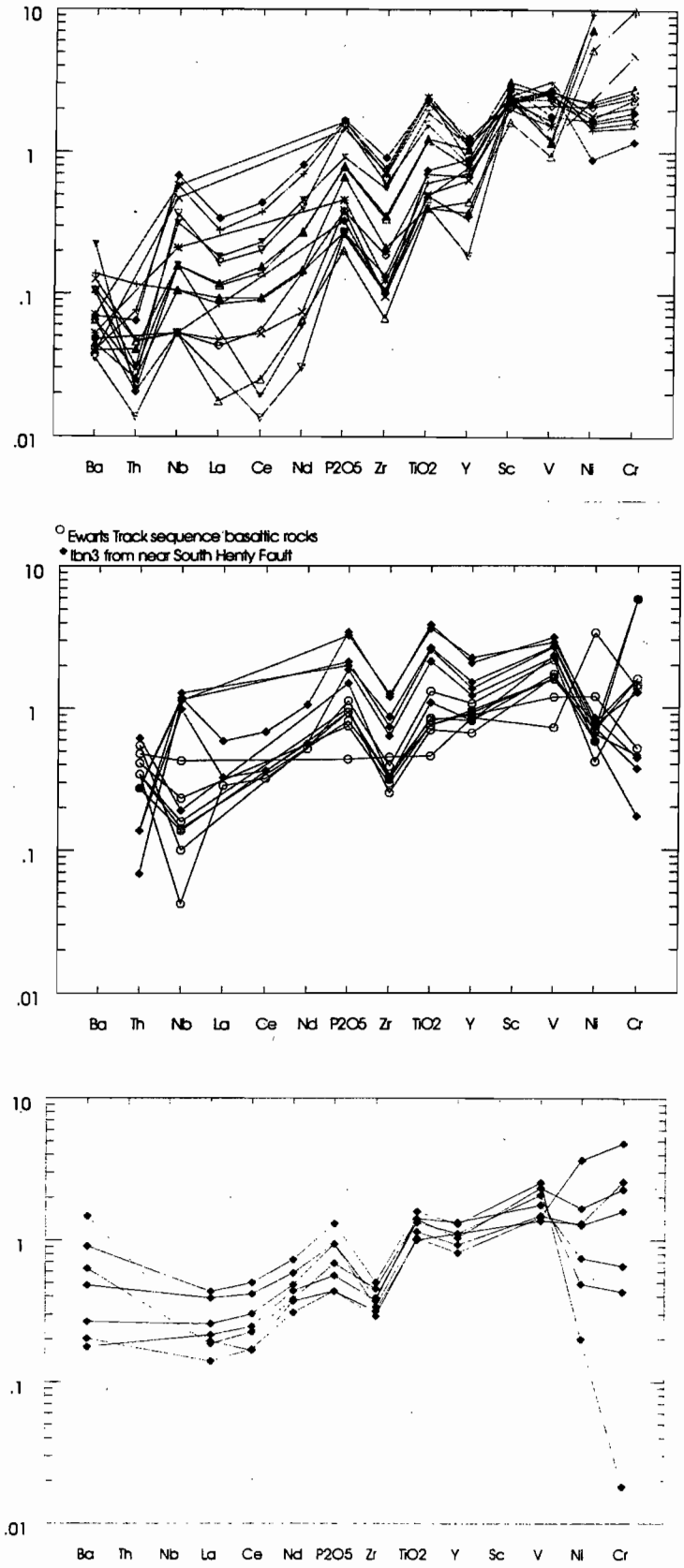

Figure 3—Spidergrams normalised to Post-Archean Australia shales (PAAS, Taylor & McClennan 1985). (a) Montgomery basalts (Brown & Stolz unpubl data); (b) Henty Fault Wedge basalts (Poltock 1992); (c) Henty dykes (Crawford et al 1992); (d) Suite 3 basalts (Crawford et al 1992); (e) Suite 2 andesites (Crawford et al 1992).

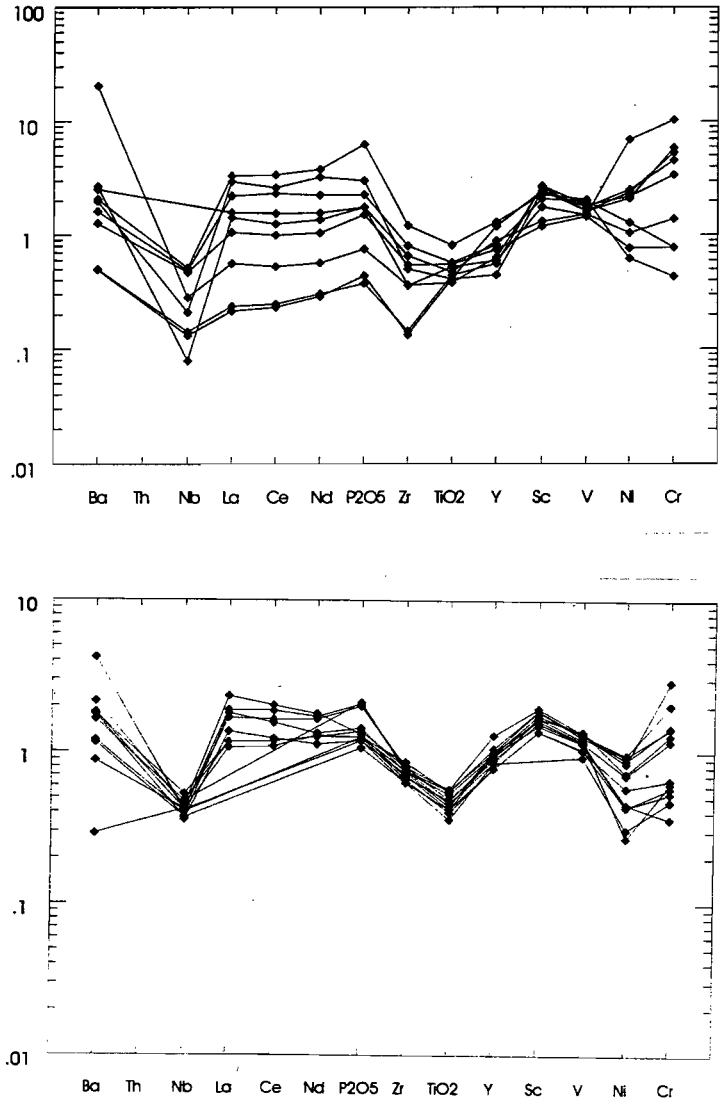

Figure 3 cont.

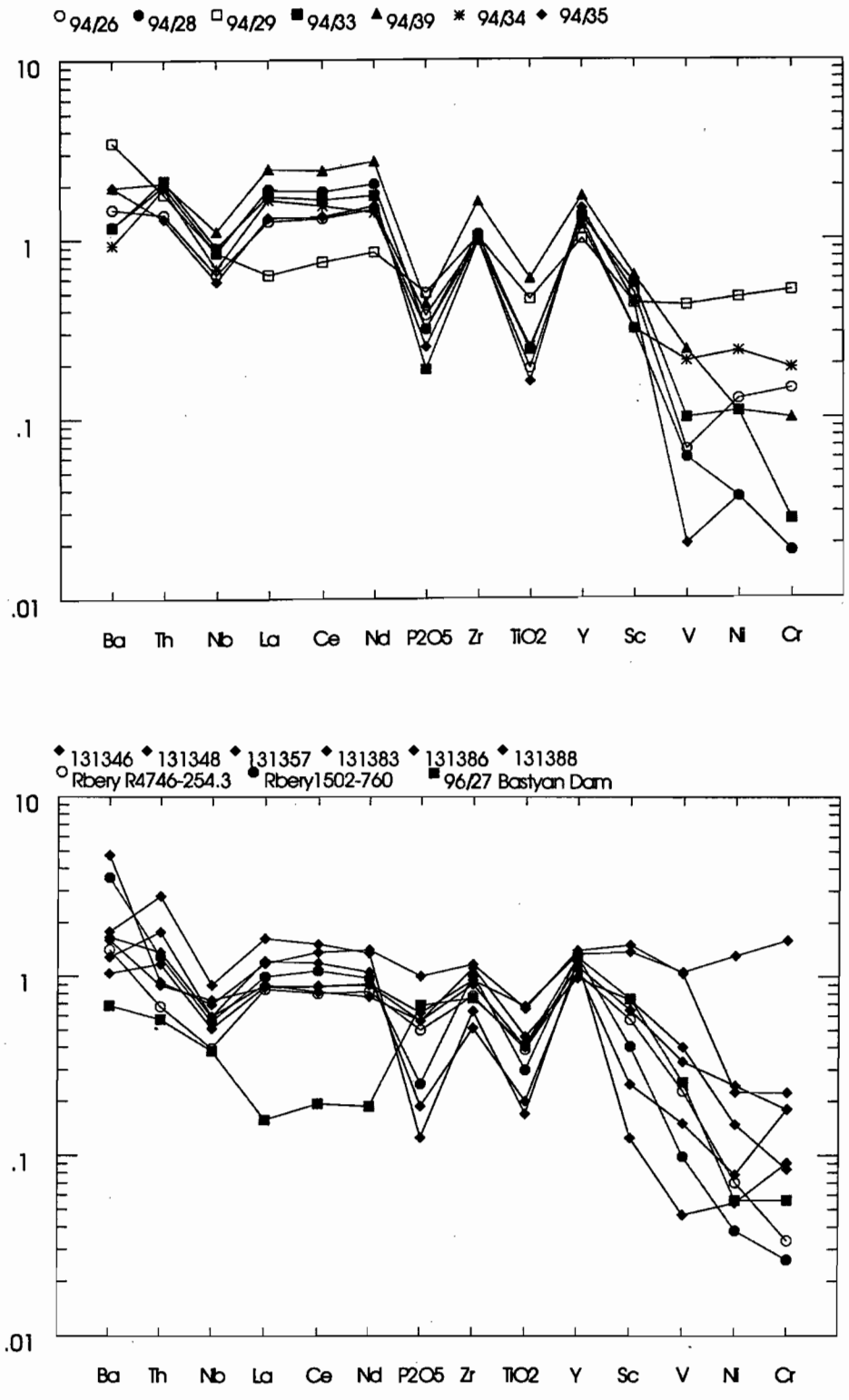

Figure 4.—Spidergrams normalised to Post-Archean Australia shales (PAAS, Taylor & McClennan 1985). (a) Volcaniclastic rocks from the Yolande River Group (94/26, 94/28, 94/29, 94/33, 94/39) and CVC (94/34, 94/35); (b) White Spur Formation and Rosebery hanging wall stratigraphy; (c) Boco Road and Silver Falls track.

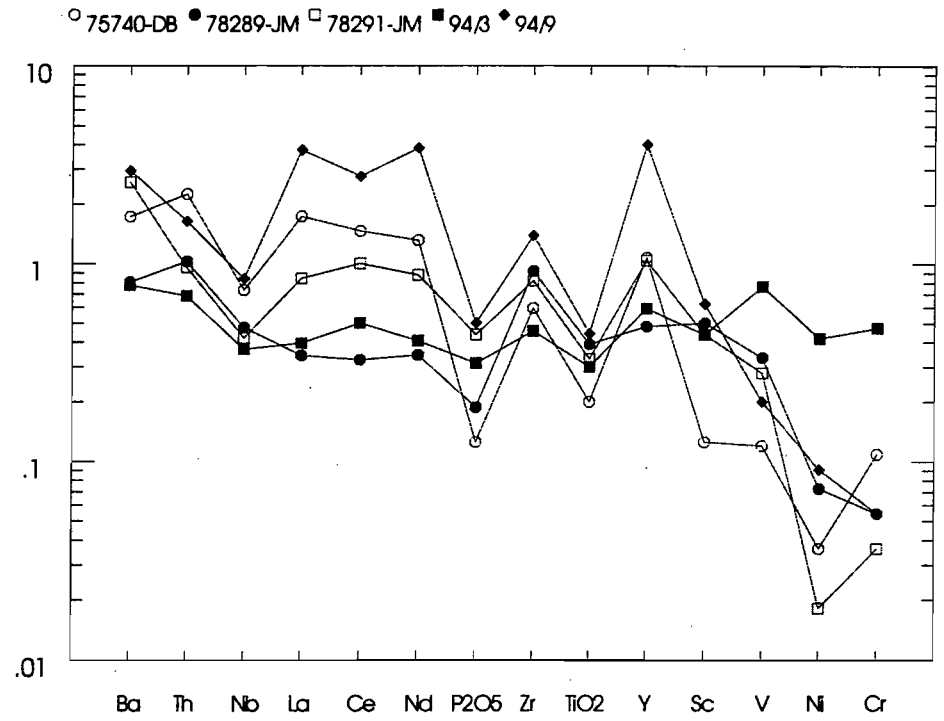
75740-DB 78289-JM 78291-JM 94/3 94/9
10
1
.1
.01
Ba Th Nb La Ce Nd P2O5 Zr TiO2 Y Sc V Ni Cr

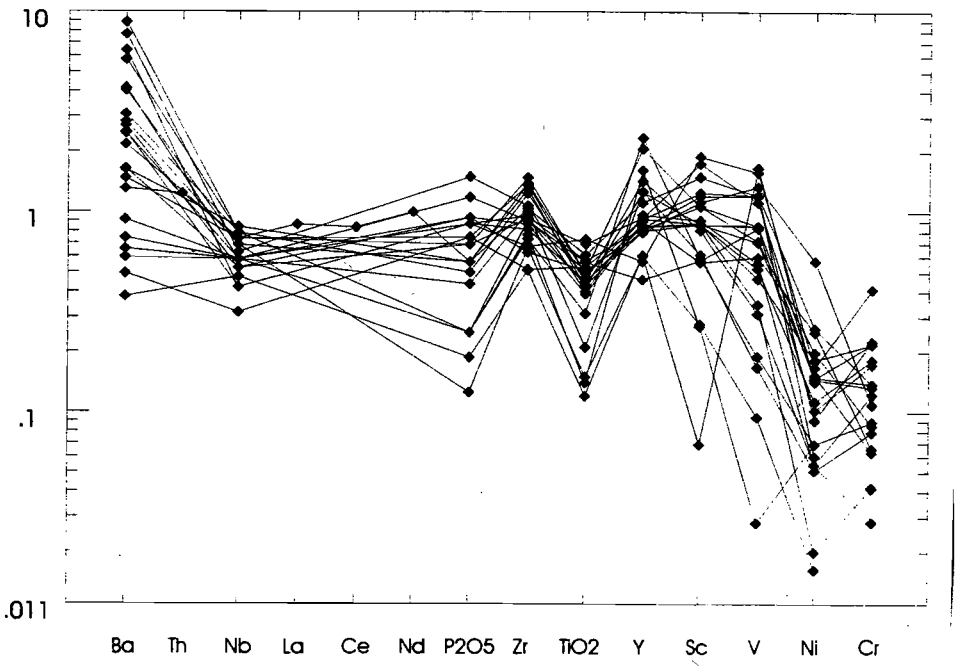
10
1
.1
.011
Ba Th Nb La Ce Nd P2O5 Zr TiO2 Y Sc V Ni Cr

samples from the CVC on the Jukes Road and a range of sample from the Yolande River Group. These sample all show a slope to the right on the PAAS normalised diagram typical of an evolved composition. They have strong negative anomalies for Ti and P and a weaker anomaly for Nb. All samples show a high Th/Nb and a low Sc/Y, distinct from the Lynchford Member pattern and on the outside of the range for other Tyndall Group samples.

A group of samples from the White Spur Formation on Halls Rivulet and the Rosebery host sequence are shown in Figure 4b. They show an incompatible enriched pattern with Ti, P and Nb anomalies. While they are not in general as LREE enriched as the CVC and Yolande River Group there is no great distinction between these rock types. Both are different from the Tyndall Group.

Samples of the mixed volcanic package above the CVC along the Boco Road are shown in Figure 4c. All of these have high Th and a general slope to the right. They have Nb, P and Ti anomalies except the very depleted Browns road sequence (94/3) and a qtz feldspar crystal sandstone (78289). Sample 94/9, a coarse quartz phyric unit similar to McPhie & Allen unit B, has very strong LREE enrichment.

The Eastern Quartz-phyric sequence is not well represented in the analyses included here. Analyses from this area that were included in the previous study are shown in Figure 4d. This dataset lacks Th and REE . Overall, the dataset suggests a slope to the left with fairly high Sc and P and a weak Nb anomaly. One dataset which includes a number of these rocks and includes a fairly complete set of trace elements is the Mt Read Project physical properties dataset. The volcanic and volcaniclastic rocks from this dataset are shown in Figure 5. There is a large variability, but 16 out of 27 samples do not have a negative P anomaly and most of these 16 have high REE. Only one sample shows a low Th (normalised Th < Nb). Thus the EQPS shows more basaltic influence than CVC and Yolande River Group discussed here. It is unlike the Tyndall Group and perhaps reflects the influence of Suite 3 lavas of Crawford et al. (1992) with their high P and REE.

The results of this analysis suggest the Tyndall Group can be recognised from other volcanic rocks in the Mt Read Volcanics. This signature is tested against two problematic datasets below.

Within the Halls Rivulet Canal there is a small section of volcaniclastics which have typical Tyndall Group style of alteration. On all other grounds they would be considered as part of the White Spur Formation. The samples from Halls Rivulet Canal (Fig. 6) have a relatively flat pattern. They have high Th/Nb, and negative P and Ti anomalies. There are samples from the Tyndall Group which match these trends but they are also very similar to White Spur Formation and lack any of the critical features. The geochemistry does not support including these samples in the Tyndall Group. They cannot be used to demonstrated that the Tyndall Group interfingers with the White Spur Formation.

There are a number of discrete volcaniclastic units which are interbedded with the Dundas Group in the Dundas area. It has always been difficult to correlate these units with more volcanogenic units. Amongst the samples analysed from the Dundas area, only samples 982 and D158 have any of the features of the Lynchford Member (Fig. 7). Sample D158 has a strong slope to the left, lacks a Nb or P anomaly, has a weak negative Ti anomaly but Sc/Y is low. This sample is like some Tyndall Group rocks and is unlike most other lithologies. The similarity provides some support for considering this rock a Tyndall correlate. Sample 982 has a strong slope to the left, high Sc/Y and lacks a Ti or P anomaly. However the P is very high and there is a weak Nb anomaly. These features are more like the shoshonitic association of Suite 3 than typical Lynchford member. Another sample with high P and REE is 883 which again appears to have a Suite 3 signature. Other samples from the Dundas area look very similar to the White Spur Formation. Sample H5 from the Husskisson River has been correlated with Unit B (of McPhie & Allen 1992). It also has a normal White Spur type composition. Only a single possible Tyndall Group volcaniclastic was recognised in the Dundas area despite the wide range in stratigraphy available and the fact that Tyndall correlates are recognised to the north of this section.

Mature sandstone

Further analyses of Sticht Range Formation (Table 1) were carried out to determine if a distinction could be found between these rocks and the Stitt Quartzite, as well as older basement rocks such as the Oonah Formation and the possibly older section in the Moores

Pinnacle area. While analysis of heavy minerals is likely to be more useful in this regard, this is still in process and will be reported at the next meeting. At the last meeting it was noted that the Sticht Range Formation (SRF) plots close to the Stitt Quartzite in most diagrams reflecting a lack of a basaltic or felsic volcanic source component. The sample 94/42 (SRF) is extremely similar to SQ1 and 93/4 which are Stitt Quartzite of similar maturity. These two samples also have a similar pattern of heavy minerals including the ratio of rounded to euhedral zircons. When looking at the heavy mineral suite alone this correlation was missed. The only distinction of Sticht Range Formation from Stitt Quartzite that we have found is the presence of small amounts of chromite in the latter.

The PAAS normalised spidergrams for Stitt Formation and Sticht Range Formation (Fig. 8) emphasizes the extremely close similarity in composition between these two units. The only exception is sample B197 which has the highest SiO_2 is very low in most other components perhaps reflecting the higher level of maturity. The P here is below detection limit. The jagged nature of the REE may reflect the analytical precision at these low abundances. The Cr levels of the Sticht Range Formation is very similar to the Stitt Quartzite suggesting that there will be chromite in the mineral separates. These lithologies are not distinguishable from Oonah Formation or the Moores sandstones on this type of diagram. The only visible difference is the lower Ba in the latter rocks (Fig. 9).

The Animal Creek Greywacke (including the Farrell slates) have a different pattern (Fig. 10) with lower Zr and weaker negative Ti and P anomalies. They also show the influence of a large component of ophiolite source in the high Ni and Cr content. The source region of this rock type is substantially different from the Sticht Range Formation. Micaceous sandstones from the Yolande River Group are more variable and do not show the very consistent trace element pattern of the Animal Creek Greywacke.

The Crimson Creek Formation sandstones (Fig. 11) have a flat pattern. They differ from the Animal Creek Formation in having lower Th and a less distinct Cr and Ni anomaly. Here sample 94/24 was originally considered as a sample of Westcott Argillite but the detrital chromite from this sample does not include any high-Ti grains and it is now included with the Crimson Creek Formation.

Chromite

Chromite chemistry is the best available method of distinguishing Crimson Creek Formation from Dundas Group. The analysis which have previously been reported are summarised on Figure 12. Here the best indicator of source is a combination of TiO_2 and Cr# (c.f. Arai 1992). The tholeiitic Crimson Creek Formation should contain high-TiO_2 chromite. Sample 94/24 supports this suggestion with TiO_2 of 0.5–5.0% (Fig. 12). Other Dundas Group samples are dominate by low-TiO_2 chromites including some very refractory high Cr# examples. The exceptional case is 94/22 which is nominally a Dundas Group sample but comes from less than 200 m from the boundary fault. It is totally dominated by high-TiO_2 chromite. The alternatives are that this near the basin boundary fault the sediment is totally dominated by the Crimson Creek Formation source or the boundary is slightly misplaced on the Mt Read Project maps and this sample is part of the Crimson Creek Formation. The latter interpretation is is accepted at this stage but this provenance of this sample needs more work.

Detailed work in the Dundas area by one of the authors (DS) has assessed the significance of location in terms of provenance. There is one example of near source dominance of the provenance of sandstones in the Dundas field. This example is of MUC dominance of some sandstones in the Ring River near the Serpentine Hill Complex. The component of Crimson Creek Formation is so low in these rocks that the incompatible elements in the whole rock analysis reflects the extremely refractory MUC compositions. In all other samples the trace elements reflect an enriched basaltic source even thogh all the chromite found in them is from the MUC.

Amongst Dundas Group sandstones most have low-TiO_2 chromites. The exception is the Fernfields Conglomerate in which a Crimson Creek source is totally dominant (Fig. 13). In the Ring River as it crosses the Rosebery tectonic zone there is a number of sandstone blocks which contain only high-TiO_2 chromites. These are interpreted here as blocks of Crimson Creek Formation. A third transitional chromite assemblage has been found associated with sandstones with a large component of Suite 3 basalts. This association blurs the distinction between the units but is thought to be very restricted in spatial distribution.

Nunn (1995) analysed chromites from the siliciclastic sandstones along the Halls Rivulet Canal (Fig. 14). These chromites were exclusively low-TiO_2. In contrast Greenhill (1995) analysed chromite from sandstone in the Cuni area. Chromite was rare in these rocks but has TiO_2 of 0.5–1.9% unlike the typical distribution in Dundas Group sandstone.

The composition of chromite as a tracer for ophiolite source in sediments has the potential to solve several of the difficult stratigraphic problems in western Tasmania. In following this up a further 40 samples are being processed including a range of samples from the Crimson Creek Formation and from various elements across northern Tasmania. These samples will be analysed over the next few months.

Summary

1. The Tyndall Group has a distinctive source composition which has contributed to the magnetic susceptibility of this unit. This composition is best reflected in the Lynchford Member and reflects an andesitic character with a tholeiitic incompatible element pattern. The closest match to this pattern in western Tasmania is the Henty dykes and the basalts of the Henty Fault wedge.
2. The Eastern Quartz-phyric sequence shows a stronger component of Suite 3 basalts than the CVC.
3. The shoshonitic Suite 3 signature is recognisable in parts of the Dundas area.
4. The Sticht Range Formation is compositional identical to the Stitt Quartzite. The Oonah Formation and Moores sandstone unit have marginally lower Ba, but are otherwise indistinguishable from this unit. The Animal Creek Greywacke has a distinctive compositional signature.
5. The MUC are very rich in chromite and even a small contribution from this source leads to a dominance low-TiO_2 chromite in the heavy mineral assemblage. Chromite composition is the clearest indicator of a MUC contribution to the provenance of sandstones in western Tasmania. The whole rock chemistry usually reflects more enriched sources such as the Crimson Creek Formation. The Animal Creek Greywacke has a contribution from the MUC and but the metamorphic basement signature associated with the Stitt Quartzite and Sticht Range Formation was not recognised.

References

Arai S 1992. Chemistry of chromian spinel in volcanic rocks as a potential guide to magma chemistry. *Mineralogical Magazine* 56: 173–184.

Berry RF & Fulton R 1995. Heavy minerals, provenance and lithostratigraphy. AMIRA P291A report 3: 1–19.

Crawford AJ, Corbett KD & Everard JL 1992. Geochemistry of Cambrian volcanic-hosted massive-sulfide-rich Mount Read Volcanics, Tasmania, and some tectonic implications. *Econ. Geol.* 87: 597–619.

Greenhill P 1995.The geological setting and mineralisation of the Cuni Cu/Ni deposits. Unpubl. BSc Hons. thesis, Univ.Tas.

McKibben J A J 1993. The geology and geochemistry of the North Pinnacles Ridge, western Tasmania. Unpubl. BSc Hons. thesis, Univ. Tasm.

McPhie J & Allen RL 1992. Facies architecture of mineralized submarine volcanic sequences: Cambrian Mt Read Volcanics, western Tasmania. *Econ. Geol.* 87: 587–596.

Nunn T 1995. Geology of the Hall Rivulet Canal, western Tasmania. Unpubl. BSc Hons. thesis, Univ Tas.

Poltock R 1992. Geology of the Henty Fault wedge, western Tasmania. Unpubl. M Econ Geol thesis, Univ Tasm: 76 pp.

Taylor SR & McClennan SM 1985. *THE CONTINENTAL CRUST: ITS COMPOSITION AND EVOLUTION.* Blackwell Sci. Pub., Oxford: 312 pp.

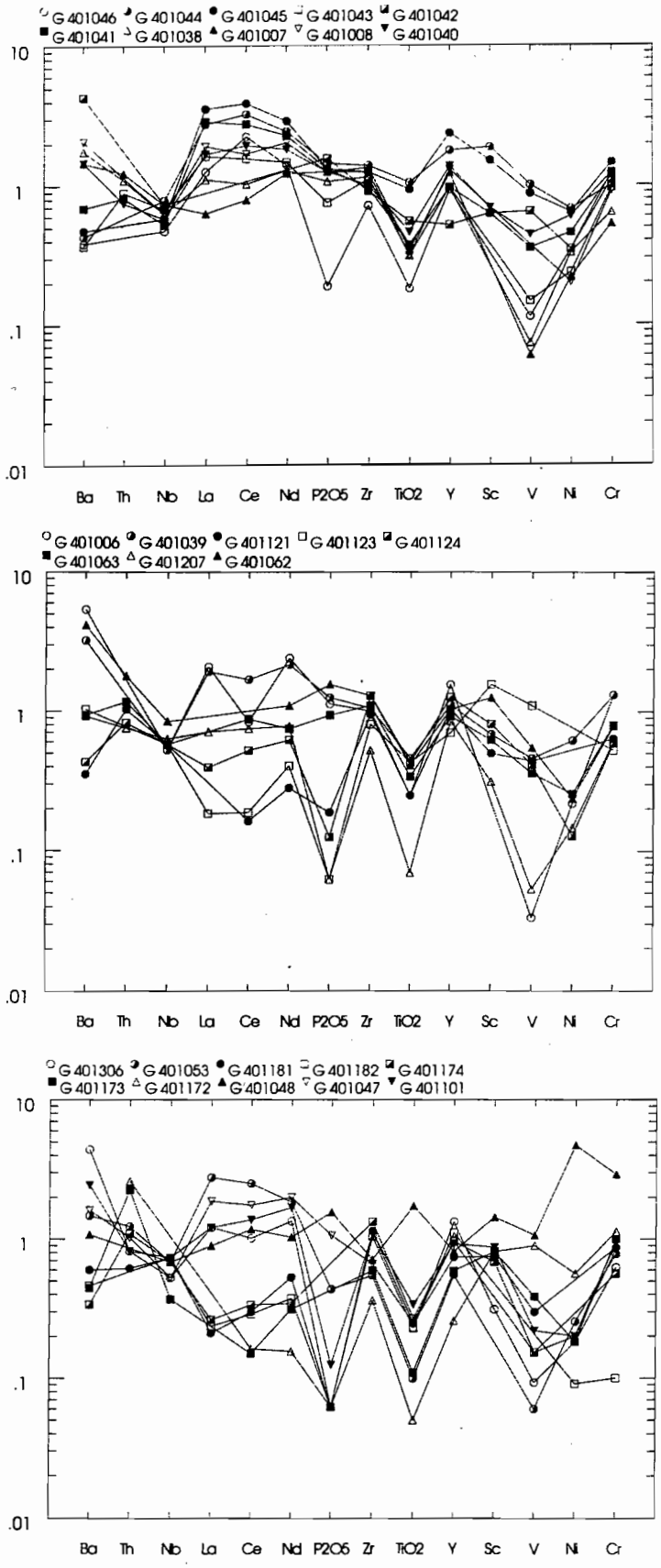

Figure 5—Spidergram normalised to Post-Archean Australia shales (PAAS, Taylor & McClennan 1985). Eastern Quartz-phyric sequence.

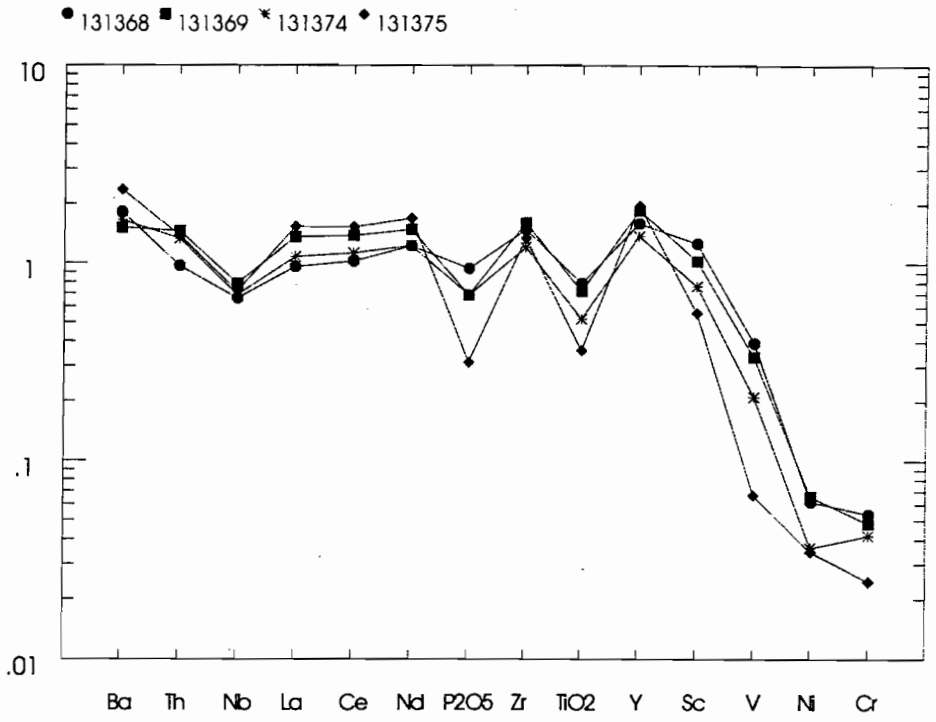

Figure 6—Spidergram normalised to Post-Archean Australia shales (PAAS, Taylor & McClennan 1985). Green and pink banded volcaniclastic rocks from the Halls Rivulet Canal.

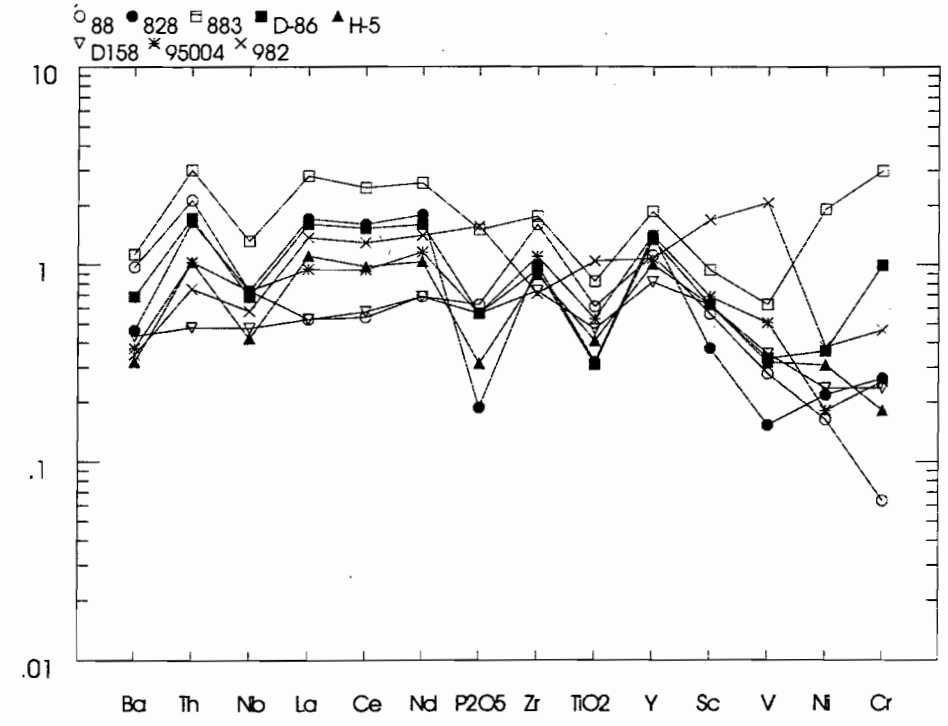

Figure 7—Spidergram normalised to Post-Archean Australia shales (PAAS, Taylor & McClennan 1985). Volcaniclastic rocks from the Dundas area.

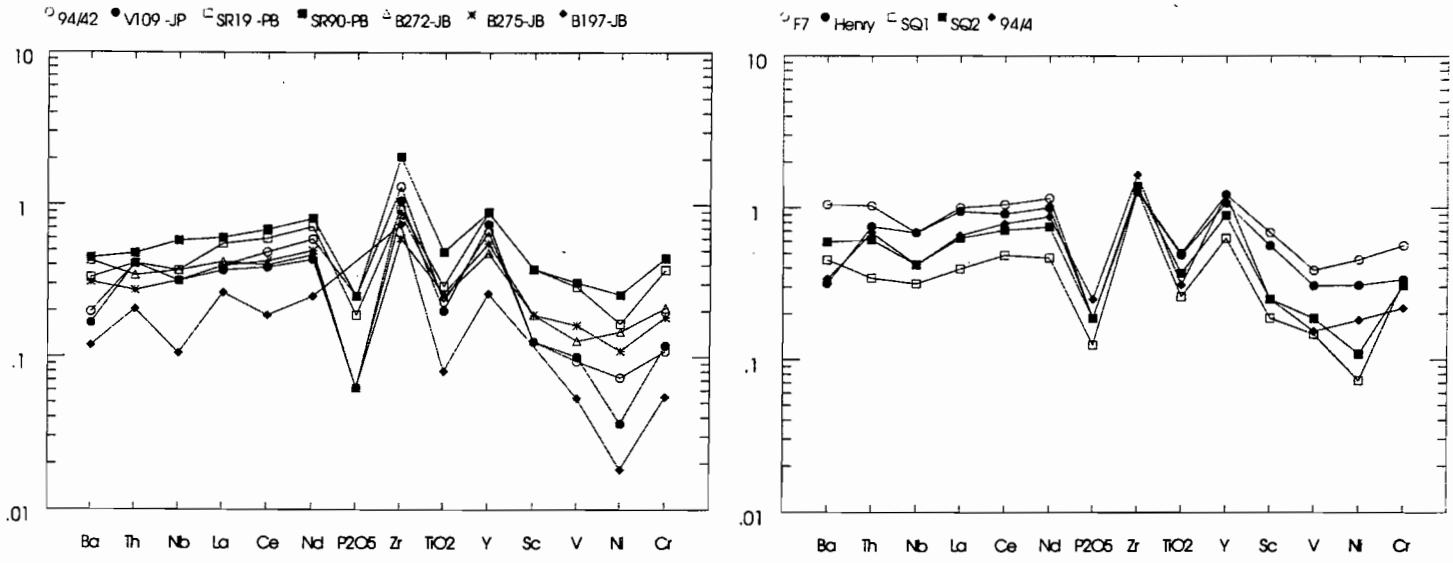

Figure 8—Spidergrams normalised to Post-Archean Australia shales (PAAS, Taylor & McClennan 1985). (a) Sticht Range Formation; (b) Stitt Quartzite.

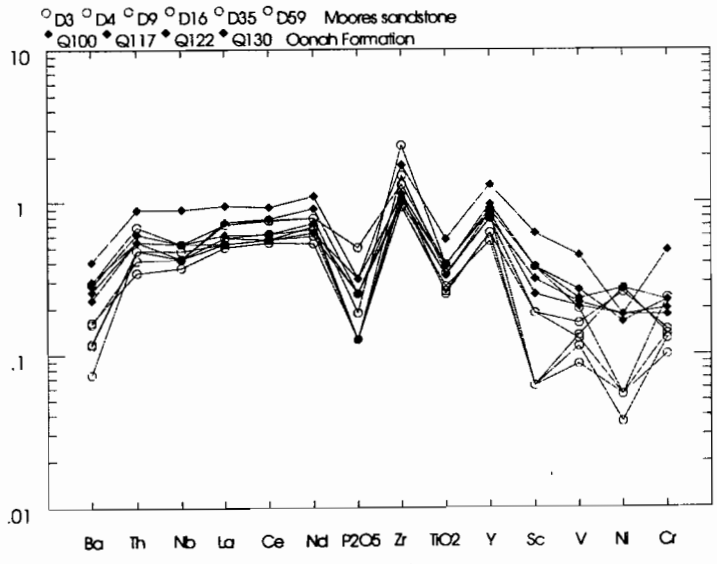

Figure 9—Spidergram normalised to Post-Archean Australia shales (PAAS, Taylor & McClennan 1985). Oonah Formation (Q100-Q132) and Moores sandstone (D3-D59).

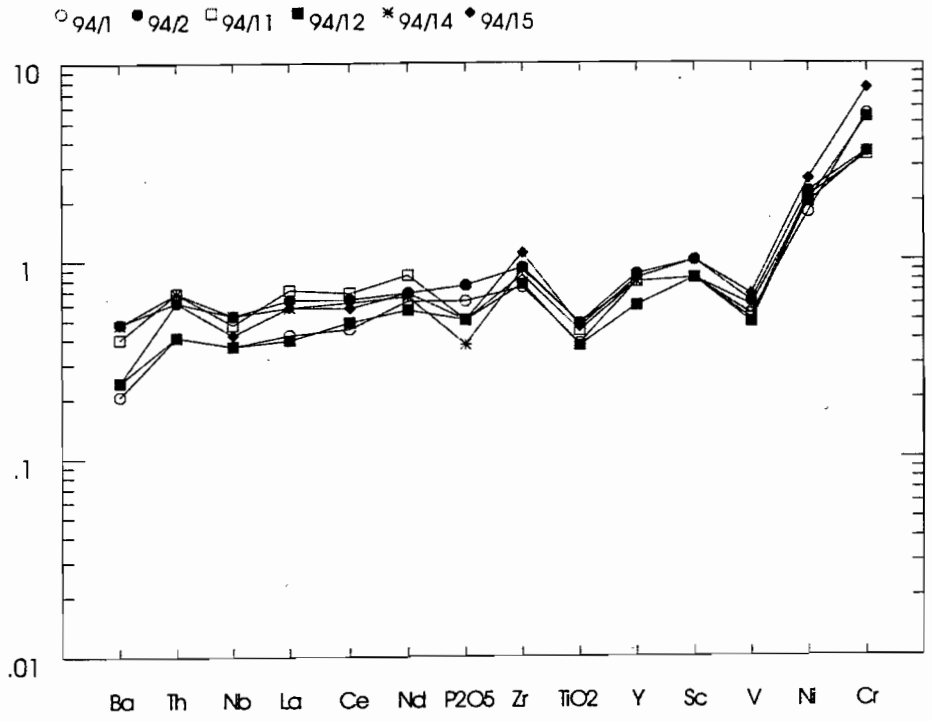

Figure 10—Spidergram normalised to Post-Archean Australia shales (PAAS, Taylor & McClennan 1985). Animal Creek Greywacke.

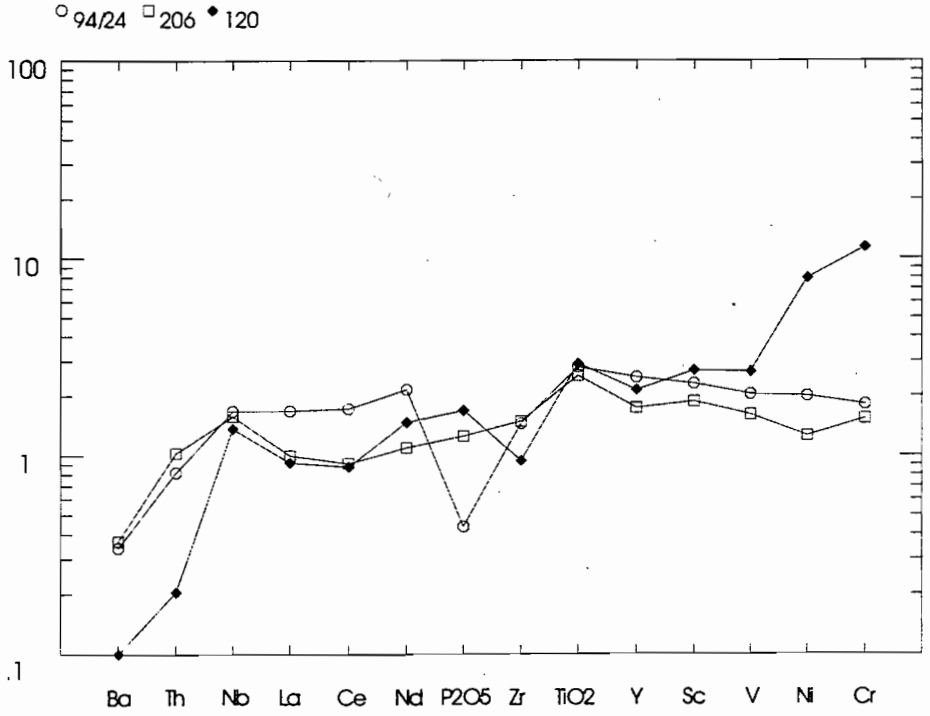

Figure 11—Spidergram normalised to Post-Archean Australia shales (PAAS, Taylor & McClennan 1985). Crimson Creek Formation sandstone.

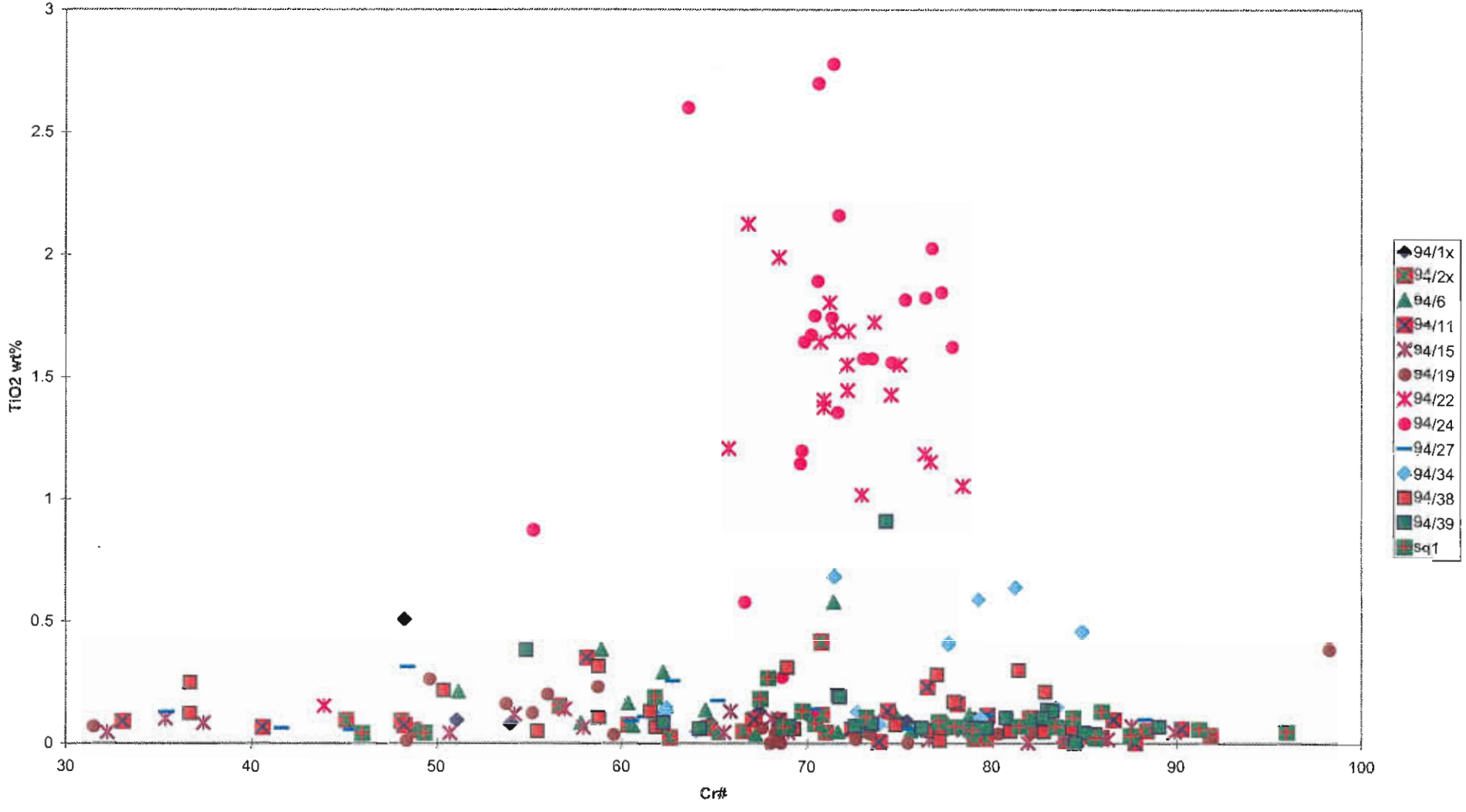

Figure 12—Composition of chromites analysed in this study.

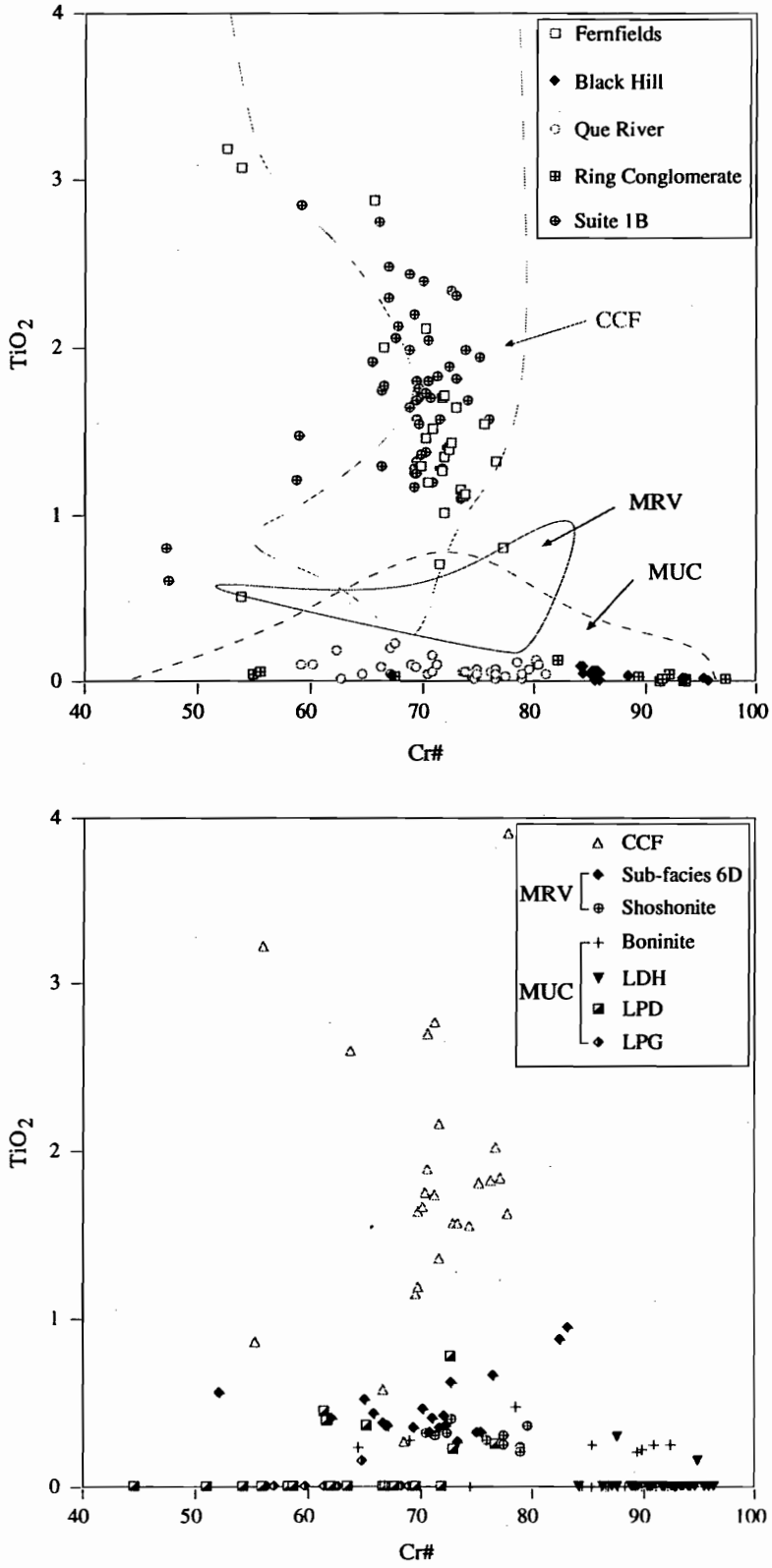

Figure 13—Composition of chromites from the Dundas area analysed by Selley (in prep.).

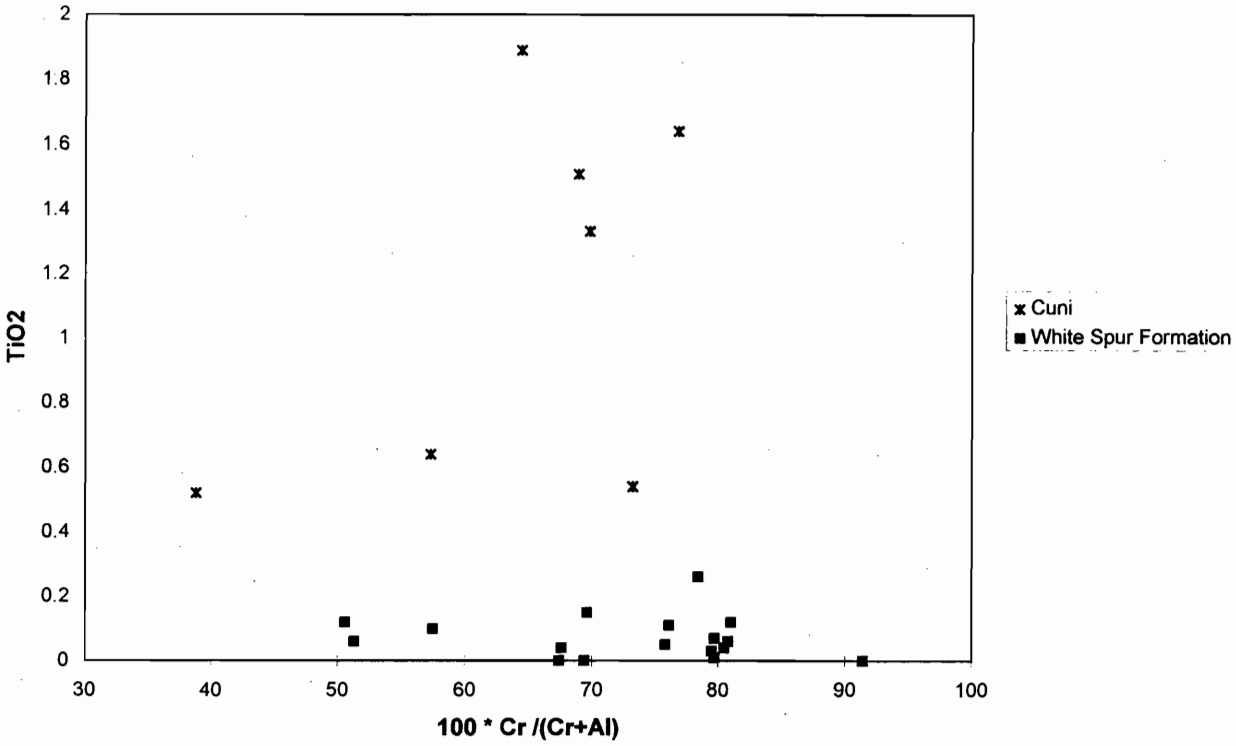

Figure 14—Composition of chromites from White Spur Formation (Nunn 1995) and Cuni area (Greenhill 1995).

Mt Cripps Fault
Evidence for Cambrian movement: provisional results

Ron Berry and Keith Corbett
Centre for Ore Deposit and Exploration Studies, University of Tasmania

Introduction

The Mt Cripps Fault was identified as a major Cambrian transfer fault in the final report of the AMIRA project P291. The evidence for this was largely based on differences between structure and stratigraphy north and south of this fault. The model proposed suggested a major Cambrian normal fault roughly in the position of the Henty Fault was offset along this structure and this offset was not entirely a result of Late Cambrian and Devonian compressional tectonics. The aim here is to consider sedimentological evidence in the context of an improved structural assessment of the immediate environment.

In order to clarify the structure in this area. new cross-sections were drawn north (5396000nM) and south (5392000mN) of the Mt Cripps Fault. These sections include detailed information from the Que River and Hellyer Mine Leases made available by Aberfoyle Ltd.

The most suitable sedimentological target for the recognition of growth faulting is the Murrays Road Greywacke, a sandstone/granule–pebble conglomerate sequence 150–200 m thick within the Southwell Subgroup. The unit extends from north of the Cradle Mountain Link Road down the eastern side of the Southwell River to where it is truncated by the Mt Cripps Fault (Vicary & Pemberton 1988, Komyshan 1986). The unit dips and faces east, and is underlain and probably intruded by a sill like body of felsic porphyry. The aim was to apply sedimentological tests for a proximal source of different composition along the Mt Cripps Fault. The exposures proved unsuitable for normal facies studies but sufficient material was available for a general consideration of grain size variations and the sampling of pebbly units to look at provenance.

A second aspect of this study was to look at the Animal Creek Greywacke near the Henty Fault between the Que River mine and the Sharks Tooth. At this point the Animal Creek Greywacke is exposed within a few hundred metres of the Henty Fault. No examples of Animal Creek greywacke are known immediately east of the Henty Fault. The exposures in this area were not sufficient to support a facies analysis and no variations in grainsize were detected. Provenance studies on these rocks are still in progress.

Murrays Road Greywacke

The relevant outcrops of Murrays Road Greywacke are shown on Figure 3. There are two substantial outcrops of micaceous siliciclastic rocks in this area: A is 300 m north of the Mt Cripps Fault and B is 150 m north. In addition, at C (100 m from the fault) there is a large amount of siliciclastic float which represents a normal progression from B. There is no evidence that this material has been transported from elsewhere. A boulder train from this float runs down to the creek but no similar material was found above it to the NNE or east.

At A there is a nearly continuous exposure for 30 m. In this section there is only one bed exposed with a pebbly component. This contrasts with the 50 m of discontinuous exposure at B. Here there is a substantial component of coarser pebbly units. Based on a visual estimate this was about 30% of the rock exposed. The ratio of coarser component appeared to be greater than 50% in the area of float at C but this may be a biased sample. The contrast between these locations suggests a simple rapid change in grain size in the 300 m away from the Mt Cripps Fault.

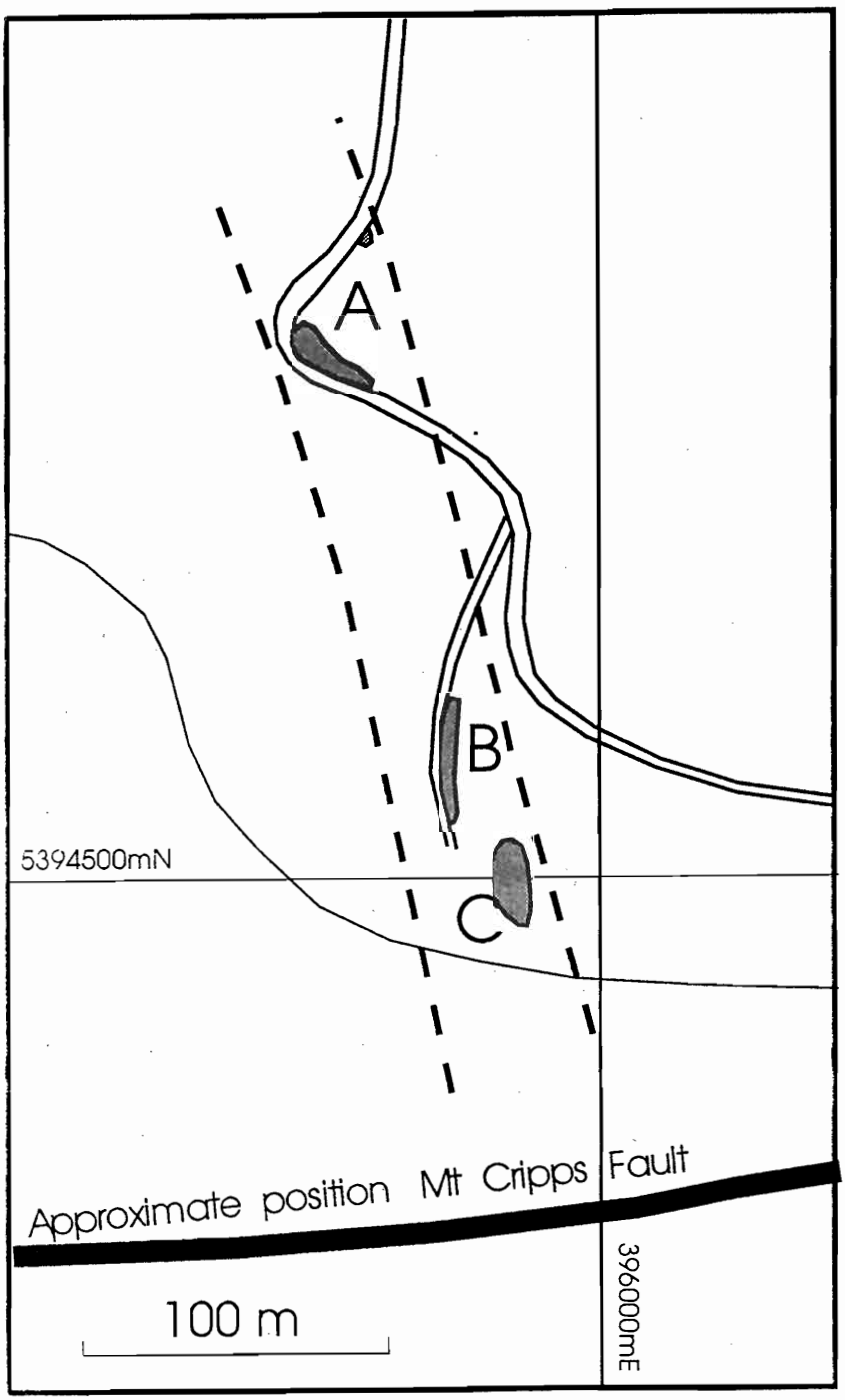

Fig. 1. Location map for exposures of Murrays Road Greywacke near the Mt Cripps Fault.

The zonation of clast size is more complex than indicated in this small area. The next available outcrop (location D — 800m north of the Mt Cripps Fault) at 39571E 539520N is along a track. The ratio of pebbly units is relatively low here but there are examples of units with 5 mm grainsize lithics. Unfortunately these were too deeply weathered to sample successfully. The sample discussed below was not the coarsest material in the section. Given the length of outcrop exposed on this track the coarse facies was less than 10% of total stratigraphy.

The Murrays Road Greywacke was also exposed on the Cradle Mountain Link Road (394800E 5398500mN). In 50m of section exposed in the cutting examined a bed of granule size material was found representing about 5% of the section. At MXRD-1 a further 5 km to the north there is 40 m of section present but there are no granule conglomerates present. The coarsest unit examined was a coarse sandstone. The largest fragments in this rock are black shales and there is no evidence for coarse quartz grains.

The original mapping of Komyshan (1986) suggests the Murrays Road Greywacke is lenticular and the exposures near the Mt Cripps Fault form a discrete lens separate from those on the Cradle Mountain Link Road. More recent mapping of Aberfoyle geologists supports this distinction. The observations here indicate there is a complex variation in grain size but the existing dataset indicates there is an anomalously high proportion of coarse units in the near vicinity of the Mt Cripps Fault. A more formal measure of this variation is required to put this observation on a firm footing.

Provenance

Of the four granule–pebble grade samples from locality C, three are consistent in their detrital composition and one (MC3-3) consists entirely of volcanic material and is probably a primary volcaniclastic. Samples MC3-1, MC3-4, and MC3-5 are closed framework with low matrix and consist of rounded to subrounded clasts 1–10mm long, commonly elongated in shape (Fig. 1). The clast components in order of abundance are:

1. Metamorphic quartzite to quartz muscovite phyllite probably derived from the Tyennan block.
   ~ 60% of the clasts
2. Chert and fine grained siliceous rocks of possible volcanic origin; usually internally structureless; colourless to brownish grey; rarely with internal quartz (-hematite) veining.
   ~ 20% of the clasts
3. Felsic volcanics/intrusives, of which the most abundant type is a feldspar porphyry with scattered small quartz phenocrysts in a greenish dusty groundmass. The feldspar phenocrysts are typically of two sizes. One grain had a spherulitic groundmass. A second type, represented by only two grains, was a coarsely intergrown quartz-feldspar granitic rock with a well developed graphic intergrowth texture (in MC3-4).
   ~ 10% of the clasts.
4. Mafic-intermediate volcanics, mostly consisting of fine plagioclase laths in a dark green chloritic groundmass.
5. Sedimentary clasts including sandstone, siltstone and dark mudstone.
6. Other components include large quartz and feldspar grains of probable igneous origin.

Sample MC3-3 consists entirely of volcanic material and appears to be a modified volcaniclastic rock, possibly of local derivation. Clasts and matrix are of similar feldspar porphyritic composition, and are similar to the porphyry clasts seen in the other samples from this locality. This porphyry type is unlike the Bond Range Porphyry (which is characterised by large embayed quartz phenocrysts, abundant altered biotite and altered feldspar) but may correlate with the felsic porphyry which occurs immediately to the west of, and probably intrudes, the Murrays Road Greywacke. As described by Corbett & Komyshan (1989) and Pemberton et al. (1991), this unit has feldspar phenocrysts and rare small quartz phenocrysts in a groundmass that is commonly spherulitic.

Sample MC2-2 from locality C is a coarse sandstone and is dominated by metamorphic quartzite clasts with little volcanic material.

The two samples from locality B (MC2-1, MC2-2) are mostly of granule grade (1–4 mm) and have similar compositions. Both are dominated by metamorphic quartzite detritus (~ 90%), with no obvious chert clasts

and no obvious volcanic material. There are some large clear quartz grains of possible volcanic derivation, and some probable sedimentary grains.

The one sample from locality A (MC1-1) is of a coarse sand to granule grade and is dominated by quartzite clasts (~95%). The are no identifiable volcanic clasts.

The sample from 800 m to the north (MC4) is a medium grained sandstone and is too fine grained to have recognisable lithic fragments. It contains clasts of quartzite and chert and some possible igneous quartz.

We have not looked in detail at the coarse facies from the Cradle Mountain Link Road. The only sample that we have appears to have a similar provenance including metamorphic grains, felsic volcanics and coarse "igneous" quartz. The sample (Fig.) appears to have less siliceous fragments, The grain size is more uniform (2–5 mm) and the grains are both more rounded and more spherical (c.f. Figs.). A sample of similar grainsize and weathering from location B has much more prominent black shale clasts. Red chert is a minor component in locations B and C but not seen in the sample from the road. The sample is too weathered to expect preservation of basaltic clasts.

The present evidence supports a rapid change in grainsize towards the Mt Cripps Fault consistent with erosion from a local source. This source includes metamorphic rocks, Mt Read style volcanics, siliceous rocks and granite. There are some indications that the Murrays Road Greywacke has a substantial variability and we have not yet demonstrated that the changes near the Mt Cripps Faults are exceptional with regard to the normal variations.

Structural sections

Two new structural sections (Figs 3, 4) were drawn to compare the structure north and south of the Mt Cripps Fault. The basic dataset for this interpretation is the Mt Read Project Maps 1 (Komyshan 1986), 2 (Corbett & McNeill 1986), and 7 (Vicary & Pemberton 1988), the Mackintosh 1:63,360 sheet (Barton et al. 1966) and the Tullah 1:50,000 compilation (Green & Bamford 1986). The new sections draw on the original sections and data in P291 report 1 and 5. The western end of these sections is drawn directly from the section given in the P291 final report. The dips of structures are shallower because these lines are now drawn E–W to facilitate application of geophysical modelling and match the orientation of proposed Cambrian structures. The previous versions were drawn perpendicular to Devonian fold axes. The area over the Que–Hellyer region has been improved by reference to Aberfoyle confidential data. The sections here are drawn at a smaller scale than the data made available so some of the smaller structures recognised by Aberfoyle geologists could not be shown. The Black Harry beds are shown here as continuing to thicken to the east as a distal apron to a thinning CVC. This is taken as a mirror of the relation of the Yolande River Group to the southern CVC. The truncation of the Que Hellyer volcanics against the Southwell Subgroup is based on Aberfoyle data. This would require a steep topographic surface on this side of the volcanic edifice (~10∞).

The eastern section is much clearer because the sections do not cross the Mt Cripps fault obliquely as occurred in previous versions. The structure along the line 5396000mN is relatively well constrained by the surface geology and follows the subsurface interpretation of Pemberton et al. (1991). The dip of the Henty Fault extension is taken as parallel to dips measured to the south. The deeper structure with growth faults are projected from south of the section.

South of the Mt Cripps Fault the whole section east of the Henty Fault is covered in Owen Conglomerate or younger units. The surface structure is simple. In the far west against the Henty Fault the underlying material is based on Aberfoyle mapping south of the Sharks Tooth. The central section is poorly constrained. The provenance data from the Murrays Road Greywacke above suggests that there is a source for basement, porphyry and siliceous rocks in this section. The interpretation here is that this indicates a thin cover of Southwell Subgroup over basement,. and the Bond Range Porphyry does not extend this far west. This interpretation is consistent with the structure north of the Mt Cripps Fault and suggests that this fault was a relatively small feature at the time of deposition of the Southwell Subgroup having an offset in this position of less than the thickness of the Southwell Subgroup, but sufficient to lift the southern block into a subaerial position.

Conclusions

Detailed investigations along the Mt Cripps Fault have provided supporting evidence that the fault was present during the deposition of the Southwell Subgroup. No additional evidence has been found for the existence of this structure during the earlier part of the Mt Read depositional cycle.

References

Barton CM et al 1966. Geological atlas one mile series Sheet 44 (8014N) Mackintosh. Dept Mines Tasmania.

Corbett KD & Komyshan P 1989. Geology of the Hellyer– Mt Charter area.. Mt Read Volc. Project Tasm. Geol. Rep. 1.

Corbett KD & McNeill AW 1986. Mt Read Project. Map 2. Geology of Rosebery –Mt Block area. 1:25,000. Dept. Mines Tasm.

Green GR & Bamford AL 1986 Mt Read Volcanics Project, 1:50,000 Metallic mineral deposit map series: Tullah. Dept Mines Tasm.

Komyshan P 1986. Mt Read Project. Map 1. Geology of the Mt Charter–Hellyer area. 1:25,000. Dept. Mines Tasm.

Pemberton J, Vicary MJ & Corbett KD 1991. Geology of the Cradle Mountain Link Road–Mt Tor area (Maps 7 and 8). Mt Read Volc. Project Tasm. Geol. Rep. 4.

Vicary MJ & Pemberton J 1988. Mt Read Project. Map 7. The geology of the Back Peak–Cradle Mountain Link Road area. 1:25,000. Dept. Mines Tasm.

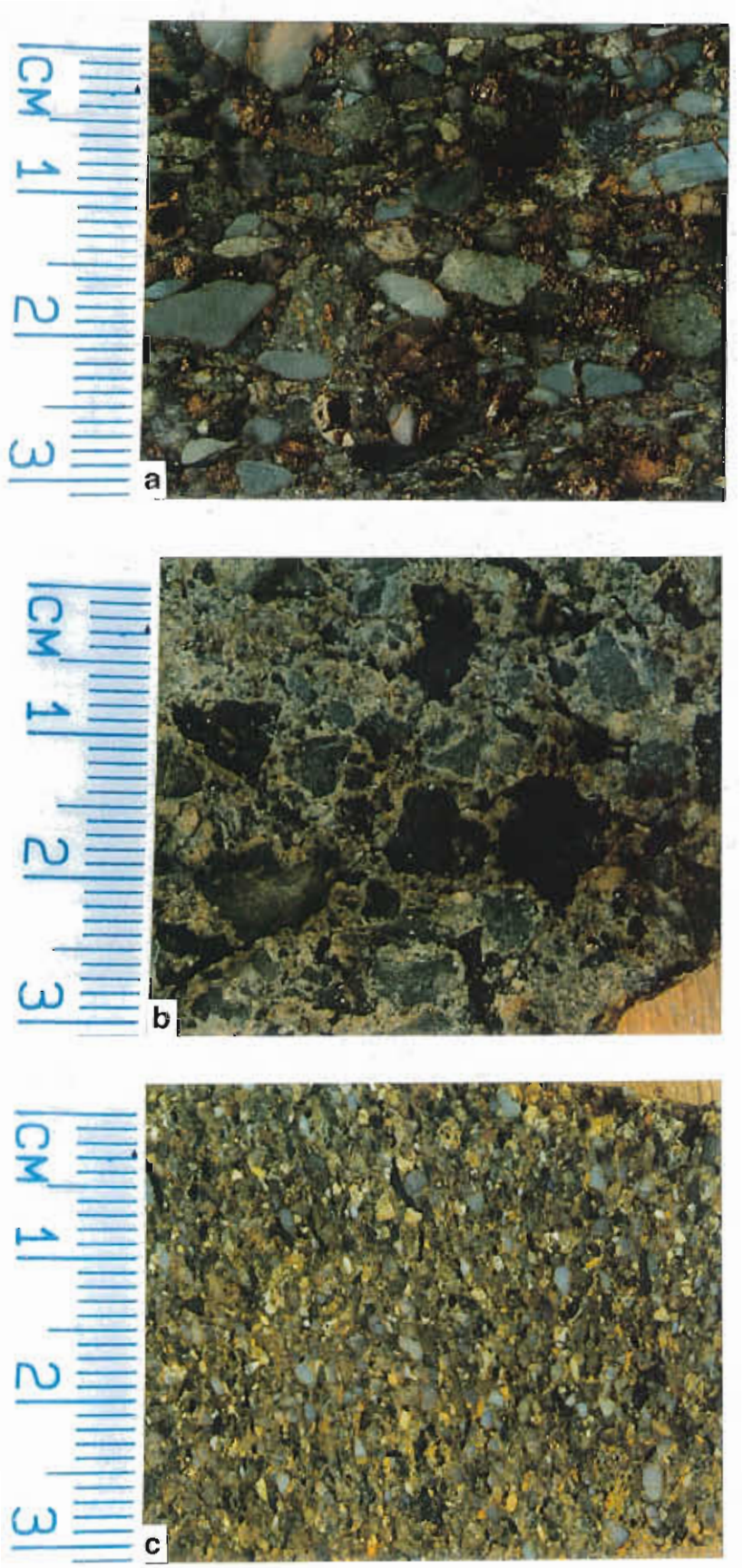

Fig. 2. Textures of coarser sediments from the Murrays Road Greywacke: (a) granule conglomerate from location C, (b) Volcaniclastic unit from location C, (c) coarse sandstone from location C.

Fig. 2. Textures of coarser sediments from the Murrays Road Greywacke: (d) granule conglomerate from location B, (e) coarse sandstone from location A, (f) granule conglomerate from the Cradle Mountain Link Road.

Fig. 4. Geological section at 5392000mN

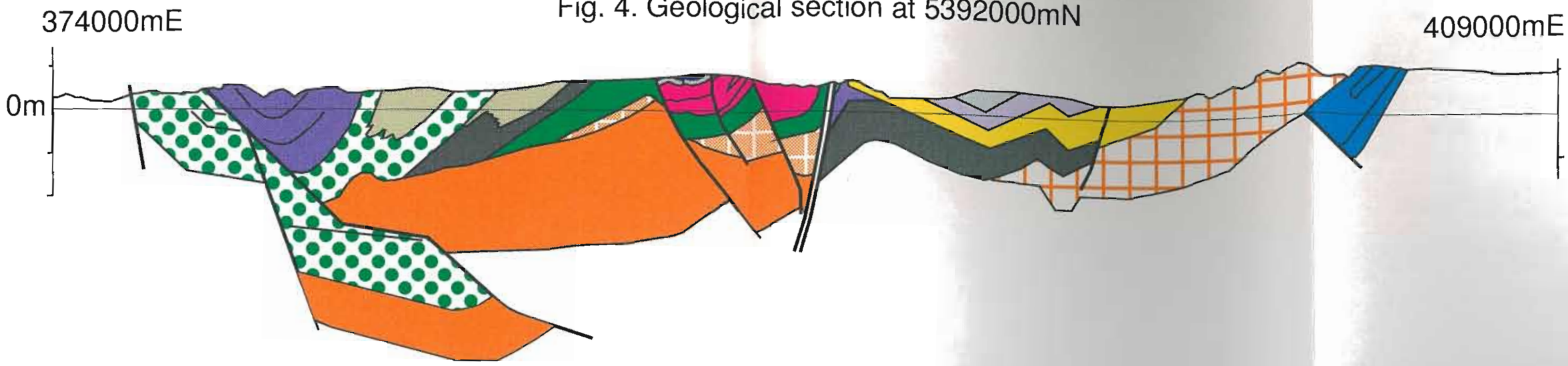

Fig. 3. Geological section at 5396000mN

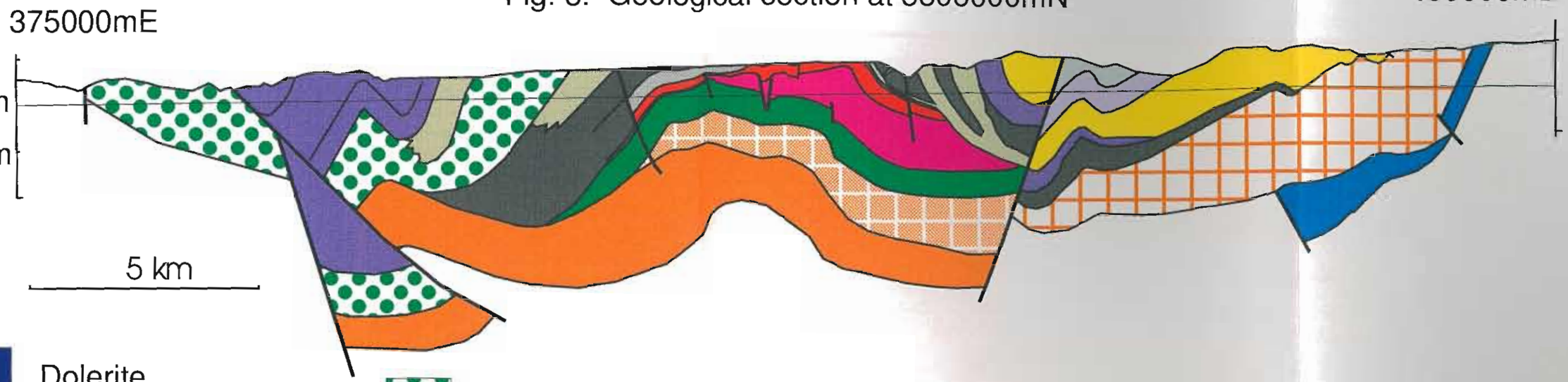

Dolerite

Animal Creek Greywacke

Black Harry beds

CVC

Basement

Upper Dundas Group

Qtz feldspar porphyry

Que River Shale

Hellyer basalt

Que Hellyer footwall

Tyndall correlates

Southwell Subgroup

Bond Range Porphyry

Sticht Range Formation
Back Peak beds

Silurian clastics

Gordon Group

Owen Conglomerate

Trace Element Investigation of Pyrite: a possible discriminator for Cambrian and Devonian fault structures

Paul A. Kitto
Centre for Ore Deposit and Exploration Studies, University of Tasmania

SUMMARY

A new multi-trace element ratio Pyrite Discriminator Index (PDI), base on electron microprobe analyses of pyrite (Co, Ni, Cu, Zn, Pb, As, Se, Ag, Au), provides for the first time a low cost method to differentiate between Cambrian VHMS mineralisation and Devonian granite related hydrothermal mineralisation. The PDI is based on the ratio of trace elements most common to Cambrian pyrite mineralisation (i.e., Co, Zn, As, Se, and Pb) compared to those elements more nearly associated with Devonian granite related pyrite mineralisation (i.e., Ni, Cu, Ag, and Au). The proposed PDI equation is:

$$PDI = \frac{100x(CambrianEnrichedElements)}{(CambrianEnrichedElements)+(DevonianEnrichedElements)}$$

$$PDI = \frac{100x(Co+0.2Zn+2As+20Se+0.1Pb)}{(Co+0.2Zn+2As+20Se+0.1Pb)+(Ni+2Cu+Ag+4Au)}$$

Based on the available pyrite trace element data, a PDI value greater than 50 is indicative of a Cambrian VHMS style of mineralisation, and a PDI value less than 50 is indicative of a Devonian granite related style of mineralisation.

INTRODUCTION AND PREVIOUS STUDIES

A major aim of AMIRA P.291a ∇ Structural Controls on Mineralisation in Western Tasmania, is to geochemically characterise and identify potential Cambrian transfer faults. Until now, no one single geochemical technique (eg., $\delta^{18}O_{qz}$, $\delta^{13}C/\delta^{18}O_{carb}$, $\delta^{34}S$, $^{204/206}Pb$, fluid inclusions, FeS/Cd/Mn ratio sphaler ite), be it expensive or inexpensive, exists to discriminate between Cambrian and Devonian faults and related mineralisation in western Tasmania.

Previously described geochemical techniques have been dependent on a specific mineral assemblage that may or may not be present at each location. Pyrite, be it abundant or in minute concentrations, is ubiquitous to western Tasmania. As such, its trace element concentrations could prove diagnostic in differentiating the nature of hydrothermal fluid flow within a fault zone and therefore the likely Cambrian and/or Devonian origin and/or reactivation of the fault.

Most pyrite contains high levels of trace elements, either as inclusions or within the crystal lattice. Loftus-Hills and Solomon (1967) using atomic absorption spectrophotometry on pyrite separates from Tasmania identified the following three groups based on cobalt and nickel ratios (Fig. 1):

(i) sedimentary or diagenetic origins in shales (high Co & Ni; Co:Ni < 1),
(ii) probable volcanic origin without accompanying Pb & Zn minerals (Co:Ni > 1), and
(iii) probable volcanic origin associated with Pb & Zn minerals and those with cassiterite or argentiferous galena related to granitic intrusions (low Co & Ni; Co:Ni < 1).

Further they showed that relatively high cobalt and selenium contents in pyrite may be related to volcanic processes. Groves (1968) extended this initial study on pyrite separates in western Tasmania and identified five groupings based on cobalt and nickel ratios (Fig. 2):

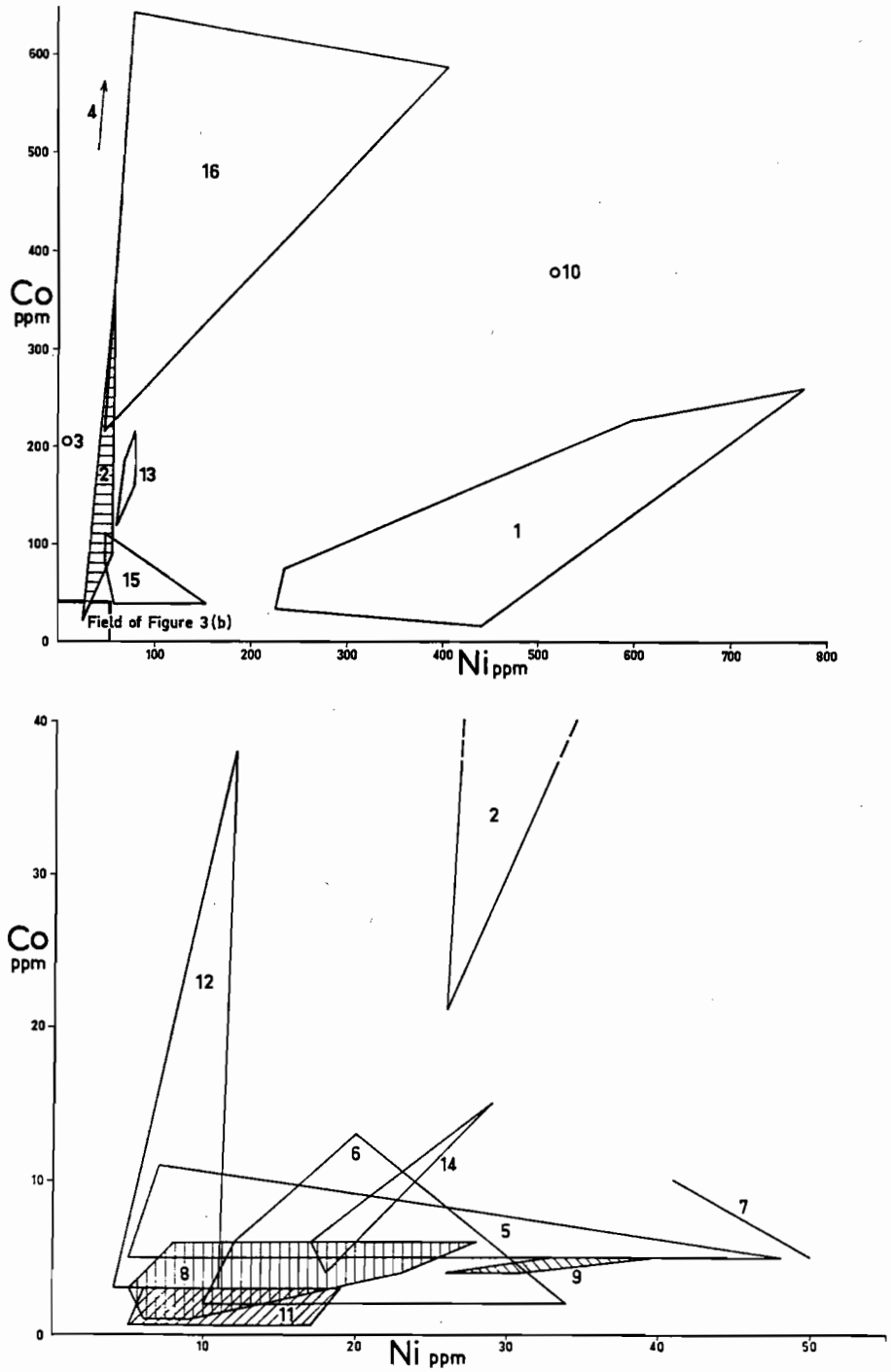

Fig. 1 (upper) Distribution of cobalt and nickel contents of pyrites from West Tasmania. 3b. (lower) Enlargement of part of Fig. 3a. 1 — Sedimentary. 2 — Murchison Granite. 3 — Mount Read Volcanics. 4 — Powerful Mine. 5 — Heemskirk Granite. 6 — Zeehan. 7 — Dundas. 8 — Mt. Bischoff. 9 — Storys Creek. 10 — Rosebery, 12-level, shales. 11 — Rosebery, 12-level, and Hercules. 12 — Rosebery, 14-level. 13 — Royal Tharsis. 14 — Tasman and Crown Lyell. 15 — West Lyell quartz veins. 16 — West Lyell

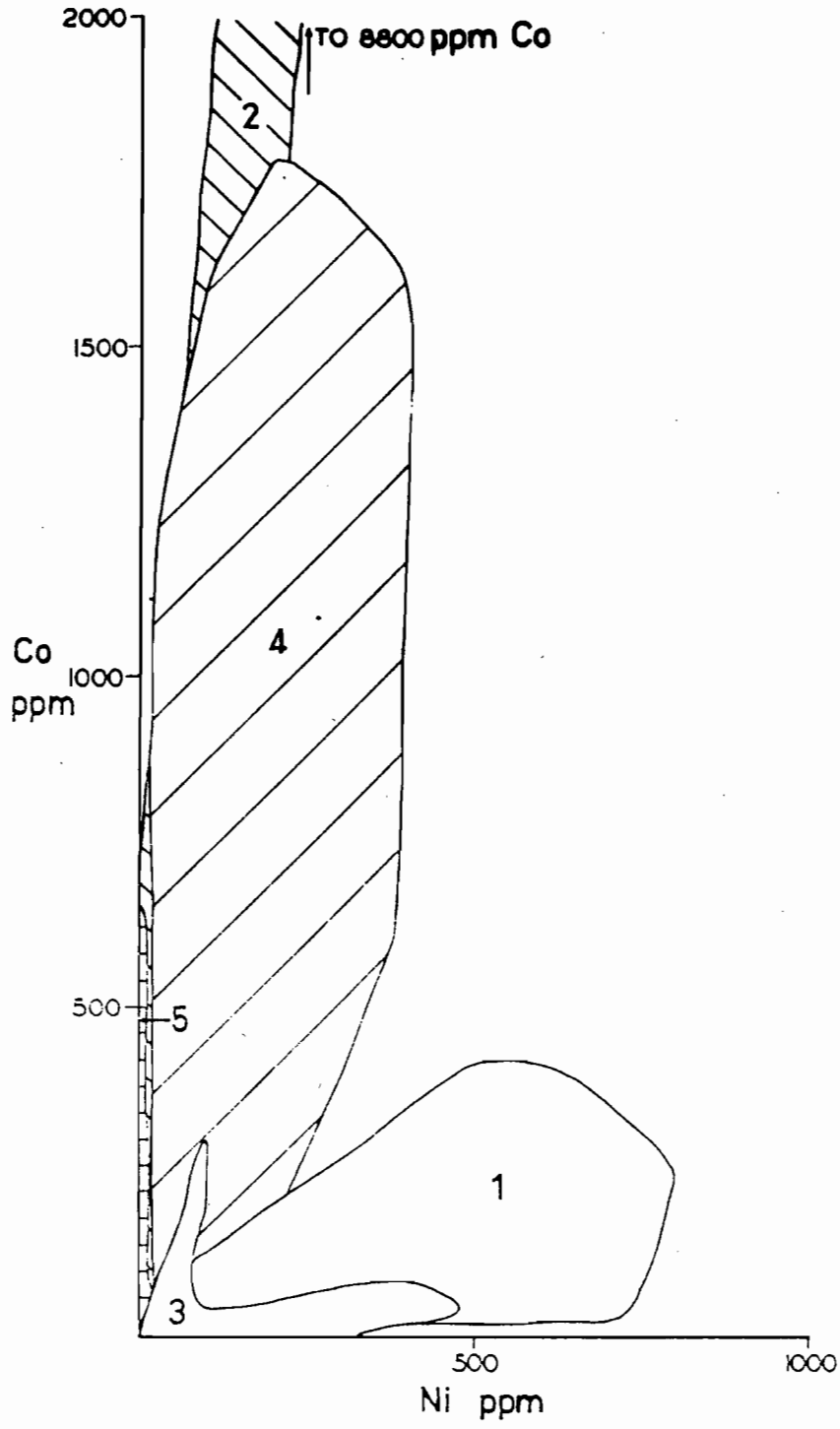

Fig. 2

DISTRIBUTION OF Co AND Ni IN TASMANIAN PYRITES

FIELD 1 SEDIMENTARY — DIAGENETIC
2 CAMBRIAN IGNEOUS ROCKS
3 DEVONIAN GRANITES AND ORES
4 MT LYELL ORES
5 ROSEBERY-HERCULES ORES

(i) sedimentary–diagenetic pyrites (high Ni; Co:Ni < 1),
(ii) Mt Read Volcanics & associated intrusives (very high Co; Co:Ni >> 1),
(iii) Devonian related granites, cassiterite–sulphide deposits and Pb–Zn–Ag deposits (low Co & Ni, i.e. <100 ppm),
(iv) Cu-rich Mt. Lyell deposits (high Co; Co:Ni > 1),
(v) Pb/Zn-rich Rosebery & Hercules (high Co & very low Ni; Co:Ni >> 1).

Additional investigations by Green et al. (1981), using the Co content of pyrite separates, defined hydrothermal vents at Rosebery, and Walshe and Solomon (1981) showed that the Co content of pyrite separates from Mt Lyell correlate well with Cu grade.

These studies were carried out using wet chemical analyses of pyrite flotation separates. Analyses were not selective of any trace element variation in pyrite grains. As a result, many samples included multiple generations of geochemically distinct pyrite. These studies demonstrate that pyrite trace element concentrations provide useful information about pyrite compositions but they fail to adequately discriminate or differentiate Cambrian from Devonian mineralisation (see later discussion). Analysis of pyrite separates also suffer from several limitations (Huston et al., 1996):

(a) the relative large quantity of sample required for analysis,
(b) difficulty in obtaining pure separates, and
(c) difficulty in separating grains of differing habit.

Electron microprobe and pixeprobe studies of trace elements in pyrite have been undertaken on a number of the Cambrian VHMS deposits in western Tasmania, and the results have been made available for this investigation. Raymond (1992) and McArthur (pers. comm.) undertook electron microprobe studies of the Prince Lyell and Hellyer deposits, respectively. More recently, Huston et al. (1996) analysed the trace elements abundances of Rosebery pyrite (North-end of the mine) as part of a larger pixeprobe investigation of eastern Australian VHMS deposits. These authors recognised that pyrite trace elements could be divided into three groups according to the likely occurrence of the elements:

(i) elements mainly as inclusions (Cu, Zn, Pb, Ba, Bi, Ag, Sb),
(ii) elements as non-stoichiometric substitutions in the lattice (As, Tl, Au, Mo), and
(iii) elements as stoichiometric substitutions for Fe (Co, Ni) or S (Se, Te).

Furthermore, it was suggested that hydrothermal and metamorphic recrystallisation cleans pyrite of Group 1 and Group 2 elements, but does not appear to effect the concentration of Group 3 elements. They noted that rapidly precipitated colloform pyrite grains had the highest levels of As and Au. Similar observation were noted by McArthur (pers. comm.) for As, Pb and Zn in colloform pyrites at Hellyer.

Electron microprobe studies are limited to relatively high detection limits (20–500 ppm) but this is somewhat compensated by the low cost of analysis and the accessibility of the instrument at the CSL, University of Tasmania. Ion microprobe and proton microprobe analyses, on the other hand, have detection limits of <0.1 ppm and 5–20 ppm respectively, but such scientific instruments are not readily accessible and are expensive to use.

In this geochemical investigation of the trace element contents of pyrite the major aims are:

(i) to establish a low cost, but effective means to discriminate geochemically between Cambrian and Devonian faults,
(ii) to establish whether electron microprobe techniques have sufficiently low detection limits to discriminate geochemical differences between Cambrian and Devonian pyrite sources,
(iii) to identify which trace elements are most diagnostic of Cambrian and Devonian pyrites,
(iv) to confirm if the Co:Ni ratio patterns established by Loftus-Hills & Solomon (1967) and Groves (1968) can be reproduced using the electron microprobe, and
(v) to develop a new pyrite discriminator (PD) to differentiate Cambrian and Devonian mineralisation, based on electron microprobe multi-trace element analyses.

ANALYTICAL TECHNIQUES

Trace element analyses of pyrite were performed on a Cameca SX-50 electron microprobe at the Central Science Laboratories of the University of Tasmania under the supervision of Mr W. Jablonski. Analyses were performed on 7μm spot sizes but detection limits were far greater than for bulk pyrite studies using wet chemical methods and for pixe microprobe analyses. Operating conditions using a voltage of 20 kv and a current of 250 namps with count times of 70 minutes per analysis reduced detection limits for the majority of the trace elements to <30 ppm (Table 1; Mn — 20 ppm, Co — 21 ppm, Ni — 20 ppm, Cu — 24 ppm, Zn — 30 ppm, Se — 48 ppm, Ag — 24 ppm, Cd — 27 ppm, Sb — 25 ppm, Hg — 111 ppm, Au — 88 ppm, Pb — 150 ppm, As — 702 ppm). Poor detection limits for lead and arsenic resulted from large overlap problems with the sulphur Kα peak on the lead Mα peak at trace lead levels, and overlap of the lead Lα peak on the arsenic Kα peak, respectively.

Prior to analysis 30–40 μm thick polished thin sections were prepared, examined microscopically and pyrite grains free of surficial inclusions identified. The depth of penetration of the electron beam is thought to be less than 5 μm during the analysis but this depth of penetration of the electron beam makes the incorporation of inclusions in some analyses highly likely.

RESULTS

Samples of pyrite multi-trace element analyses from a variety of western Tasmanian deposits have been collected from various sources (Appendix 1; Hellyer, n = 542, McArthur, pers. comm.; Prince Lyell, n = 421, Raymond, 1992; Rosebery, n = 59, Huston, 1996), together with new analyses undertaken in this study (Renison, n = 13).

A comparison of Co:Ni ratios for these deposits (Fig. 3) immediately shows that a far greater range of Co and Ni exists for these deposits than that initially suggested by Loftus-Hills & Solomon (1967) and Groves (1968). This brings into question their interpretation of Co:Ni ratios for Cambrian and Devonian mineralisation in western Tasmania based on the small number of analyses used in their studies.

Given this simple observation, and the wider range of trace elements analysed in pyrite from each of the deposits previously mentioned, a new pyrite discriminator was attempted in this study.

The suite of trace elements analysed and common to the pyrite data sets for Hellyer, Prince Lyell, Rosebery and Renison include: Co, Ni, Cu, Zn, As, Se, Ag, Au and Pb. Of this suite of elements Au was not analysed for the Prince Lyell data set of Raymond (1992). Empirical observations of trace element ranges and means for each pyrite data set (Appendix 1) are presented in Table 1. Stacked histograms for each of the pyrite trace elements are presented in figure 4 (a–i). A summary of comparative findings are presented below.

(NOTE: at the time of writing this report the Devonian database was very limited and the following findings are therefore preliminary)

Cobalt (ppm)
Prince Lyell ≥ Hellyer ≈ Rosebery ≥ Renison

Nickel (ppm)
Prince Lyell ≥ Hellyer > Rosebery ≥ Renison

Selenium (ppm)
Prince Lyell ≥ Hellyer > Rosebery > Renison

Copper (ppm)
Rosebery ≥ Hellyer ≈ Prince Lyell ≥ Renison

Zinc (ppm)
Hellyer ≥ Rosebery ≥ Prince Lyell ≥ Renison

Lead (ppm)
Hellyer ≥ Rosebery ≥ Prince Lyell ≥ Renison

Arsenic (ppm)
Hellyer ≥ Rosebery ≥ Prince Lyell > Renison

Silver (ppm)
Hellyer ≥ Prince Lyell ≥ Rosebery ≥ Renison

Gold (ppm)
Hellyer ≥ Renison ≥ Rosebery (NB no Prince Lyell data)

TABLE 1 SUMMARY OF MULTI ELEMENT ANALYSIS OF PYRITE

ELEMENT		PRINCE LYELL (n = 421)	HELLYER (n = 542)	ROSEBERY (n = 59)	RENISON (n = 13)
Cobalt	Range	BDL - 29880	BDL - 1319	BDL - 980	BDL - 275
	Mean	2954	53	48	57
	PADL	77% (DL = 100 ppm)	31% (DL = 57 ppm)	13% (DL = 50 ppm)	46% (DL = 21 ppm)
Nickel	Range	BDL - 4710	BDL - 3492	BDL - 640	BDL - 278
	Mean	257	104	27	52
	PADL	88% (DL = 100 ppm)	45% (DL = 54 ppm)	12% (DL = 50 ppm)	77% (DL = 20 ppm)
Copper	Range	BDL - 6960	BDL - 13446	BDL - 19700	BDL - 1091
	Mean	193	72	837	175
	PADL	74% (DL = 100 ppm)	6% (DL = 100 ppm)	95% (DL = 10 ppm)	69% (DL = 24 ppm)
Zinc	Range	BDL - 50710	BDL - 14692	BDL - 8090	BDL - 349
	Mean	239	1258	584	166
	PADL	62% (DL = 350 ppm)	71% (DL = 100 ppm)	75% (DL = 10 ppm)	100% (DL = 30 ppm)
Lead	Range	BDL - 2300	BDL - 45880	BDL - 20300	BDL - 757
	Mean	843	3962	1453	152
	PADL	70% (DL = 800 ppm)	89% (DL = 400 ppm)	87% (DL = 30 ppm)	46% (DL = 150 ppm)
Arsenic	Range	BDL - 10910	BDL - 64526	BDL - 11600	BDL
	Mean	751	6843	1593	BDL
	PADL	92% (DL = 300 ppm)	78% (DL = 31 ppm)	95% (DL = 25 ppm)	0% (DL = 702 ppm)
Selenium	Range	BDL - 1070	BDL - 1093	BDL - 33	BDL
	Mean	142	78	2	BDL
	PADL	62% (DL = 350 ppm)	37% (DL = 50 ppm)	13% (DL = 5 ppm)	0% (DL = 48 ppm)
Silver	Range	BDL - 330	BDL - 1530	BDL - 375	BDL - 59
	Mean	46	173	25	24
	PADL	49% (DL = 150 ppm)	54% (DL = 75 ppm)	58% (DL = 5 ppm)	54% (DL = 24 ppm)
Gold	Range	NA	BDL - 2327	BDL - 50	BDL - 268
	Mean	NA	21	2	67
	PADL	NA	3% (DL = 100 ppm)	7% (DL = 30 ppm)	38% (DL = 88 ppm)

BDL - below detection limits
NA - not analysed
PADL - percentage of samples above the detection limit

Fig. 3

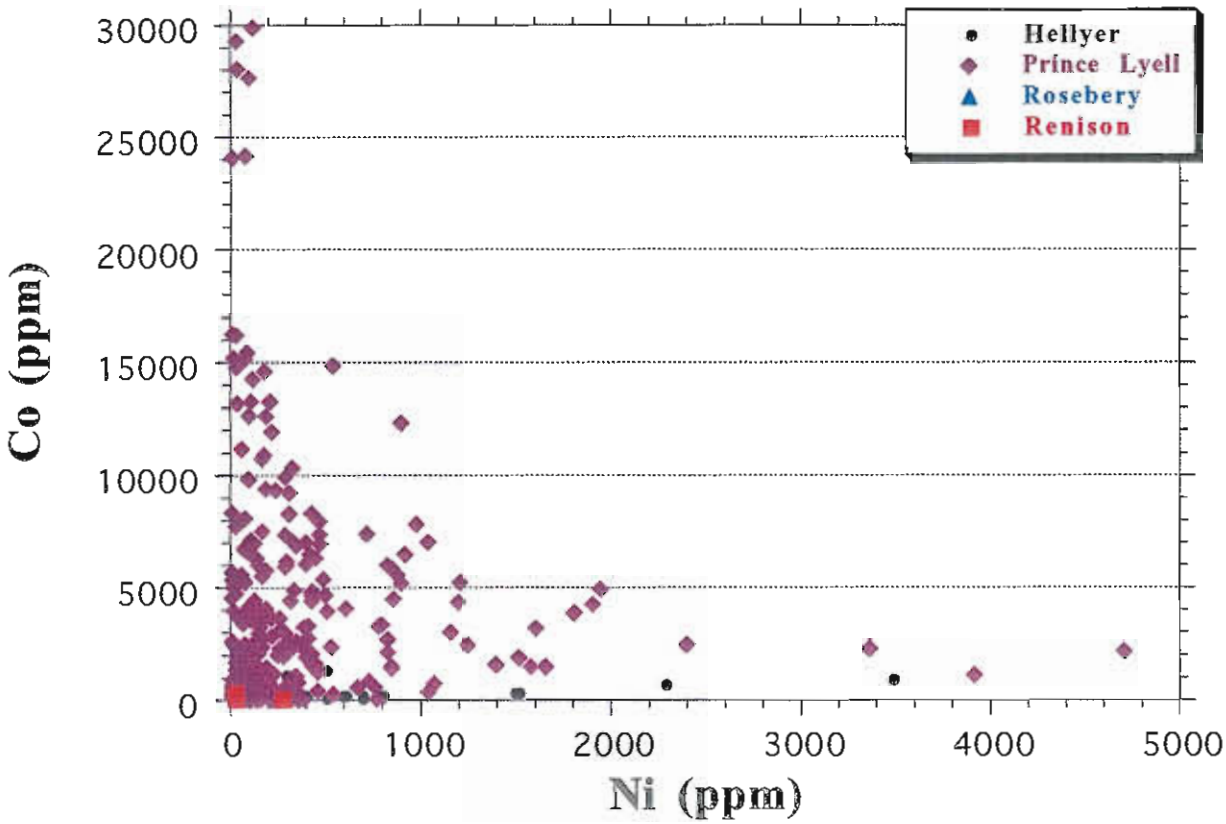
Hellyer
Prince Lyell
Rosebery
Renison
Co (ppm)
30000
25000
20000
15000
10000
5000
0
0
1000
2000
3000
4000
5000
Ni (ppm)

DISCUSSION

Cobalt

Co has the greatest concentrations in Prince Lyell pyrites (Table 1; Fig. 4a; BDL — 29880 ppm, mean = 2954 ppm, PADL = 77%). In comparison the remaining deposits have cobaltiferous-poor pyrite decreasing from Hellyer, to Rosebery and finally Renison. The percentage of pyrite analyses above the detection limit for cobaltiferous-poor deposits was less than fifty percent, indicating that very low detection limits are required to successfully analyse for cobalt in western Tasmanian ore deposits. Note: the mean Co ≈ 0.3% in Prince Lyell pyrite is an economic cut off grade for this element!

In summary, Co ranges from highest values in Cambrian Cu-rich VHMS deposits, to intermediate values in Pb/Zn-rich VHMS deposits, with the lowest Co concentrations occurring in Devonian Sn-rich systems. As Co occurs in pyrite as a stoichiometric substitution for Fe the Co concentrations are expected to remain constant regardless of hydrothermal or deformation processes post-mineralisation.

Nickel

Ni, like Co, has the greatest concentrations in Prince Lyell pyrite (Table 1; Fig. 4b; BDL — 4710 ppm, mean = 257 ppm, PADL = 88%). Similarly, the range of Ni analyses decreases from Hellyer, to Rosebery and finally Renison. The percentage of pyrite analyses with Ni values below the detection limit for the Pb/Zn-rich VHMS deposits was greater than fifty percent. Once again, this indicates that the detection limits used to analyse the Pb/Zn-rich VHMS deposits requires improvement. The new pyrite label on the electron microprobe with longer count times and increased nano-amps may be sufficient to overcome these difficulties.

In summary, Ni ranges from highest values in Cambrian Cu-rich VHMS deposits, to intermediate values in Pb/Zn-rich VHMS deposits, with the lowest Ni concentrations occurring in Devonian Sn-rich systems. The low mean count for Ni in Rosebery pyrite is most probably a reflection of the detection limits. As Ni occurs in pyrite as a stoichiometric substitution for Fe the Ni concentrations are expected to remain constant regardless of hydrothermal or deformation processes post-mineralisation.

Copper

Strangely enough, the copper-rich end of the North Rosebery orebody has pyrite containing significantly more copper than Prince Lyell (Table 1; Fig. 4c; BDL — 19700 ppm, mean = 837 ppm, PADL = 95%). Hellyer has an expansive range in Cu values but the percentage of samples above the detection limit was only 6%. The increased detection limits on the microprobe may be sufficient to overcome this problem. The range and mean of Cu values in Renison pyrites is significantly lower than for the Cambrian systems with the exception of the mean for Hellyer pyrites.

In summary, Cu ranges have highest values in Cambrian Pb/Zn-rich VHMS deposits, intermediate values in Cu-rich VHMS deposits, and lowest Cu concentrations in Devonian Sn-rich systems. The low mean count for Cu in Hellyer pyrite is most probably a reflection of the detection limits. As Cu typically occurs as inclusions in pyrite, hydrothermal or deformation processes post-mineralisation may affect Cu concentrations in similar ores types.

Zinc

As expected the Pb/Zn ore bodies from Hellyer and Rosebery had pyrites containing the highest zinc concentrations (Table 1; Fig. 4d; Hellyer BDL — 14692 ppm, mean = 1258 ppm, PADL = 71%; Rosebery BDL ∇ 8090 ppm, mean = 584 ppm, PADL = 75%) although a single pyrite analysis from Prince Lyell did record 50710 ppm. This was most certainly a surficial inclusion, as the mean for Zn in Prince Lyell pyrite was only 239 ppm (PADL = 62%). Re-crystallisation of the Rosebery pyrites may have removed significant concentrations of micro-sphalerite inclusions from the pyrites resulting in the lower Zn values, relative to Hellyer pyrites. The range and mean of Zn values in Renison pyrites is significantly lower than for the Cambrian systems.

In summary, Zn ranges have highest values in Cambrian Pb/Zn-rich VHMS deposits, intermediate values in Cu-rich VHMS deposits, and lowest Zn concentrations in Devonian Sn-rich systems. As Zn typically occurs as inclusions in pyrite, hydrothermal or deformation processes post-mineralisation may affect Zn concentrations in similar ores types.

Lead

As expected, the Cambrian Pb/Zn-rich ore bodies from Hellyer and Rosebery had pyrites containing the highest Pb concentrations (Table 1; Fig. 4e; Hellyer BDL ∇ 45880 ppm, mean = 3962 ppm, PADL = 89%; Rosebery BDL — 20300 ppm, mean = 1453 ppm, PADL = 87%). Recrystallisation of Rosebery pyrites may have removed significant concentrations of micro-galena inclusions from the pyrites resulting in lower Pb values, relative to Hellyer pyrites. The range and mean of Pb values in Renison pyrite is at least an order of magnitude lower than for the Cambrian systems.

In summary, Pb ranges have highest values in Cambrian Pb/Zn-rich VHMS deposits, intermediate values in Cu-rich VHMS deposits, and lowest Pb concentrations in Devonian Sn-rich systems. As Pb typically occurs as inclusions in pyrite, hydrothermal or deformation processes post-mineralisation may affect Pb concentrations in similar ores types.

Arsenic

The highest range of arsenic levels analysed in pyrites are from the Cambrian Pb/Zn-rich ore bodies at Hellyer and Rosebery (Table 1; Fig. 4f; Hellyer BDL ∇ 64526 ppm, mean = 6843 ppm, PADL = 78%; Rosebery BDL — 11600 ppm, mean = 1593 ppm, PADL = 95%). Recrystallisation of Rosebery pyrites may have removed significant concentrations of arsenic from non-stoichiometric lattice location in pyrites, resulting in lower As values, relative to Hellyer pyrites. Arsenic was not detected in Renison pyrite but is most probably a reflection of the very high detection limits for As (DL = 702 ppm).

In summary, As ranges have highest values in Cambrian Pb/Zn-rich VHMS deposits, intermediate values in Cu-rich VHMS deposits, and lowest As concentrations in Devonian Sn-rich systems. Hydrothermal or post mineralisation deformation of arseniferous-pyrite may decrease As levels because this element occurs within non-stoichiometric lattice locations.

Selenium

Se like Ni and Co, has the greatest concentrations in Prince Lyell pyrite (Table 1; Fig. 4g; BDL — 1070 ppm, mean = 142 ppm, PADL = 62%). Similarly, the range of Se analyses decreases from Hellyer, to Rosebery and finally Renison. The percentage of pyrite analyses with Se values below the detection limit was greater than sixty percent for the Pb/Zn-rich VHMS deposits, and no selenium was detected in Renison pyrite. Once again, this indicates that the detection limits used to analyse for Se on the electron microprobe requires improvement.

In summary, Se in pyrite ranges from highest concentrations in Cambrian Cu-rich VHMS deposits, to intermediate values in Pb/Zn-rich VHMS deposits, with the lowest Se concentrations (i.e. below detection limit) occurring in Devonian Sn-rich systems. The low mean count for Se in Rosebery pyrite is apparently real, because it does not reflect the detection limits of the PIXIE probe used for the analyses (DL = 5 ppm), nor does it reflect hydrothermal or post-mineralisation deformation as Se occurs in pyrite as a stoichiometric substitution for S.

Silver

The highest range of silver levels analysed in pyrites are from the Cambrian Pb/Zn-rich ore bodies at Hellyer and Rosebery (Table 1; Fig. 4h; Hellyer BDL — 1530 ppm, mean = 173 ppm, PADL = 54%; Rosebery BDL ∇ 375 ppm, mean = 25 ppm, PADL = 58%). Recrystallisation of Rosebery pyrites may have removed significant concentrations of silver from non-stoichiometric lattice location in pyrites, resulting in lower Ag values, relative to Hellyer pyrites. The range of Ag levels in Prince Lyell pyrites are just below Rosebery values but the mean Ag values for Prince Lyell pyrite are almost twice that of Rosebery. At Renison the range of silver levels in main ore stage pyrite are considerably lower than the Cambrian deposits.

In summary, Ag ranges have highest values in Cambrian Pb/Zn-rich VHMS deposits, intermediate values in Cu-rich VHMS deposits, and lowest Ag concentrations in Devonian Sn-rich systems. Hydrothermal or post mineralisation deformation of argentiferous-pyrite may decrease Ag levels because this element occurs within non-stoichiometric lattice locations.

Gold

No conclusive comments can be made for gold in pyrite because detection limits are poor and data from Prince Lyell is absent. However, the Cambrian

Fig. 4A

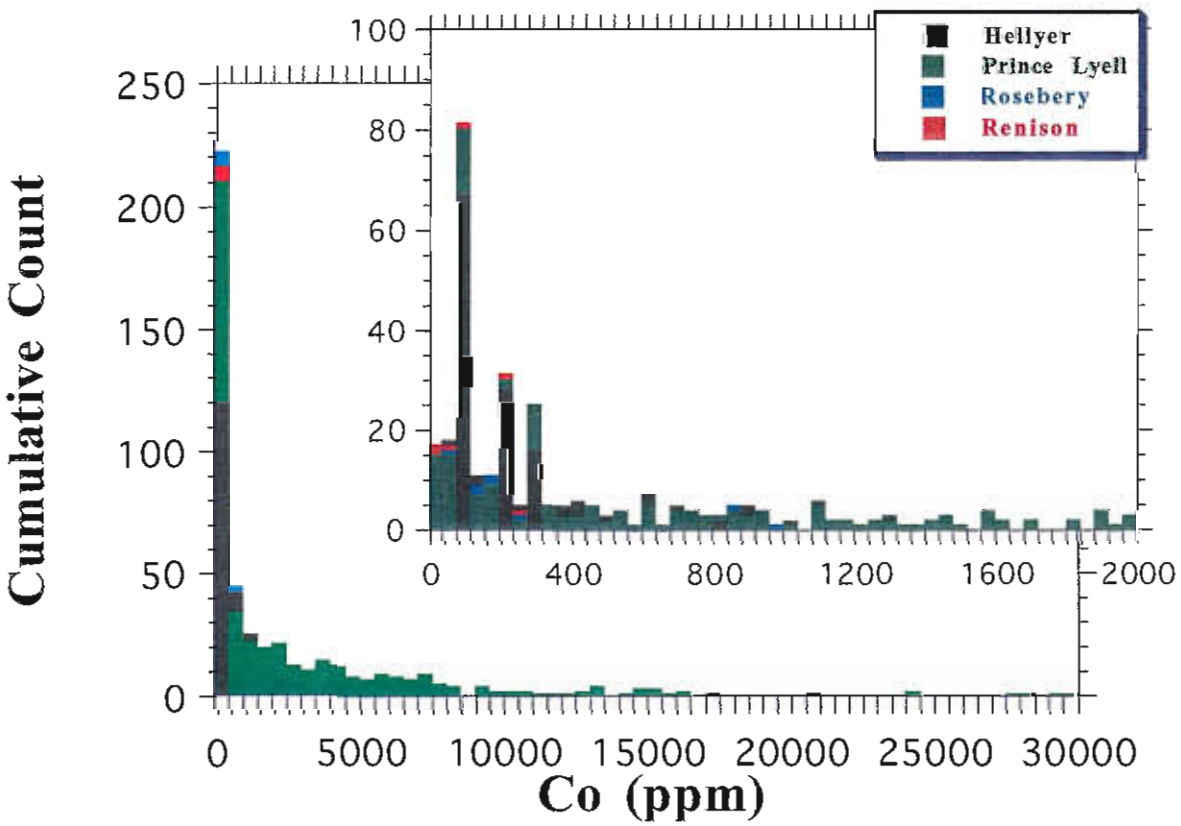
Hellyer
Prince Lyell
Rosebery
Renison
Cumulative Count
Co (ppm)
0
50
100
150
200
250
0
5000
10000
15000
20000
25000
30000
0
20
40
60
80
100
0
400
800
1200
1600
2000

Fig. 4B

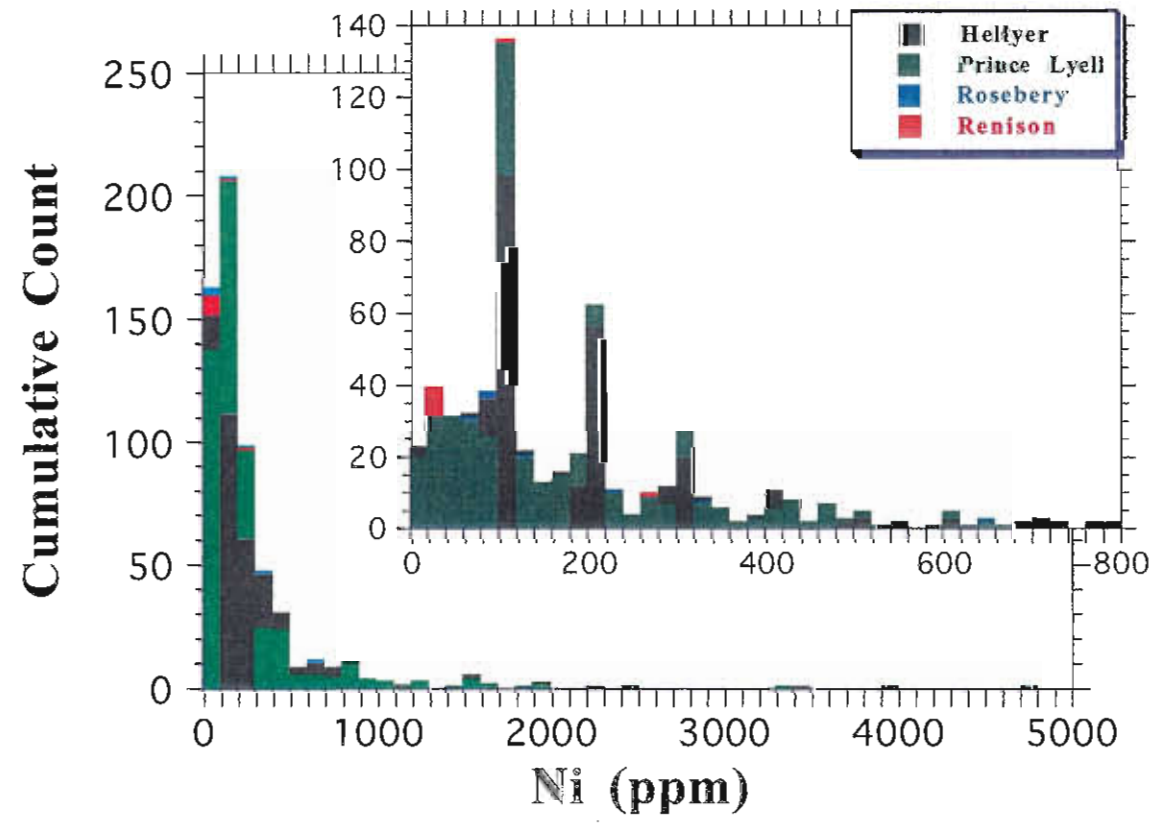
Hellyer
Prince Lyell
Rosebery
Renison
Cumulative Count
Ni (ppm)
0
50
100
150
200
250
0
1000
2000
3000
4000
5000
0
20
40
60
80
100
120
140
0
200
400
600
800

Fig. 4C

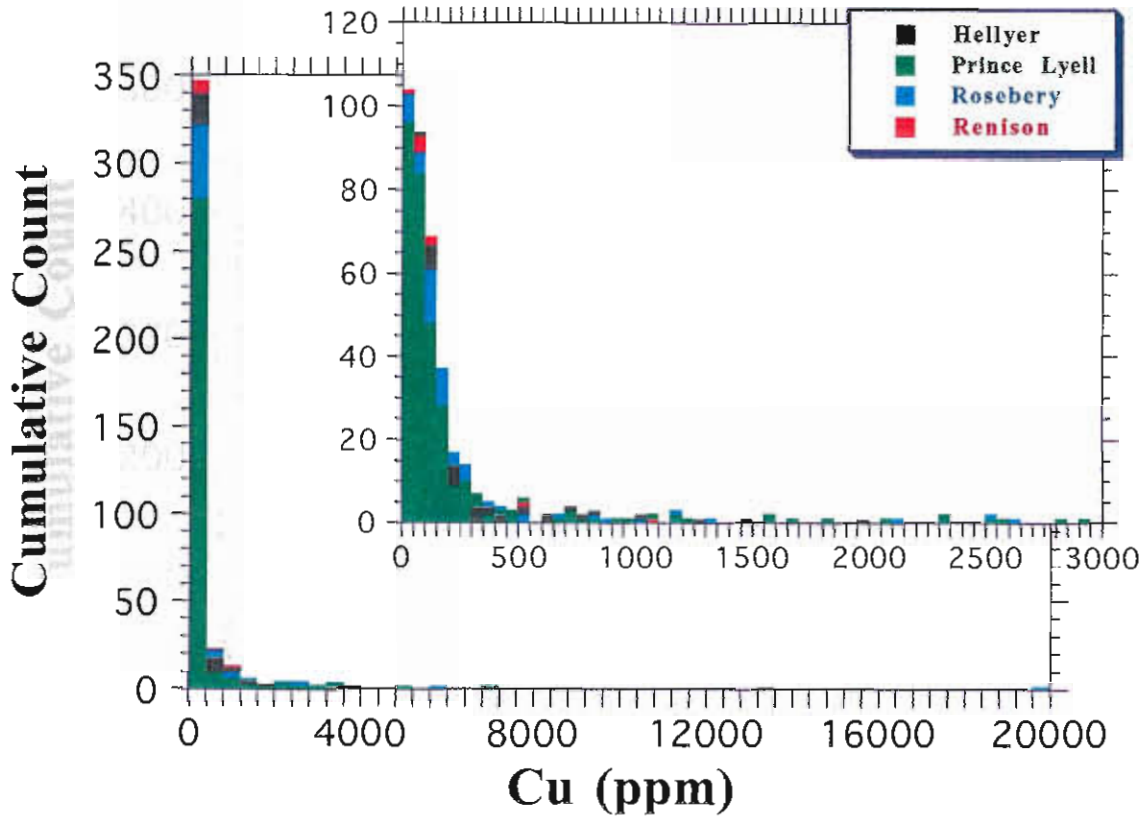
Hellyer
Prince Lyell
Rosebery
Renison
Cumulative Count
Cu (ppm)
0
50
100
150
200
250
300
350
0
4000
8000
12000
16000
20000
0
20
40
60
80
100
120
0
500
1000
1500
2000
2500
3000

Fig. 4D

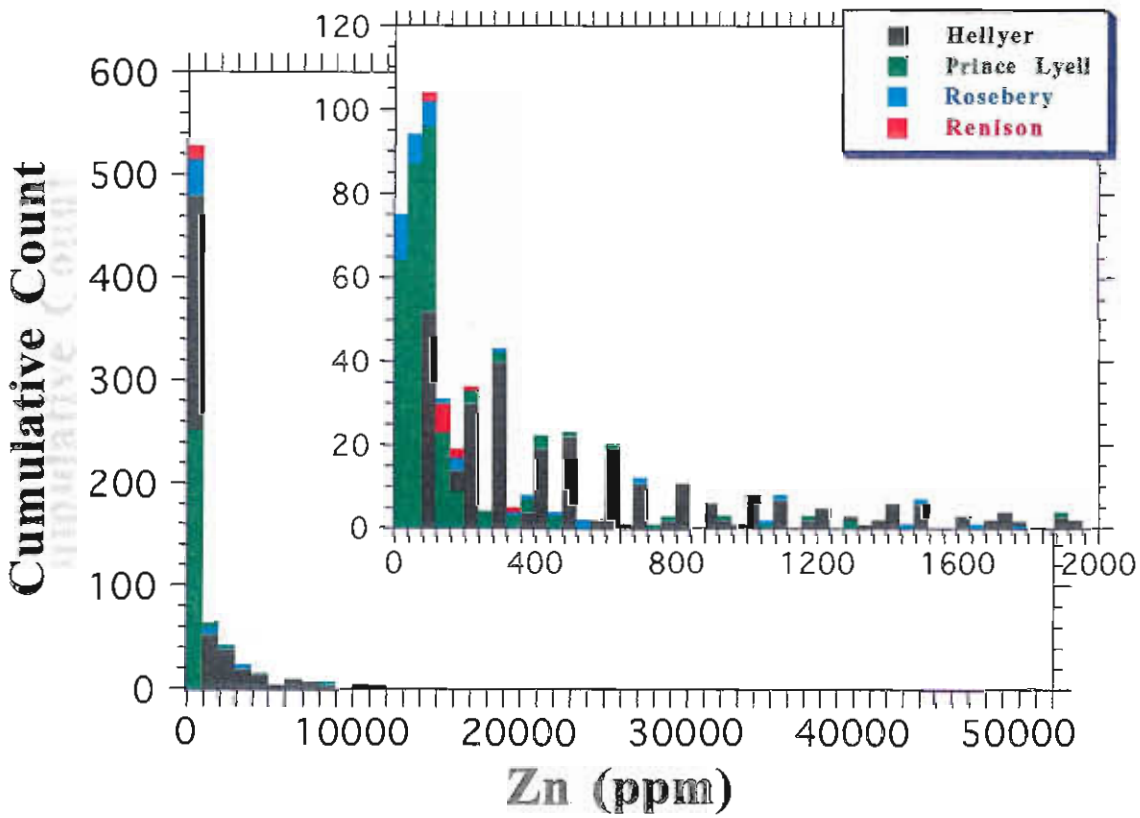
Hellyer
Prince Lyell
Rosebery
Renison
Cumulative Count
Zn (ppm)
0
100
200
300
400
500
600
0
10000
20000
30000
40000
50000
0
20
40
60
80
100
120
0
400
800
1200
1600
2000

Fig. 4E

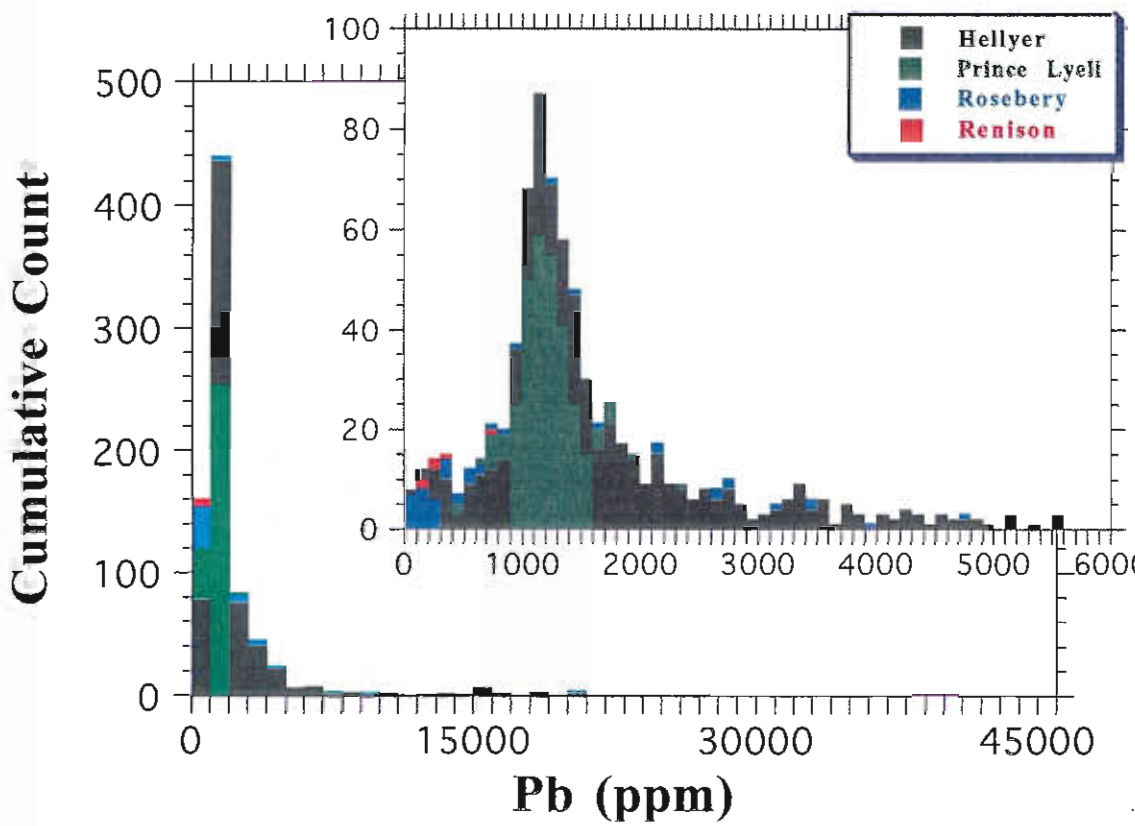
Hellyer
Prince Lyell
Rosebery
Renison
Cumulative Count
Pb (ppm)
0
100
200
300
400
500
15000
30000
45000
20
40
60
80
1000
2000
3000
4000
5000
6000

Fig. 4F

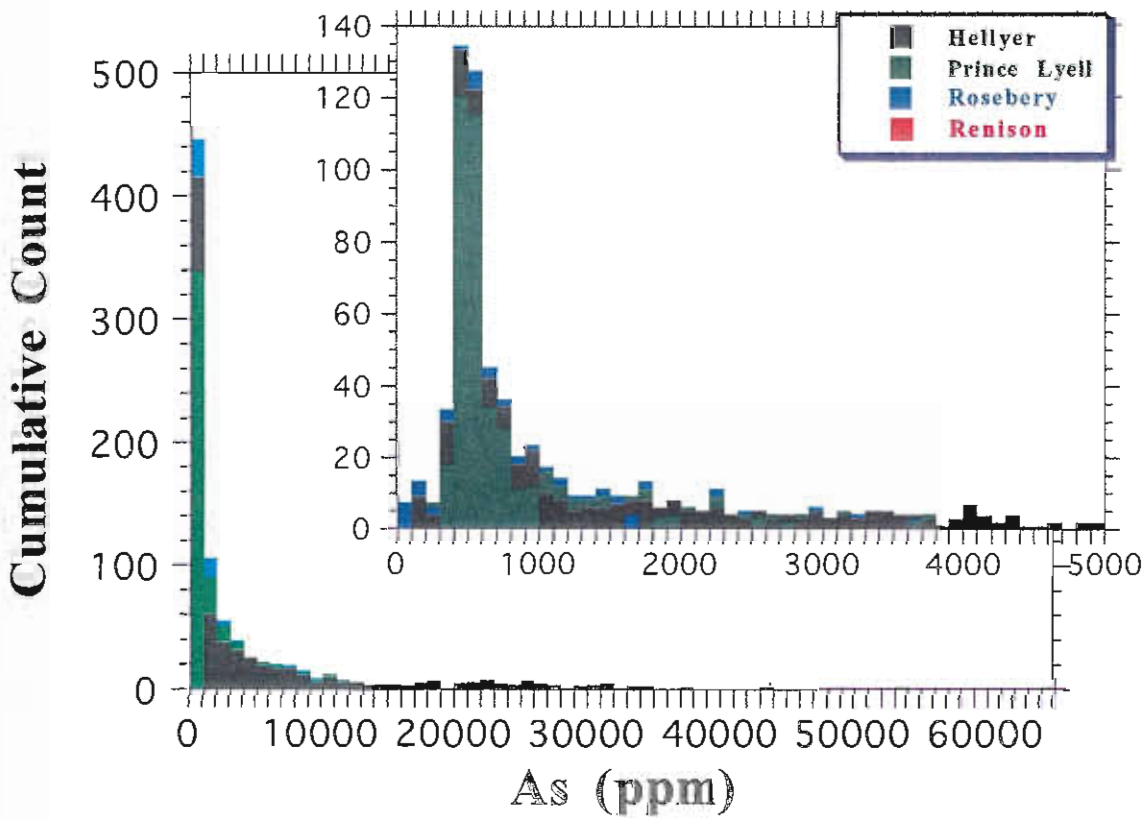
Hellyer
Prince Lyell
Rosebery
Renison
Cumulative Count
As (ppm)
0
100
200
300
400
500
20
40
60
80
100
120
140
1000
2000
3000
4000
5000
10000
20000
30000
40000
50000
60000

Fig. 4G

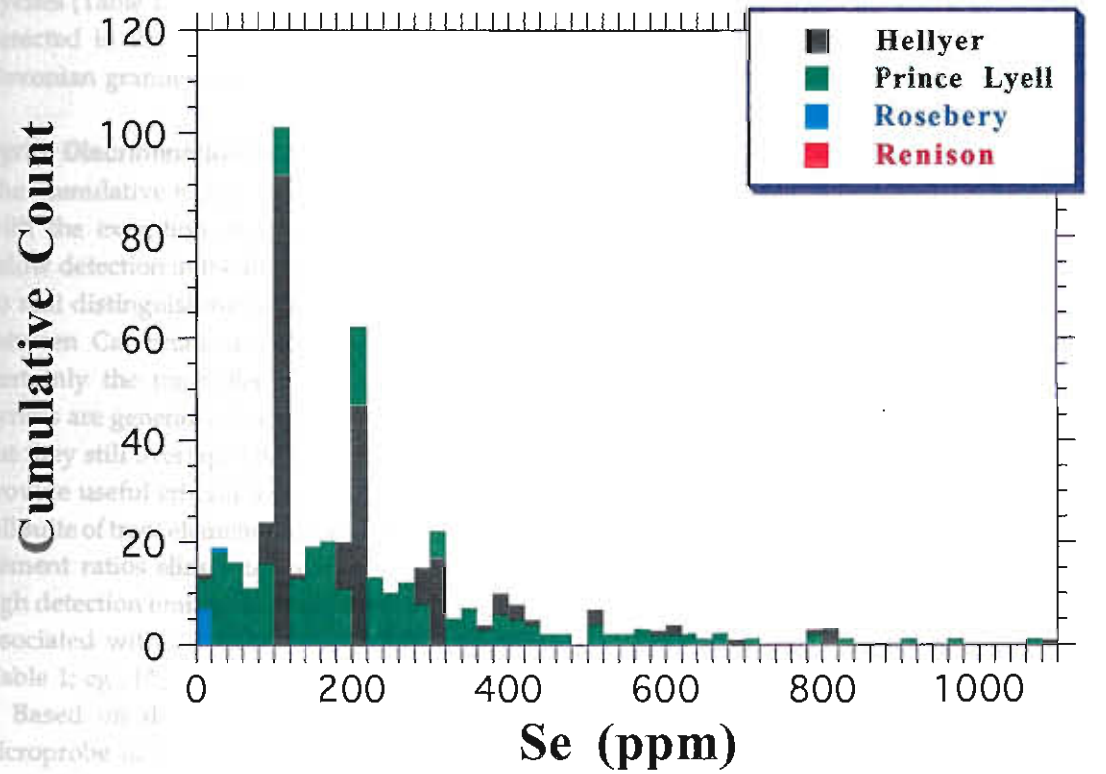
Hellyer
Prince Lyell
Rosebery
Renison
Cumulative Count
0
20
40
60
80
100
120
0
200
400
600
800
1000
Se (ppm)

Fig. 4H

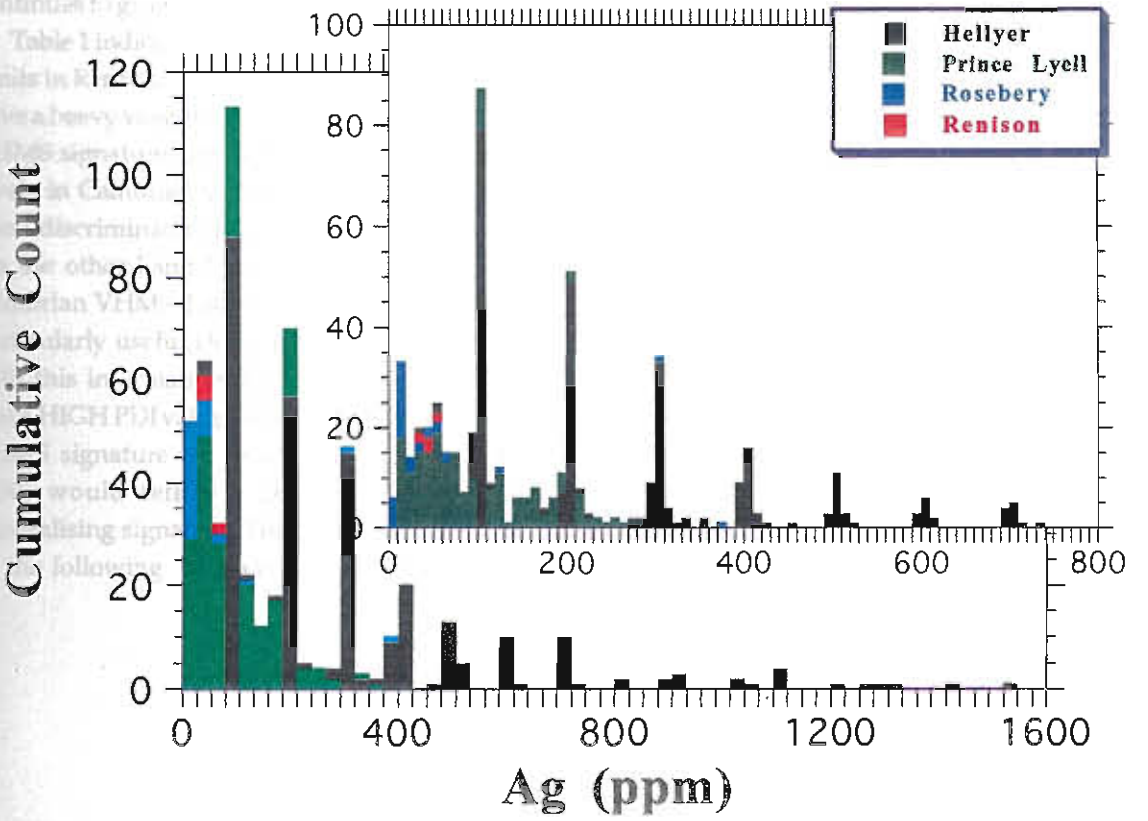
Hellyer
Prince Lyell
Rosebery
Renison
Cumulative Count
0
20
40
60
80
100
120
0
400
800
1200
1600
Ag (ppm)
0
20
40
60
80
100
0
200
400
600
800

Pb/Zn-rich VHMS deposits do contain low levels of Au in non-stoichiometric lattice positions, with the lowest levels occurring in recrystallised Rosebery pyrites (Table 1; Fig 4i). Surprisingly, there was gold detected in Renison pyrite. This is unusual as the Devonian granites have extremely low Au levels.

Pyrite Discrimination Index

The cumulative histograms illustrate the point that, with the exception of selenium and arsenic being below detection in the few Renison pyrites analysed, no real distinguishing features separate the overlap between Cambrian and Devonian pyrite samples. Certainly the trace element levels in the Renison pyrites are generally lower than VHMS pyrite levels but they still overlap. Multi-element ratio plots may provide useful criteria for pyrite classification if the full suite of trace elements are combined. Use of multi-element ratios eliminate some of the difficulties of high detection limits on various elements, in this case associated with the use of the electron microprobe (Table 1; eg., Pb, As, Se, Au).

Based on the detection limits of the electron microprobe and the concentrations of the various elements in pyrite from the Cambrian and Devonian data sets, a pyrite discrimination index (PDI) has been developed. The PDI may need refining as the database of multi-element analyses on pyrite continues to grow and more deposits are investigated.

Table 1 indicates that As and Se are below detection limits in Renison pyrite and so these elements should have a heavy weighting in any PDI toward a Cambrian VHMS signature. Similarly, the high Co, Zn, and Pb levels in Cambrian VHMS pyrites would also made good discriminators in a Cambrian pyrite signature. On the other hand Ni, Cu, Ag and Au make poor Cambrian VHMS discriminators and equally are not particularly useful Devonian discriminators. Armed with this information the PDI was developed such that a HIGH PDI value (>50) would reflect a Cambrian VHMS signature for pyrite and a LOW PDI value (<50) would reflect a Devonian granite related mineralising signature. The PDI was therefore based on the following equation:

$$PDI = \frac{100x(CambrianEnrichedElements)}{(CambrianEnrichedElements) + (DevonianEnrichedElements)}$$

$$PDI = \frac{100x(Co + 0.2Zn + 2As + 20Se + 0.1Pb)}{(Co + 0.2Zn + 2As + 20Se + 0.1Pb) + (Ni + 2Cu + Ag + 4Au)}$$

Figure 5 (a–i) plots the trace elements versus PDI. In each instance it is apparent that greater than 98∠ 99% of all the Cambrian pyrite data (n = 1022) have PDI values above 50 when plotted against each of the trace elements. In fact 90% of all Cambrian pyrite data have PDI values greater than 80. In contrast all the Devonian pyrite data have PDI values less than 50. PDI values for each pyrite analysis are given in Appendix 1. It is apparent from looking at these tables that the lower PDI values for Cambrian pyrites occur when only one or two elements from the complete suite analysed are detected, or when extremely high trace element analyses occur (eg. 30,000 ppm Pb) due to the detection of mineral inclusions within he pyrite. Filtering of the data after probing to remove such anomalous results from the data set (1–2% of the data set) would immediately eliminate these few *"rogue"* PDI values.

CONCLUSIONS

Based on the new Pyrite Discriminator Index (PDI) it is apparent that we now how developed a low cost but effective means to discriminate geochemically between Cambrian and Devonian faults, if hydrothermal pyrite mineralisation is present. This technique overcomes the difficulties associated with previous geochemical techniques which require hydrothermal galena, sphalerite, quartz, or carbonate to be present to undertake isotopic analyses or fluid inclusion studies.

The PDI technique establishes the fact that the electron microprobe does has sufficiently low detection limits to discriminate geochemical differences between Cambrian and Devonian pyrite sources. The suite of elements necessary to discriminate between the different pyrite sources consists of Co, Ni, Cu, Zn, Pb, As, Se, Ag and Au. Care must be taken however to eliminate those pyrite analyses (<1–2%) which do not contain a sufficient number of

the trace elements, or those analyses that have obviously detected mineral inclusions within the pyrite. The PDI is based on the ratio of trace elements most common to Cambrian pyrite mineralisation (i.e., Co, Zn, As, Se, Pb) compared to those elements more nearly associated with Devonian granite related pyrite mineralisation (i.e., Ni, Cu, Ag, Au). The proposed PDI equation is:

$$PDI = \frac{100x(CambrianEnrichedElements)}{(CambrianEnrichedElements)+(DevonianEnrichedElements)}$$

$$PDI = \frac{100x(Co+0.2Zn+2As+20Se+0.1Pb)}{(Co+0.2Zn+2As+20Se+0.1Pb)+(Ni+2Cu+Ag+4Au)}$$

Based on the available pyrite trace element data, a PDI value greater than 50 is indicative of a Cambrian VHMS style of mineralisation, and a PDI value less than 50 is indicative of a Devonian granite related style of mineralisation.

This study has also shown that the Co:Ni ratio patterns established by Loftus-Hills & Solomon (1967) and Groves (1968) for Cambrian and Devonian pyrites can not be reproduced using the electron microprobe technique and therefore their interpretation is brought into question.

REFERENCES

Green, G. R., Solomon, M., and Walshe, J. L., 1981. The formation of the volcanic-hosted massive sulfide ore deposit at Rosebery, Tasmania. *Econ. Geol.* 76: 304∠338.

Groves, D. I., 1968. The cassiterite∠sulphide deposits of western Tasmania. Unpubl. PhD thesis, University of Tasmania: 294 pp.

Huston, D. L., Sie, S. H., Suter, G. F., Cooke, D. R., and Both, R. A., 1996. Trace elements in sulfide minerals from eastern Australian volcanic-hosted massive sulfide deposits. *Econ. Geol.*, in press.

Loftus-Hills, G. and Solomon, M., 1967. Cobalt, nickel and selenium in sulphides as indicators of ore genesis. *Mineralium Deposita* 2: 228∠242.

Raymond, O. L., 1992. Geology and mineralisation of the southern Prince Lyell Deeps, Queenstown, Tasmania. Unpubl. Masters thesis, University of Tasmania: 161 pp.

Walshe, J. L., and Solomon, M. 1981. An investigation into the environment of formation of the volcanic-hosted Mt. Lyell copper deposits using geology, mineralogy, stable isotopes, and a six-component chlorite solid solution model. *Econ. Geol.* 76: 246∠284.

Fig. 4I

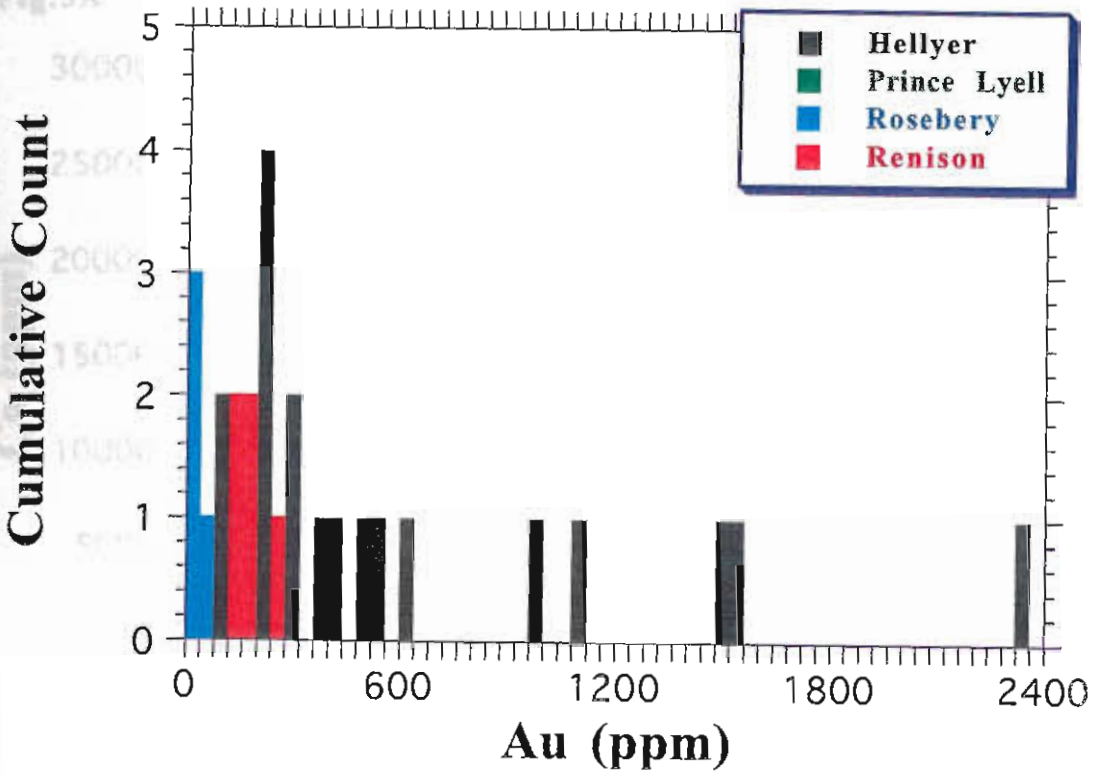
Cumulative Count
0
1
2
3
4
5
0
600
1200
1800
2400
Au (ppm)
Hellyer
Prince Lyell
Rosebery
Renison

Fig.5A

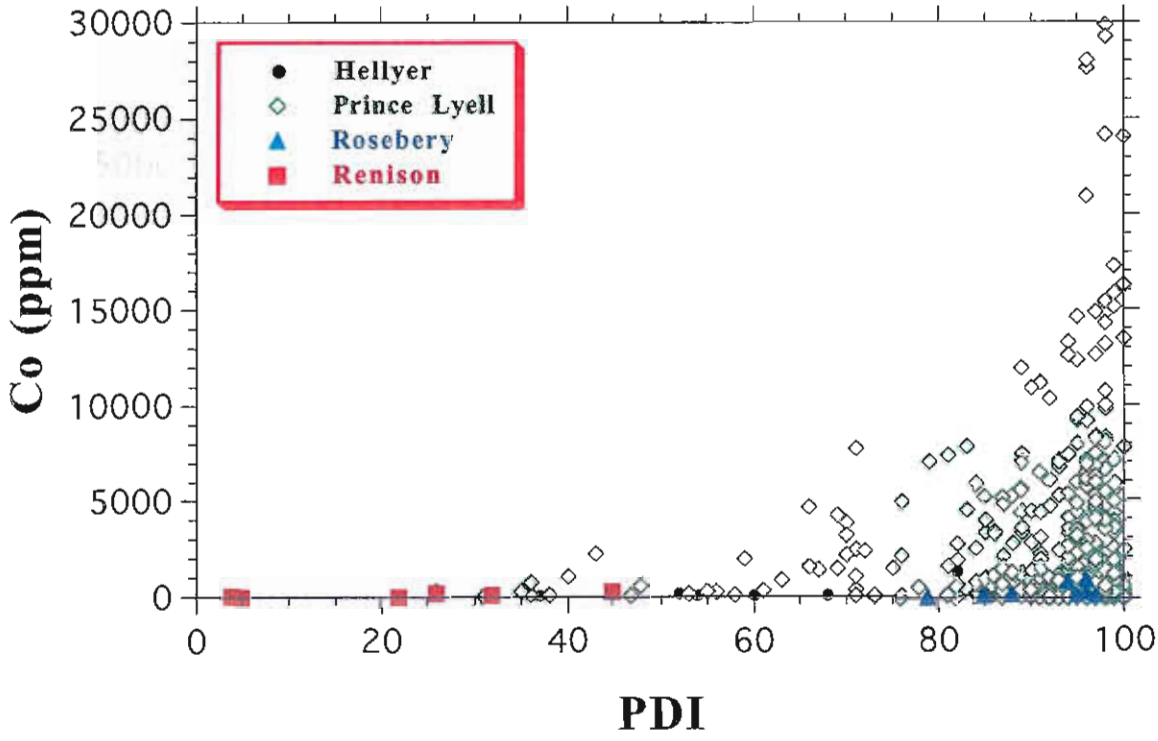
Hellyer
Prince Lyell
Rosebery
Renison
Co (ppm)
30000
25000
20000
15000
10000
5000
0
0
20
40
60
80
100
PDI

Fig.5B

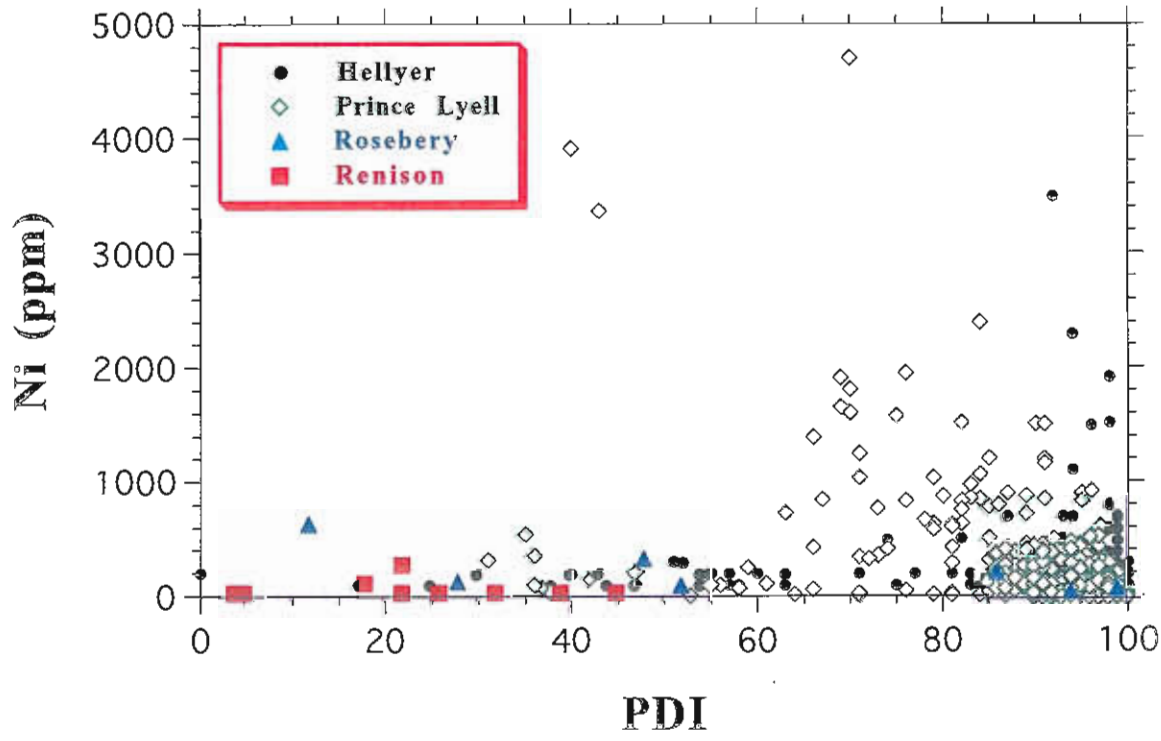
Hellyer
Prince Lyell
Rosebery
Renison
Ni (ppm)
5000
4000
3000
2000
1000
0
0
20
40
60
80
100
PDI

Fig.5C

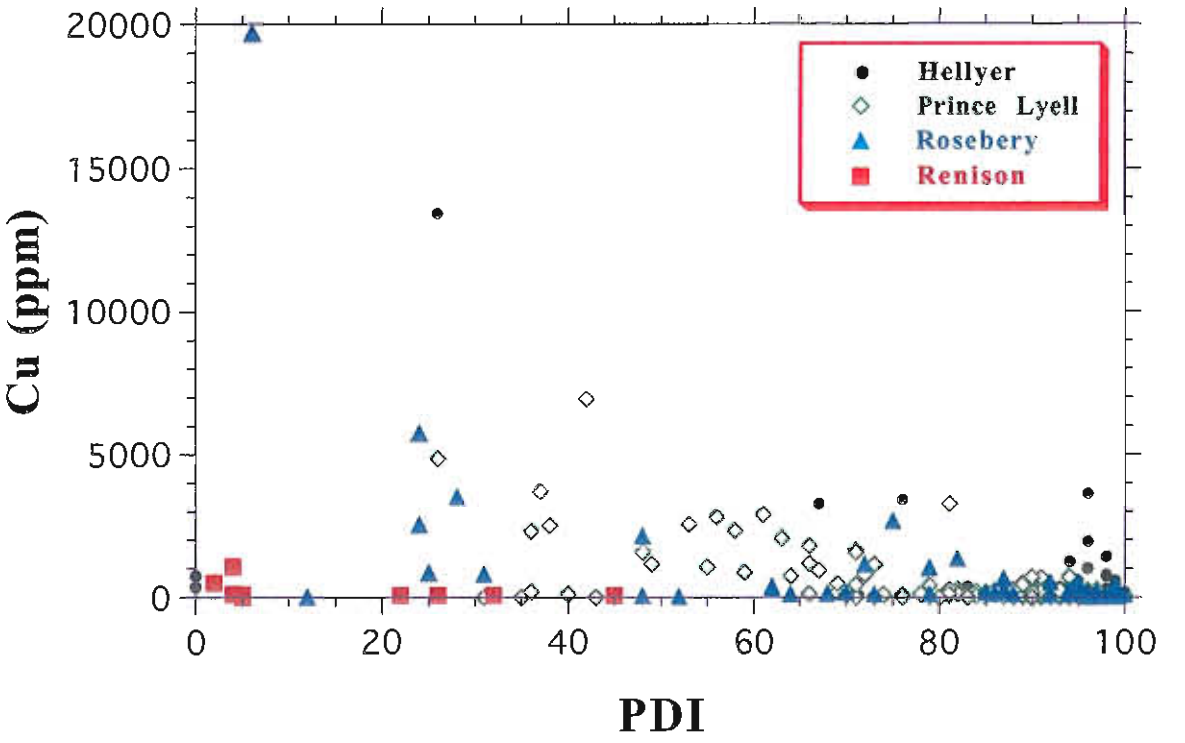
Hellyer
Prince Lyell
Rosebery
Renison
Cu (ppm)
20000
15000
10000
5000
0
0
20
40
60
80
100
PDI

Fig.5D

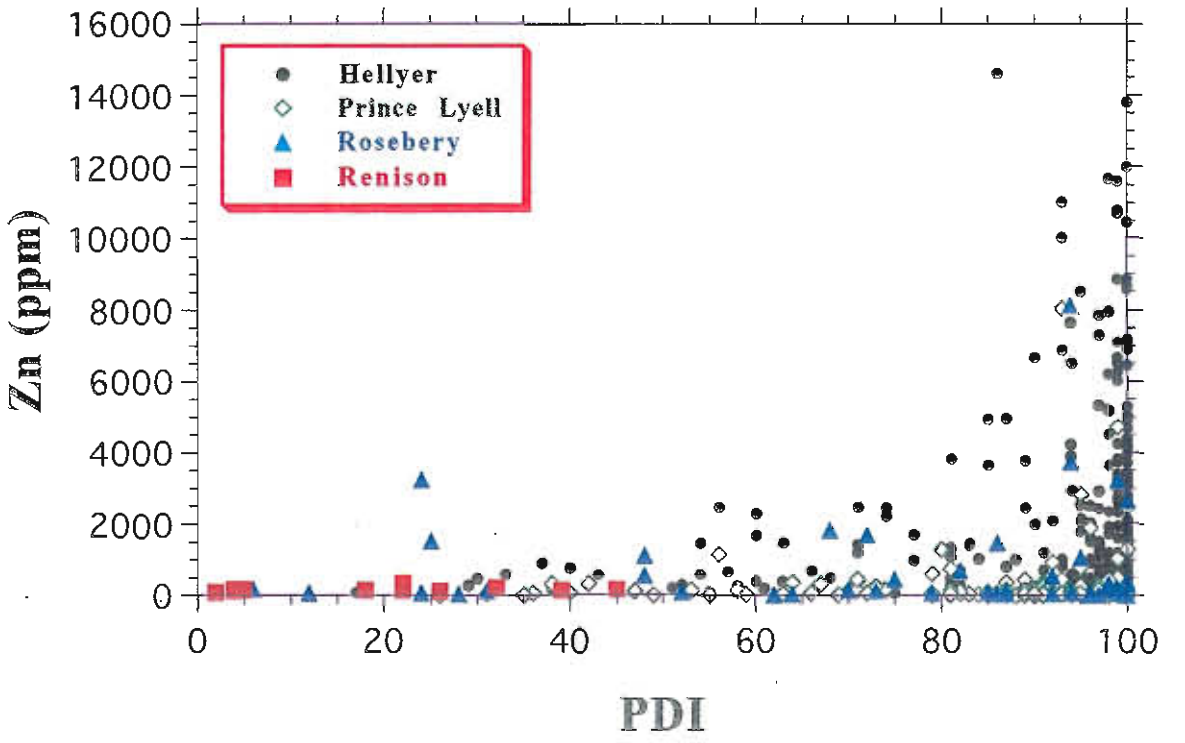
Hellyer
Prince Lyell
Rosebery
Renison
Zn (ppm)
16000
14000
12000
10000
8000
6000
4000
2000
0
0
20
40
60
80
100
PDI

Fig.5E

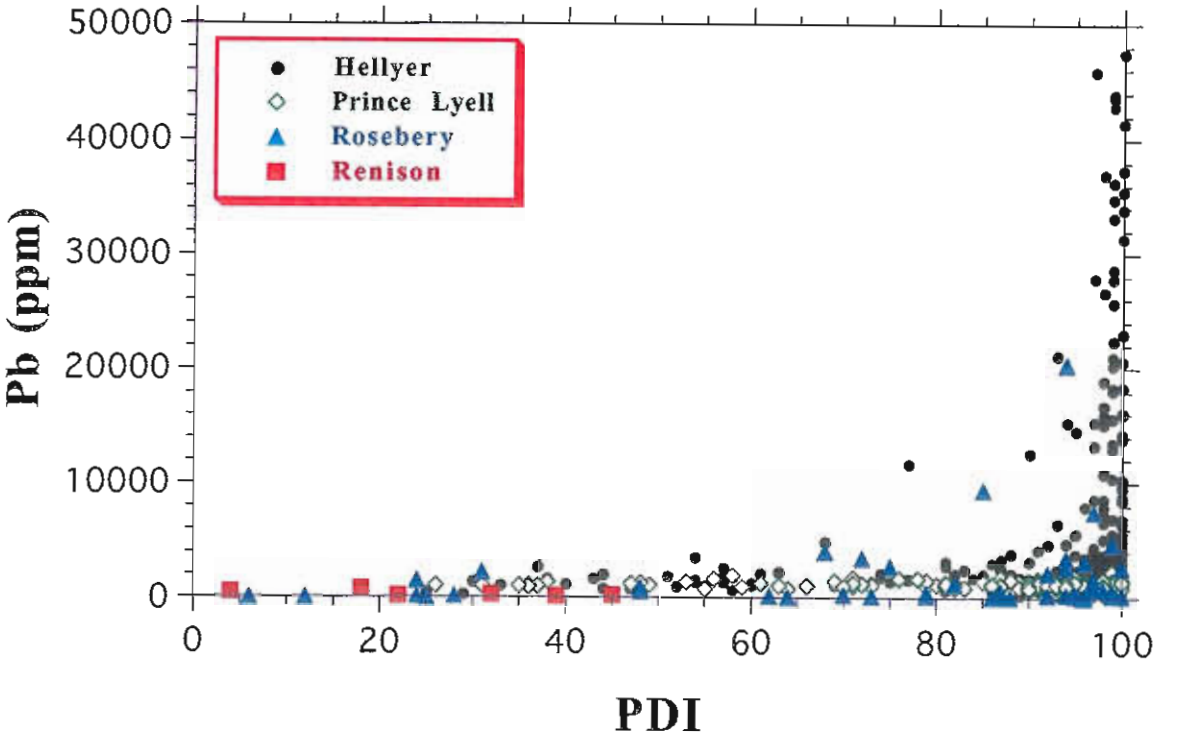
Hellyer
Prince Lyell
Rosebery
Renison
Pb (ppm)
50000
40000
30000
20000
10000
0
0
20
40
60
80
100
PDI

Fig.5F

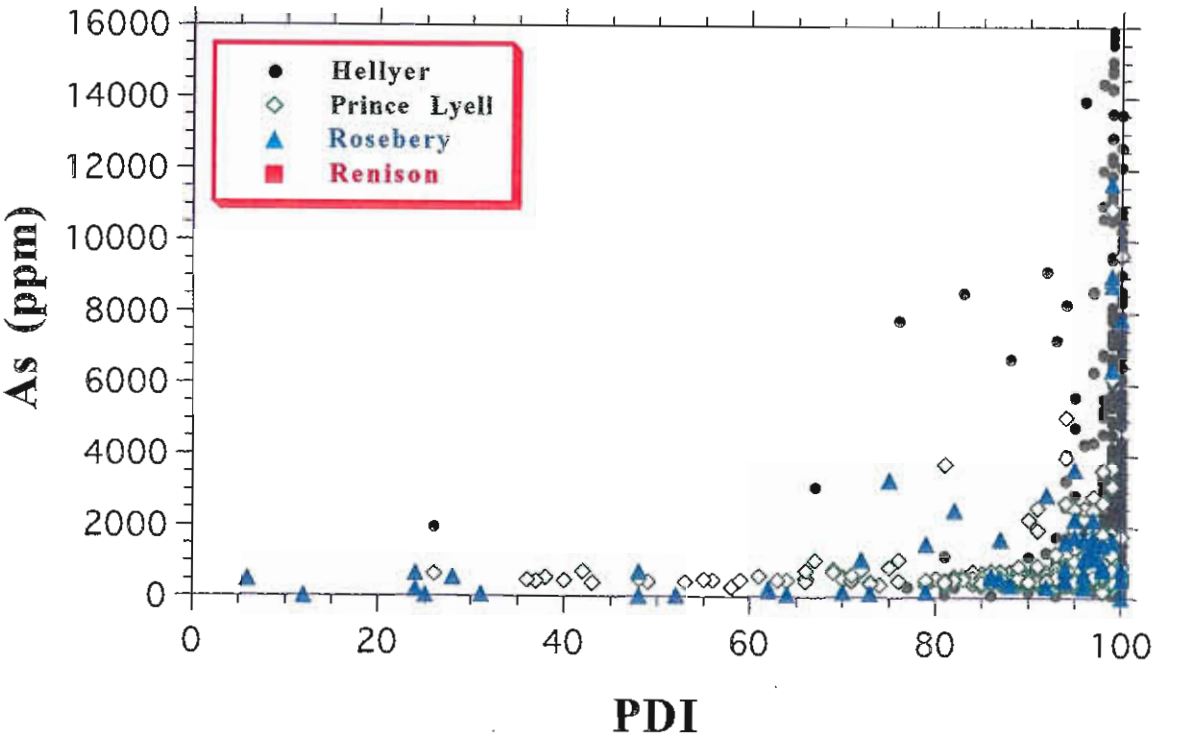
Hellyer
Prince Lyell
Rosebery
Renison
As (ppm)
16000
14000
12000
10000
8000
6000
4000
2000
0
0
20
40
60
80
100
PDI

Fig.5G

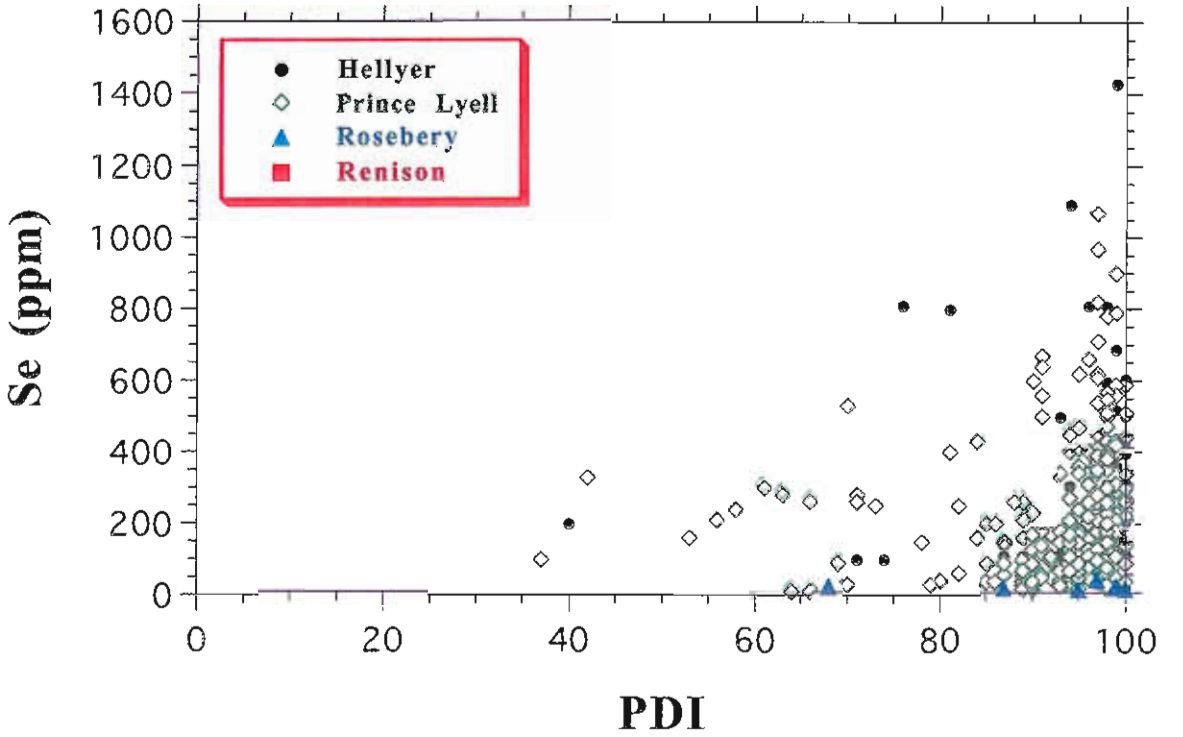
Hellyer
Prince Lyell
Rosebery
Renison
Se (ppm)
PDI
0
200
400
600
800
1000
1200
1400
1600
0
20
40
60
80
100

Fig.5H

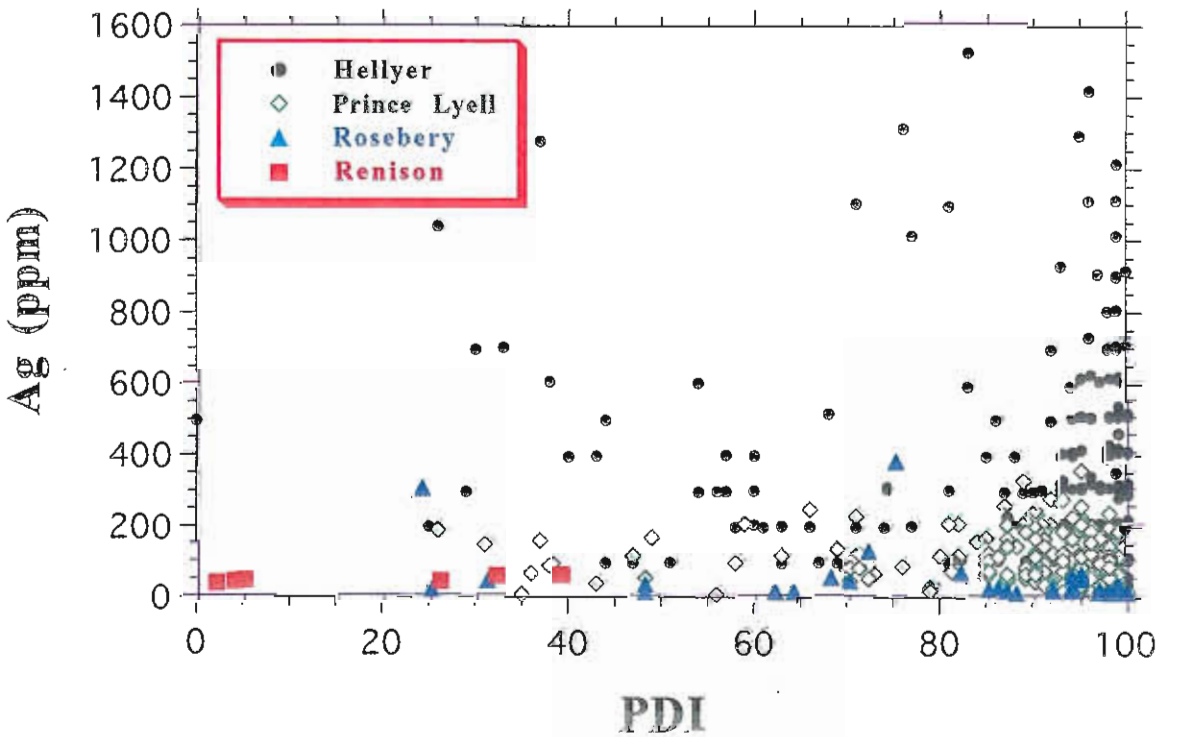
Hellyer
Prince Lyell
Rosebery
Renison
Ag (ppm)
PDI
0
200
400
600
800
1000
1200
1400
1600
0
20
40
60
80
100

Fig.5I

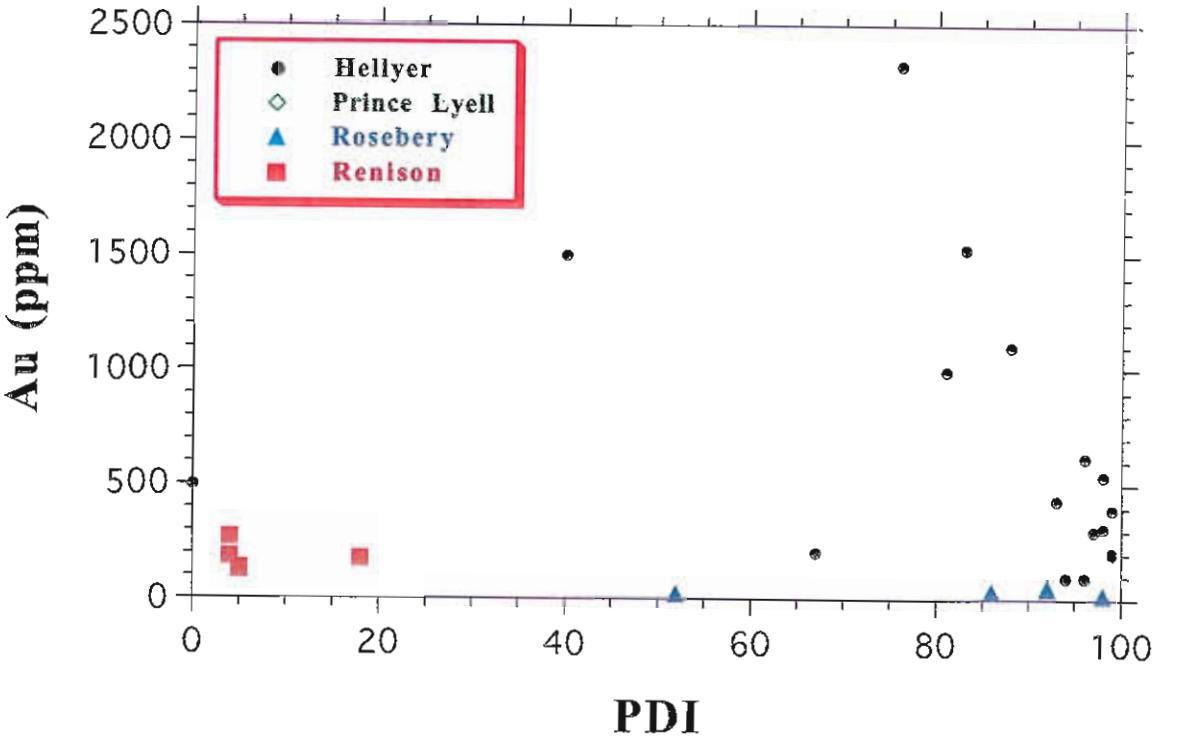
Hellyer
Prince Lyell
Rosebery
Renison
Au (ppm)
2500
2000
1500
1000
500
0
0
20
40
60
80
100
PDI

APPENDIX 1 - PYRITE TRACE ELEMENT DATA

HELLYER

Sample	Ring	Comments	Label	Co ppm	Ni ppm	Cu ppm	Zn ppm	As ppm	Se ppm	Ag ppm	Au ppm	Pb ppm	PDI*
61-452-44.1	2	Py2	PYASGOLD						200		1503		40
61-452-71.8	1	Py2	PYASGOLD			201		4627					98
61-442-69.0	1	Py2	PYRITE	200	700		900	200	500	200		300	93
61-442-69.0	1	Py3	PYRITE		100		301			200		1804	58
61-443-76.7	1	Py1	PYRITE	100	301		402	23415		301		2311	99
61-443-76.7	1	Py2	PYRITE		404		202	11119	101	202		3134	99
61-443-76.7	1	Py3	PYRITE					23232	202	404		4242	100
61-443-76.7	2	Py1	PYRITE	200	300		300					999	52
61-443-76.7	2	Py2	PYRITE							100		699	58
61-449-59.0	2	Py1	PYRITE		101		404	2424	101			707	99
61-449-59.0	3	Py1	PYRITE		101		101	22695		504		5144	99
61-449-59.0	3	Py2	PYRITE		201		503	14279		302			99
61-449-89.6	3	Py3	PYRITE	201			302	7245		101		1811	100
61-449-89.6	3	Py4	PYRITE				101	8549	201			2112	100
61-452-71.8	1	Py1	PYASGOLD			201		6828		201			98
67-229-41.6	2	Py2	PYRITE		200			1497	100	100		1298	97
67-229-41.6	2	Py3	PYRITE		100		100	801	300	100		701	98
67-231-16.3	4	Py2	PYRITE		203		101	33083	101	1015		4668	99
67-377-126.0	1	Py1	PYRITE				4228					2215	100
67-377-126.0	1	Py3	PYRITE				303					1414	100
67-377-126.0	1	Py4	PYRITE				2634	2229	101			2229	100
67-381-102.4	1	Py3	PYRITE							100		3005	86
67-381-102.4	2	Py3	PYRITE	100						299		1596	54
67-382-17.3	2	Py3 PyG?	PYRITE				1332			102		819	81
67-382-17.3	4	Py3	PYRITE				2437	1320		203		1117	97
67-382-96.1	2	Py4	PYRITE		100		200	2105	100	100		1103	98
73-151-21.1	1	Py1	PYRITE				602		100			2008	100
73-151-21.1	1	Py2	PYRITE		100				200			2096	98
73-151-21.1	1	Py5	PYRITE				200		100	299		1797	89
73-151-21.1	4	Py1	PYRITE		399			1198		300		1697	90
73-151-21.1	4	Py4	PYRITE									1204	100
73-151-21.1	5	Py5	PYRITE		100		100			100		801	47
73-157-6.3	3	Py1	PYRITE		103				103			4116	97
73-157-6.3	3	Py2	PYRITE	206	309		6903		103			2473	93
73-157-6.3	5	Py1	PYRITE	104			518			518		4868	68
73-347-20.4	4	Py1	PYRITE		102		1023	307		205		2148	88
73-347-20.4	4	Py2	PYRITE		203		812		101			1623	93
73-347-49.5	5	Py1	PYRITE				1106	3520		302		1509	98
73-347-49.5	5	Py6	PYRITE				908	10591	101			5548	100
73-347-49.5	5	Py7	PYRITE					6985	101			1114	100
73-348-30.8	1	Py1	PYRITE		101			101	302			1709	99
73-348-30.8	1	Py2	PYRITE					4396		599		799	97
73-348-30.8	1	Py3	PYRITE		301		201	3314	301	100		1707	98
73-348-30.8	1	Py4	PYRITE				201	3309		100		2708	99
73-348-30.8	1	Py5	PYRITE					10882		100		2795	100
73-348-30.8	3	Py1	PYRITE	299			299	6184				3491	100
73-348-30.8	6	Py1 Rx	PYRITE					7866		199			99
73-348-30.8	6	Py2	PYRITE		202		303	10311				1415	100
73-351-36.7	1	Py1	PYRITE				2103	4106				41458	100
73-351-36.7	1	Py2	PYRITE				606	6366		909		15360	97
73-351-36.7	1	Py5	PYRITE		102		203	1016	203	406		2031	95
73-351-36.7	2	Py1	PYRITE				101	1910				4021	100
73-351-36.7	2	Py2	PYRITE				101	2228				3444	100
73-351-36.7	2	Py3	PYRITE				604	302				3219	100
73-351-36.7	3	Py1	PYRITE	101			507	6691		304		5576	99
73-351-36.7	3	Py2	PYRITE	101	201		704	1006				4426	97
73-351-36.7	3	Py3	PYRITE		202		3125	7460		101		3831	99
73-351-36.7	4	Py2	PYRITE				101	403				3832	100
73-351-36.7	4	Py4	PYRITE				1114	2128	203	101		2330	99
73-351-36.7	5	Py1	PYRITE		101		7979	1818	202	303		5151	98
73-351-36.7	5	Py2	PYRITE				610	1017				9560	100
73-351-36.7	5	Py3	PYRITE		101			3525	201	302		15106	98
73-355-30.6	2	Py1 close to TeE	PYRITE		298		496		199			1191	94
73-355-30.6	2	Py2	PYRITE		199			696		398		3880	88
73-355-30.6	2	Py3	PYRITE					2303	200			1502	100
73-355-30.6	4	Py1	PYRITE					4857	99			1784	100
73-355-30.6	4	Py3 Gn contamination	PYRITE		98				98			33215	99
73-357-77.4	2	Py2	PYRITE				300		100	300		200	88
73-357-77.4	2	Py3	PYRITE					699	200			2296	100
61-452-57.3	2	Py2	PYASGOLD			100		5680		1295			95
61-454-82.3	3	Py2	PYRITE		698		182	617	132	223		3399	87
61-455-61.6	1	Py7	PYRITE		300		6497	7996	100			1000	99
73-349-8.0	1	Py3	PYRITE	99			297	22693	198	99		1387	100
61-452-71.8	4	Py1	PYASGOLD			408		8569		1530	1530		83
61-452-71.8	4	Py2	PYASGOLD			510		15518		102			99
61-452-84.6	4	Py1	PYASGOLD					1213		101			98

Sample	Ring	Comments	Label	Co ppm	Ni ppm	Cu ppm	Zn ppm	As ppm	Se ppm	Ag ppm	Au ppm	Pb ppm	PDI*
61-452-57.3	3	Py1	PYASGOLD			306		15732	1430				99
67-388-42.4	1	Py2	PYRITE		102		818	6541				4599	100
67-388-42.4	1	Py4	PYRITE	102			612					612	100
67-388-42.4	1	Py5	PYRITE	304			810	4251		202		1113	99
73-351-36.7	4	Py6	PYRITE	103	205		514	4931	205	103		4931	99
73-351-36.7	4	Py7	PYRITE		101		303	404				4042	97
61-452-44.1	1	Py1	PYASGOLD			605		4841					95
61-452-44.1	2	Py1	PYASGOLD			100		6866	597	697			98
61-452-44.1	3	Py2	PYASGOLD			99		23369	99		398		99
61-452-44.1	4	Py1	PYASGOLD					24420		904	201		99
61-452-57.3	1	Py1	PYASGOLD			808		11015	808				98
61-452-57.3	1	Py2	PYASGOLD			302		5335					98
61-452-57.3	3	Py2	PYASGOLD			100		5504					99
61-452-57.3	4	Py1	PYASGOLD								499		0
61-452-57.3	4	Py2	PYASGOLD					8615			301		97
61-452-71.8	2	Py2	PYASGOLD					4350	809	1113	101		96
61-452-71.8	3	Py1	PYASGOLD					4237	605	101			100
61-452-84.6	1	Py1	PYASGOLD			201		10629		702			98
61-452-84.6	2	Py1	PYASGOLD			100		6724			1104		88
61-454-58.9	2	Py2	PYASGOLD			385		7269		324	435		93
61-454-58.9	2	Py3	PYASGOLD			790							0
61-454-58.9	4	Py3	PYRITE		174			3457	113	174		6731	98
61-454-58.9	6	Py2	PYRITE		336		641	3064	92			550	98
61-454-82.3	3	Py1	PYRITE				193	1635		30		20	100
61-454-82.3	3	Py3	PYRITE	298	1502		93	13940		1420		7942	96
61-455-61.6	1	Py2	PYRITE	101	202		6659	5751	202			18061	99
61-455-61.6	1	Py3	PYRITE		202		101	506				1416	93
67-381-102.4	1	Py2	PYRITE	403	202		101	2317		202		26700	98
67-381-102.4	2	Py1	PYRITE	201				1106				13875	100
67-381-102.4	3	Py2	PYRITE	100	100		100	1407	100			43605	99
67-388-42.4	1	Py3	PYRITE		203		1016	305		1016		11683	77
73-050-356.7	1	Py3 outer Rx edge	PYRITE	101			3426	3527	101			2318	100
73-050-356.7	2	Py2	PYRITE				3994	9085				3794	100
73-050-356.7	2	Py3	PYRITE				499	4093				2496	100
73-151-21.1	3	Py2	PYRITE				101	4038	101			3230	100
73-151-21.1	3	Py3	PYRITE		304			3948				2834	99
73-151-21.1	3	Py4	PYRITE	202			101	4134				4538	100
73-347-20.4	3	Py1	PYRITE					4020		206		1752	99
73-347-20.4	3	Py2	PYRITE					4436	103	103		1444	100
73-347-20.4	3	Py3	PYRITE				206	2056	206	617		2159	96
73-347-20.4	3	Py4	PYRITE	205	103			1642		410		3796	95
73-347-49.5	2	Py2	PYRITE	402	201		1005	4119	100	100		20999	99
73-347-49.5	3	Py3	PYRITE	203			4266	3758	102	406		42864	99
73-347-49.5	4	Py3	PYRITE		200			3508	100	200		36283	99
73-347-49.5	4	Py4	PYRITE				703	5726				8438	100
73-347-49.5	4	Py5	PYRITE				500	3298		400		15492	98
73-347-49.5	4	Py7	PYRITE		301		1104	5217	100	502		16755	98
73-347-49.5	5	Py2	PYRITE		101		302	7954	201	101		20640	100
73-347-49.5	5	Py3	PYRITE				300	5607				59972	100
73-347-49.5	5	Py4	PYRITE	101			505	6058		303		15649	99
73-347-49.5	5	Py5	PYRITE	101			706	7666		101		8775	100
73-351-36.7	4	Py1	PYRITE				1719	2932		404		15974	98
73-351-36.7	4	Py3	PYRITE	102			204	3464		102		12939	99
73-351-36.7	4	Py5	PYRITE		102		818	6133	102			16150	100
61-443-76.7	1	Py4	PYRITE		1107		503	3322				1208	94
61-443-76.7	3	Py1	PYRITE		606		202	9593		101		2020	99
61-443-76.7	3	Py2	PYRITE		503			14796	101	302		2818	99
61-443-76.7	3	Py3	PYRITE		303		404	14731		202		2926	99
61-450-72.2	5	Py3	PYRITE					1113				33991	100
61-451-125.9	1	Py3	PYRITE				203	405				1722	100
61-451-99.7	1	Py3	PYRITE	101	201		5331	805		101		27862	97
61-451-99.7	5	Py4	PYRITE	101			709	43575	304	1216		4054	99
61-455-61.6	1	Py1	PYRITE	100	100		11617	2904	200	200		28643	99
61-455-61.6	1	Py4	PYRITE	101			3239	2328				31373	100
61-455-61.6	1	Py5	PYRITE		101		6247	1310				25695	99
61-455-61.6	1	Py6	PYRITE	200			4408	2805				37367	100
61-455-61.6	2	Py3	PYRITE	100	201		6019	3411				802	99
67-384-59.7	3	Py1	PYRITE					11852	203	608		2634	99
67-384-59.7	3	Py2	PYRITE		200		100	7286				1098	99
67-384-59.7	3	Py3	PYRITE	101	202		101	12232		202		2831	99
67-384-59.7	3	Py4	PYRITE		101		203	12371		406		3042	99
67-384-59.7	3	Py5	PYRITE		200		100	6700				1200	99
67-384-59.7	3	Py6	PYRITE		203			7804	101	203		1926	99
73-348-30.8	2	Py4	PYRITE	610	102		13831	10678	203	102		1831	100
73-349-8.0	1	Py1	PYRITE	898	3492			9180		698		4690	92
73-349-8.0	1	Py2	PYRITE	698	2293			8276		499		4786	94
61-442-69.0	4	Py1	PYRITE		100			199				1696	93
61-442-69.0	4	Py2	PYRITE		100		100					1394	75
61-442-69.0	4	Py3	PYRITE				1396					897	100

Sample	Ring	Comments	Label	Co ppm	Ni ppm	Cu ppm	Zn ppm	As ppm	Se ppm	Ag ppm	Au ppm	Pb ppm	PDI*
61-449-89.6	2	Py3	PYRITE		201		3220	30288	101	704		3522	99
61-449-89.6	2	Py4	PYRITE				303	11321		708		34873	99
61-450-72.2	1	Py1 inner	PYRITE				803					2308	100
61-450-72.2	1	Py2 outer	PYRITE							403		2618	57
61-454-58.9	1	Py2	PYRITE					473		111		1922	96
61-454-58.9	1	Py3	PYRITE		100		90		301			1275	98
61-454-58.9	1	Py5	PYRITE		61			17518		283		3243	100
67-377-126.0	2	Py1 outer zone	PYRITE					22820	102	102		1936	100
67-377-126.0	2	Py2 inner zone	PYRITE	202	101		202			607		1618	38
67-377-126.0	2	Py3 inner zone	PYRITE	305			203	10062	102	203		407	100
67-377-126.0	2	Py4 outer zone	PYRITE					17531		101		1008	100
67-377-126.0	2	Py5 outer outer zone	PYRITE				406	18868				2333	100
67-377-126.0	2	Py6 outer zone	PYRITE		101		101	25390				2620	100
67-377-126.0	2	Py7 inner zone	PYRITE		102		306	27137	102	612		3775	99
67-377-126.0	2	Py8 inner inner zone	PYRITE		100				201			1808	98
73-347-20.4	5	Py1	PYRITE	103			2998	11268		310		2481	99
73-348-30.8	4	Py1	PYRITE				1887	8443	99			1490	100
73-348-30.8	4	Py2	PYRITE		295		6196	5114		393		1672	98
73-348-30.8	4	Py3	PYRITE		99			3964	396	198		1784	99
73-348-30.8	4	Py4	PYRITE		199		499			698		1396	30
73-348-30.8	4	Py5	PYRITE					17497	199			1094	100
61-442-69.0	3	Py2	PYRITE		100		1504		100			1303	96
61-442-69.0	3	Py3	PYRITE	300	100		2101	6204				1701	100
61-443-76.7	4	Py1	PYRITE	201	302		302	302		101		705	81
61-443-76.7	4	Py2	PYRITE				807	3229				23005	100
61-443-76.7	4	Py3	PYRITE		100		5212	902				1002	98
61-443-76.7	5	Py2	PYRITE	101	201		2312			302		1307	60
61-443-76.7	6	Py1	PYRITE		101		202	5245	101				100
61-449-89.6	4	Py2	PYRITE				6541	503	101	402		1107	94
61-450-85.9	2	Py3	PYRITE		100		1603		100			1102	96
61-455-61.6	3	Py1	PYRITE	803			4716	1605	502			702	100
61-455-61.6	3	Py2	PYRITE	500			10792	1499	200	100		899	99
61-455-61.6	3	Py3	PYRITE	303	101		606	8186		202		2729	99
61-455-61.6	5	Py1	PYRITE	204	306		408	4591				22444	99
61-455-61.6	5	Py2	PYRITE	304	101		2738	2028				507	99
67-229-41.6	4	Py2	PYRITE	100	300		2403	5006				1001	99
67-231-16.3	3	Py1 Gn contamin?	PYRITE		100		500	2101	200			35521	100
67-377-126.0	3	Py1	PYRITE		102		1225	715		306		1633	91
67-377-126.0	3	Py2	PYRITE				410	2666				1846	100
67-377-126.0	4	Py1	PYRITE		102			918	204			2143	99
67-377-126.0	4	Py3	PYRITE		102		1118		610	305		610	97
67-377-126.0	4	Py4	PYRITE				3862			305		2744	81
67-377-59.4	1	Py1	PYRITE		100		200			200		2102	61
67-377-59.4	1	Py2	PYRITE		100		1403					1102	83
67-377-59.4	1	Py3	PYRITE		100		3811					301	89
67-377-59.4	1	Py4	PYRITE	101			2513		101	101		804	96
67-377-59.4	3	Py2	PYRITE	100			2508	602	201			903	100
67-377-59.4	3	Py3	PYRITE	200			1402	300	100			1402	100
67-378-70.8	3	Py1	PYRITE		200		6695	200		100		1199	90
67-382-17.3	3	Py2	PYRITE		303		7872	2624		101		1817	97
67-382-96.1	4	Py1	PYRITE				498	5482				1595	100
67-382-96.1	4	Py2	PYRITE	100	100		1202	6812	301			2204	100
67-384-59.7	1	Py1	PYRITE							499		1996	44
67-385-39.9	1	Py3 Gn contamin?	PYRITE		306		2546	509	102	102		14564	95
67-385-39.9	1	Py4	PYRITE	203			102	813	203			1117	100
67-385-39.9	1	Py5	PYRITE		204		1428	9794				1530	100
67-385-39.9	2	Py1 furthest from As	PYRITE				508	15022		406		1421	99
67-385-39.9	2	Py2 closer to As	PYRITE				101	2221				909	100
67-385-39.9	2	Py3 closest to As	PYRITE		202			808				1211	95
67-385-39.9	2	Py4	PYRITE	101				8320	101			913	100
67-385-39.9	2	Py7 remnant	PYRITE					406				304	100
73-050-356.7	3	Py1	PYRITE				1400			100		13300	97
73-050-356.7	3	Py2 recrsyt.d	PYRITE				400	3799	200	100		600	100
73-050-356.7	3	Py3	PYRITE						303			16080	100
73-050-356.7	3	Py4	PYRITE				2022					2831	100
73-050-356.7	4	Py1	PYRITE				405	2128	101	608		203	95
73-050-356.7	4	Py2	PYRITE		202		1923	2024	202			1316	99
73-050-356.7	5	Py2	PYRITE	99			4175	2982				1193	100
73-050-356.7	5	Py3	PYRITE					4983		299		299	99
73-050-356.7	5	Py4	PYRITE		301		8842	2914	100			18288	99
73-050-356.7	6	Py1	PYRITE		101		506	3137				1417	99
73-050-356.7	6	Py2	PYRITE		101		4549	1011				1011	98
73-050-356.7	6	Py3	PYRITE		102		1018	3053		204		7938	98
73-151-21.1	5	Py2	PYRITE				301	502	301	100		1907	99
73-151-21.1	5	Py3	PYRITE		100		1098	799				6790	98
73-157-6.3	1	Py2	PYRITE		102		307			102		15374	94
73-157-6.3	2	Py1	PYRITE				2247			306		2145	74
73-157-6.3	2	Py2	PYRITE				407		204	204		36969	98
73-157-6.3	2	Py4	PYRITE				613		204	204		18897	98

Sample	Ring	Comments	Label	Co ppm	Ni ppm	Cu ppm	Zn ppm	As ppm	Se ppm	Ag ppm	Au ppm	Pb ppm	PDI*
73-157-6.3	4	Py1	PYRITE		102		1024					1740	84
73-157-6.3	4	Py2	PYRITE				310			103		2069	82
73-157-6.3	5	Py4	PYRITE		102		818					2556	87
73-347-20.4	6	Py2	PYASGOLD			398							0
73-347-49.5	3	Py1	PYRITE		201		503	1813		201		3021	96
73-348-30.8	2	Py2	PYRITE				902	41086		501		2305	100
73-348-30.8	2	Py3 closer to Is Gn	PYRITE	1004			301	5020				5120	100
73-348-30.8	2	Py5	PYRITE	200			100			300		12587	90
73-355-30.6	3	Py1	PYRITE				5289	4391	100			1896	100
73-355-30.6	3	Py2	PYRITE	100	200		1198	1997	300	100		1298	98
73-355-30.6	3	Py3	PYRITE		198		1489			99		1092	63
73-355-30.6	5	Py4	PYRITE				2976		397	595		1488	94
73-357-77.4	1	Py1	PYRITE		199		795			397		1192	40
73-357-77.4	1	Py2	PYRITE		99				99			596	95
73-357-77.4	1	Py3	PYRITE		100		199	499				897	96
73-357-77.4	4	Py1	PYRITE		199		1495			299		1396	54
73-357-77.4	4	Py2	PYRITE	201			702			100		4214	91
61-443-76.7	6	Py3	PYRITE				2513	5730	101			905	100
61-450-72.2	1	Py3 (Co contam.?)	PYRITE				315	26639				2098	100
67-382-96.1	2	Py2 outer o'growth	PYRITE		201		1404					1103	71
73-151-21.1	1	Py4	PYRITE				1390					1489	100
73-151-21.1	2	Py4	PYRITE		100			902	100			1002	99
73-349-8.0	3	Py1 o'growth on SiB	PYRITE		299		100	24349	200	299		2595	100
73-349-8.0	3	Py3 o'growth on SiB	PYASGOLD			1039		20781	208	312	623		96
61-449-59.0	2	Py2 inner	PYRITE					1103				1704	100
61-449-59.0	2	Py3 outer s-spongy	PYRITE				405	7804		203			99
61-451-99.7	1	Py1	PYRITE		204		204	64526		510		6422	100
61-451-99.7	1	Py2	PYRITE				101	53251	101	710		2130	100
61-451-99.7	5	Py1	PYRITE	102			1735	46944		918		4388	100
61-451-99.7	5	Py2	PYRITE		101		303	43979				1921	100
61-451-99.7	5	Py3	PYRITE		100		603	24814	402	603		1708	99
61-454-58.9	1	Py1	PYRITE	40			202	3457				615	100
67-385-39.9	1	Py1	PYRITE							102		1119	69
67-385-39.9	1	Py2	PYRITE	102			102	1937				2548	100
73-348-30.8	2	Py6	PYRITE	399			8572	18040	299			2591	100
73-355-30.6	1	Py1	PYRITE				12010		197			886	100
61-443-76.7	5	Py1	PYRITE				11695	2722		302		3629	98
61-451-112.3	4	Py1	PYRITE	203	406		101	7202	203			2130	99
61-451-112.3	4	Py2	PYRITE	102			610	1728		305		1829	97
61-451-112.3	4	Py3	PYRITE				1738					1431	100
61-451-125.9	3	Py1	PYRITE	399			1296						100
61-451-99.7	4	Py1	PYRITE				610	21028		203		6908	100
61-451-99.7	4	Py2	PYRITE		400		1901	3102				500	98
61-452-44.1	1	Py2	PYASGOLD			100		1197	798	1097	997		81
61-452-44.1	3	Py1	PYASGOLD					9903	200				100
61-452-44.1	4	Py2	PYASGOLD			1292		4074	1093				94
67-382-17.3	3	Py4	PYRITE				7134	1427				3363	100
67-385-39.9	2	Py6	PYRITE				1727			203		1626	77
67-388-42.4	1	Py1	PYRITE		102			3877		204		27851	99
61-442-69.0	3	Py1	PYRITE	100			14629			501		1002	86
61-449-89.6	3	Py2	PYRITE	100			3919	703		301		301	94
61-449-89.6	4	Py1	PYRITE				7204					1401	100
61-450-72.2	2	Py1	PYRITE				2616	101				3522	100
61-450-72.2	3	Py1	PYRITE				403	1611	101	503		2215	95
61-450-85.9	3	Py1	PYRITE				1203	5612		501		2105	98
61-451-112.3	1	Py1	PYRITE				704			201		1207	66
61-451-112.3	1	Py2	PYRITE		202		2824	16137		101		1614	100
61-451-112.3	1	Py3	PYRITE		203		2127	405					92
61-451-112.3	1	Py4	PYRITE				2423	10296	101			808	100
61-451-112.3	4	Py4	PYRITE	102	102		813	5388		305		1728	99
61-454-45.0	1	Py1	PYRITE		91		7112	3662	688	273		1872	99
61-454-58.9	4	Py1	PYRITE	291			8857	1222				381	100
61-454-58.9	4	Py2	PYRITE				3413	5028	363	454			99
61-454-58.9	5	Py1	PYRITE	121			3835	6772		353		1332	99
61-454-58.9	5	Py2	PYRITE	120			6904	2077	10			1776	100
61-454-58.9	6	Py1	PYRITE	102			924			1279		2690	37
61-454-71.3	1	Py1	PYRITE	241			1226	462		90		2031	97
67-377-126.0	1	Py2	PYRITE	101	203		1013	912				3545	96
67-377-126.0	4	Py2	PYRITE		102		511		204			2862	98
67-377-59.4	3	Py1	PYRITE	101			4925	1709				1005	100
67-377-59.4	3	Py4	PYRITE				4705	4004		200		1802	99
67-378-70.8	3	Py2 inner	PYRITE	100	100		897		199	100		797	96
67-378-70.8	3	Py3 outer	PYRITE				2488			100		1493	89
67-381-102.4	4	Py1	PYRITE	400	200		4994					1199	87
67-382-17.3	2	Py1	PYRITE	101			5046					303	100
67-382-17.3	3	Py3 corroded PyZ?	PYRITE		102		406			203		2234	63
67-382-96.1	4	Py3	PYRITE	99			10721	2879		99		1985	99
67-385-39.9	1	Py6	PYRITE				305	2444				1426	100
67-385-39.9	2	Py5	PYRITE				1730	8650		204		305	100

Sample	Ring	Comments	Label	Co ppm	Ni ppm	Cu ppm	Zn ppm	As ppm	Se ppm	Ag ppm	Au ppm	Pb ppm	PDI*
67-388-42.4	2	Py1	PYRITE				3137	2833		101		405	99
73-050-356.7	1	Py1	PYRITE				804	6428	100	301		1306	99
73-151-21.1	5	Py1	PYRITE		100		2505			301			56
73-157-6.3	1	Py1 Sp contamination	PYRITE				10046		101	304		812	93
73-347-20.4	6	Py1	PYRITE				3452					1117	100
73-347-49.5	2	Py1	PYRITE				4390					2993	100
73-347-49.5	2	Py3	PYRITE	99	99		4549	1286		99		1978	98
73-347-49.5	3	Py2	PYRITE				3300	2500		200		3200	99
73-348-30.8	2	Py1	PYRITE	299	199		4979	398		398		2091	85
73-355-30.6	1	Py2	PYRITE	98	98		7641		294	392		1469	94
73-355-30.6	1	Py3	PYRITE	304			3745	1518	101	101		1012	99
73-355-30.6	2	Py4	PYRITE	99			10471					1087	100
73-357-77.4	3	Py1	PYRITE				2090	995				9751	100
73-357-77.4	5	Py1	PYRITE				3080		199			1192	100
61-454-71.3	2	Py1 (contains Gn?)	PYRITE					2221				47501	100
73-151-21.1	3	Py5	PYRITE				635	1798		106		5393	99
61-455-61.6	2	Py1	PYRITE				503	2215				302	100
61-455-61.6	2	Py2	PYRITE	803			502	703				2109	100
61-450-72.2	2	Py2 outer	PYRITE				1203			200		1303	71
61-450-72.2	2	Py3 central	PYRITE					100				904	100
61-450-72.2	2	Py4 inner	PYRITE				302	1508	302			2111	100
61-450-72.2	4	Py1 unreplaced remn.	PYRITE		101					201		503	25
61-450-85.9	2	Py1 outer rim	PYRITE		201		1104					3110	81
61-450-85.9	2	Py2 inner "new orig!	PYRITE				402	6529				1507	100
61-451-112.3	2	Py1	PYRITE				6448	1008	101			101	100
61-451-112.3	2	Py2	PYRITE		303		4246	303	101				94
61-451-112.3	2	Py3	PYRITE		102		1117	7312		203		1828	99
61-451-112.3	2	Py4	PYRITE		203			29993	101			608	100
61-451-112.3	2	Py5	PYRITE				101	7485		101		809	100
61-451-112.3	3	Py1	PYRITE				306	26487				2139	100
61-451-112.3	3	Py2	PYRITE				1625	12086	102	203		2539	100
61-451-112.3	3	Py3	PYRITE				3732	34997	202			1815	100
61-451-112.3	3	Py4	PYRITE	102			203	16584	102			1831	100
61-451-112.3	3	Py5	PYRITE				102	10291				1732	100
61-451-112.3	3	Py6	PYRITE					13590		507		101	99
61-450-72.2	5	Py1	PYRITE				101					4133	100
61-450-72.2	5	Py2 borderline PyO/J	PYRITE	101	101			27188				303	100
61-452-84.6	1	Py2	PYASGOLD					1709		101	101		94
73-348-30.8	5	Py1	PYRITE							500			0
73-348-30.8	5	Py2	PYRITE				298			298		298	29
73-348-30.8	5	Py3	PYRITE				1705			401		1304	60
73-348-30.8	5	Py4	PYRITE		200		599			399		1696	43
73-348-30.8	5	Py5	PYRITE				398					2191	100
73-348-30.8	5	Py6	PYRITE		199		1794	1096		199		5580	95
61-449-89.6	1	Py1	PYRITE					7132		301		3315	99
61-449-89.6	1	Py2	PYRITE		100		300	1301		500		1701	92
61-449-89.6	1	Py3	PYRITE				100	8102		400		2200	99
67-209-42.8	1	Py1	PYRITE		102		2343	713	102			713	98
67-209-42.8	1	Py2	PYRITE					709		101		2735	98
67-209-42.8	1	Py3	PYRITE		305		102	1525		203		1525	94
67-209-42.8	1	Py4	PYRITE	909				808	404	101		1516	99
67-209-42.8	2	Py1 inner	PYRITE					2242		102		611	99
67-209-42.8	2	Py2 closer to Py^	PYRITE	204				1020	204			1020	100
67-209-42.8	2	Py3 closest to Py^	PYRITE	307			614	614				3477	100
67-209-42.8	3	Py3	PYRITE		306			1532	204	204		613	96
67-229-41.6	1	Py1	PYRITE		300		400	600	200	100		1001	95
67-229-41.6	1	Py2	PYRITE	1319	507		710	304				913	82
67-229-41.6	1	Py3	PYRITE						202			1113	100
67-229-41.6	1	Py4	PYRITE		101		201	1207	101			1811	99
67-229-41.6	2	Py4	PYRITE	200			3305	300	300			1302	100
67-229-41.6	3	Py1	PYRITE				300	200	100			1400	100
67-229-41.6	3	Py2	PYRITE	101	101		2633	1013	203			506	99
67-231-16.3	4	Py1	PYRITE					1396				1595	100
67-231-16.3	4	Py3	PYRITE					101		101		707	86
67-377-59.4	4	Py1	PYRITE				1508					1408	100
67-377-59.4	4	Py2	PYRITE		101		101		101	101		906	92
67-377-59.4	4	Py3	PYRITE		201		201	301	100			2411	95
67-377-59.4	4	Py4	PYRITE		101		1008	101	101	202		6452	93
67-382-17.3	3	Py1	PYRITE				8538			102		1728	95
73-151-21.1	2	Py1	PYRITE		100			499				2796	97
73-151-21.1	2	Py2	PYRITE					403		101		3226	96
73-151-21.1	2	Py3	PYRITE									2592	100
73-151-21.1	3	Py1	PYRITE				399	898	200			1298	100
73-357-77.4	5	Py2 outer	PYRITE				1902	3403				1501	100
73-357-77.4	5	Py3	PYRITE									501	100
73-357-77.4	5	Py4 inner	PYRITE		201							1304	57
73-357-77.4	5	Py5	PYRITE		200		100					1100	55
73-357-77.4	5	Py6 outer	PYRITE		198		1485	594		594		2476	83
61-454-45.0	2		PYTRACE		2		2012	4063					100

Sample	Ring	Comments	Label	Co ppm	Ni ppm	Cu ppm	Zn ppm	As ppm	Se ppm	Ag ppm	Au ppm	Pb ppm	PDI*
61-454-45.0	2		PYTRACE				2011	4316		51			100
61-454-45.0	2	Fb1	PYTRACE		12		2012	4108					100
61-454-45.0	2	Fb2	PYTRACE		5		2009	5263		51			100
61-454-45.0	2	Fb2A	PYTRACE		132		2014	2371		334			96
67-382-17.3	1	Py3 S-Rx	PYRITE	103			1436	3385				1641	100
67-382-17.3	1	Py5 S-Rx	PYRITE		102		1024	1741		102		1536	98
67-382-17.3	4	Py1	PYRITE				1928	406				1421	100
67-382-17.3	4	Py5	PYRITE				3676	919		102		306	98
67-381-102.4	4	Py2	PYRITE	100	100		7329	803		100		1807	97
73-349-8.0	4	Py5	PYRITE		1918		505	17367	404	404		8582	98
73-349-8.0	4	Py6	PYRITE	100	700		400	15903	300	100		43909	99
73-349-8.0	4	Py8	PYRITE	304	1522			22015	101	609		10855	98
73-349-8.0	4	Py9	PYASGOLD			1990		21265	105	733			96
61-443-76.7	6	Py2	PYRITE		201		906	8452				2314	100
61-449-59.0	1	Py1	PYRITE				8671	997	299			1196	100
61-449-59.0	1	Py2	PYRITE	602	201		2008	301		100		3213	90
61-449-59.0	4	Py1	PYRITE	1100	300		600	1801		200			95
61-449-89.6	2	Py1	PYRITE				100	5822	100			1004	100
67-229-41.6	2	Py1	PYRITE		499		200		100	200			74
67-229-41.6	3	Py3	PYRITE		299		299		399			897	96
67-229-41.6	3	Py4 edge of cube	PYRITE					903	301	100			99
67-229-41.6	3	Py5 centre of cube	PYRITE		101		402	503	201			503	99
67-229-41.6	3	Py6 edge of cube	PYRITE				994	1789	199	99		1292	99
67-229-41.6	4	Py1	PYRITE				413			207		1137	60
67-229-41.6	4	Py3	PYRITE		99					99		796	44
67-377-59.4	2	Py1	PYRITE		100		700			300		1901	57
67-377-59.4	2	Py2	PYRITE				2013	1510	101			2617	100
67-377-59.4	2	Py4	PYRITE	201	100		201	401				1304	96
67-378-70.8	1	Py1	PYRITE				1199	1399	100	100		799	99
67-378-70.8	1	Py2	PYRITE	100			601	1402				1202	100
67-378-70.8	2	Py1	PYRITE	300	100		300		200			1098	98
67-378-70.8	2	Py2	PYRITE						100	100		1396	96
67-378-70.8	2	Py3	PYRITE	100				100				1698	100
67-378-70.8	4	Py1	PYRITE		100		703	7532	100			3314	100
67-378-70.8	4	Py2	PYRITE		200		100	1497	100			699	98
67-381-102.4	1	Py1	PYRITE					995		298		1592	95
67-381-102.4	3	Py1	PYRITE	100	100			301				1808	95
67-382-17.3	1	Py1 cube centre	PYRITE				102					1427	100
67-382-17.3	1	Py2 cube corner	PYRITE				2926	504		101		1211	97
67-382-17.3	2	Py2 PyN?	PYRITE				102	8377	102	102		2145	100
67-382-17.3	4	Py2	PYRITE		203		2134	1728		305		1118	95
67-382-17.3	4	Py4	PYRITE				102	2140				1325	100
67-382-96.1	1	Py1	PYRITE	100	100		600	1501		400		901	94
67-382-96.1	1	Py2	PYRITE				4697	3398	100	100		799	100
67-382-96.1	2	Py1 inner core	PYRITE		101		101	9550		201		2413	99
67-382-96.1	2	Py3	PYRITE		101		2314	2716		101		905	99
67-382-96.1	3	Py1	PYRITE				900	400	100	100		1601	98
67-382-96.1	3	Py2	PYRITE	200			401					1703	100
67-382-96.1	3	Py3	PYRITE						101	101		403	95
73-050-356.7	1	Py2	PYRITE		298		398	3083	298			1691	99
73-050-356.7	2	Py1 Sp contamination	PYRITE		199		11037	1193		398		1491	93
73-151-21.1	1	Py3	PYRITE				298	199	99	99		3378	97
73-151-21.1	2	Py5	PYRITE					1302				3106	100
73-157-6.3	5	Py2	PYRITE		205								0
73-347-49.5	1	Py2	PYRITE	299	199		3686					1694	85
73-347-49.5	1	Py3	PYRITE		99		595	1189	99	198		4262	97
73-347-49.5	4	Py1	PYRITE				2491			299		1794	74
73-348-30.8	3	Py2	PYRITE				3282	995				2089	100
73-351-36.7	1	Py3	PYRITE				2509		100	1104		1104	71
73-351-36.7	1	Py4	PYRITE		101		604			604		3521	54
73-351-36.7	3	Py4	PYRITE				2634	1013				1925	100
73-355-30.6	4	Py2	PYRITE		200		499	100				1197	81
73-355-30.6	5	Py1	PYRITE				299	1297				1795	100
73-355-30.6	5	Py2	PYRITE				604			704		1107	33
73-355-30.6	5	Py3	PYRITE					1197	299	499		1596	96
73-357-77.4	2	Py1	PYRITE	299	100		299	5381	399			1096	100
73-357-77.4	4	Py3	PYRITE	99	99		791	29761				593	100
73-157-6.3	3	Py3 Gn contamination	PYRITE	309	206		823	1543		309		45880	97
67-209-42.8	2	Py8	PYRITE		206		103	2059				1647	98
67-209-42.8	2	Py9	PYRITE				207					207	100
67-209-42.8	3	Py1	PYRITE		306		204			102		1941	51
67-209-42.8	3	Py2	PYRITE	102	510			1019	102			611	93
67-378-70.8	4	Py3	PYRITE		100		1601	200	300			1601	99
67-381-102.4	2	Py2	PYRITE		100		100						17
61-451-125.9	1	Py1	PYRITE		716		307	30768		511		13493	99
61-451-125.9	1	Py2	PYRITE		101			30245	202	809		4350	99
61-451-125.9	2	Py1	PYRITE	202			101	27104				3337	100
61-451-125.9	2	Py2	PYRITE		101			31089		1114		3139	99
61-452-57.3	2	Py1	PYASGOLD			3650		37713	304				96

Sample	Ring	Comments	Label	Co ppm	Ni ppm	Cu ppm	Zn ppm	As ppm	Se ppm	Ag ppm	Au ppm	Pb ppm	PDI*
61-452-97.6	2	Py1	PYASGOLD			3439		7789	809	1315	2327		76
61-452-97.6	2	Py2	PYASGOLD			13446		1980		1042			26
61-452-97.6	2	Py3	PYASGOLD			3313		3106		104	207		67
67-209-42.8	2	Py4 inner o'growth	PYRITE				943	629	105	105		3774	98
67-209-42.8	2	Py5 inner o'growth	PYRITE					33405	102	102		1226	100
67-209-42.8	2	Py6 next o'growth	PYRITE				203	34731	203	102		1523	100
67-209-42.8	2	Py7 next o'growth	PYRITE	104	104			6643		311		1972	99
67-231-16.3	1	Py1	PYRITE		100			16045		199		698	100
67-231-16.3	1	Py2 framboid core	PYRITE	101	201			13569				1106	100
67-231-16.3	1	Py3 "o'growth"	PYRITE					20850		302		1108	100
67-231-16.3	1	Py4	PYRITE				201	31671				1910	100
67-231-16.3	2	Py1	PYRITE				201	25530		101		804	100
67-231-16.3	2	Py2 "o'growth"	PYRITE				499	18077	100	200		899	100
67-231-16.3	2	Py3	PYRITE	100	200		301	22351		401		1303	99
67-231-16.3	2	Py4	PYRITE		100		201	30431		201		3314	100
67-231-16.3	2	Py5 "o'growth"	PYRITE	101			302	22620	302			10355	100
67-384-59.7	2	Py1 Ns core	PYRITE				1497	699	200	299		8584	97
67-384-59.7	2	Py2 Sg interstitial	PYRITE		100		200	12906		400		1501	99
67-384-59.7	2	Py3 Ns core	PYRITE	201			302	4029				3526	100
67-384-59.7	2	Py4 Sg interstitial	PYRITE	100	200			12623				2304	100
67-384-59.7	4	Py1 Ns interstitial	PYRITE					22730	100	300		2603	100
67-384-59.7	4	Py10 Ns core	PYRITE				403	4632		201		20240	99
67-384-59.7	4	Py2 Ns core	PYRITE		101		201	3216		101		10453	99
67-384-59.7	4	Py4 Ns core	PYRITE					3121	101			6846	100
67-384-59.7	4	Py5 Ns interstitial	PYRITE				303	23605				14325	100
67-384-59.7	4	Py7 Ns interstitial	PYRITE		101			17664				4744	100
67-384-59.7	4	Py8 Ns core	PYRITE		201			10562		201		1408	99
73-151-21.1	2	Py6	PYRITE				700	2499				1899	100
73-151-21.1	4	Py2	PYRITE		200		399	40140	100			2297	100
73-151-21.1	4	Py3	PYRITE	106				10686		529		15658	99
73-151-21.1	4	Py5	PYRITE				2503	31832		200		4805	100
73-151-21.1	5	Py4	PYRITE		102		609	7209				4264	100
73-347-20.4	1	Py1 Gn contamination	PYRITE				310	1756		930		21173	93
73-347-20.4	1	Py2	PYRITE				829	3730				2590	100
73-347-20.4	2	Py1	PYASGOLD			403		2924					95
73-347-20.4	3	Py5	PYRITE				103	20631	103			3301	100
73-349-8.0	2	Py1	PYRITE		401		602	25376		301		4514	99
73-349-8.0	2	Py2	PYRITE		490		98	2644		392		2155	94
73-349-8.0	2	Py3 spongy	PYRITE	99	796		199	14421	199	398		7260	98
73-349-8.0	2	Py4 bubble core	PYRITE		695		199	2582		199			94
73-349-8.0	2	Py5 bubble inbetween	PYRITE	200	600		100	11993		500		6596	98
73-349-8.0	2	Py6 bubble edge	PYRITE	100	200		100	18144		902		6917	99
73-349-8.0	2	Py7	PYRITE		403			29930		705		4333	99
73-349-8.0	2	Py8	PYASGOLD			1467		32687	105	419			98
73-349-8.0	3	Py2	PYRITE	99	199		99	18594		199		2784	100
73-349-8.0	3	Py4	PYASGOLD			519		18999	519				99
73-349-8.0	3	Py5	PYRITE	204	612			8157				918	99
73-349-8.0	3	Py6	PYRITE	200			700	21006		400		200	100
73-349-8.0	3	Py7	PYRITE	201	805		101	18716		805		2516	98
73-349-8.0	3	Py8 colloform	PYRITE				100	21942				1202	100
73-349-8.0	4	Py1	PYRITE		198			31442	198			1483	100
73-349-8.0	4	Py2	PYRITE		200			31225	299	698		1796	99
73-349-8.0	4	Py3	PYRITE				299	24855	200			2296	100
73-349-8.0	4	Py4	PYRITE		99			26512		99		1192	100
73-349-8.0	5	Py1	PYRITE		101			19924	201	201		1912	100
73-349-8.0	5	Py10	PYASGOLD			621		28459		414			99
73-349-8.0	5	Py11	PYASGOLD			105		26233	105	315			100
73-349-8.0	5	Py12	PYASGOLD			739		33787	106	422	317		98
73-349-8.0	5	Py13	PYASGOLD			212		37930	425	106			100
73-349-8.0	5	Py14	PYASGOLD			325		27600			541		98
73-349-8.0	5	Py15	PYASGOLD			320		25619			213		99
73-349-8.0	5	Py16	PYASGOLD					20919					100
73-349-8.0	5	Py17	PYASGOLD					21518	106	212			100
73-349-8.0	5	Py18	PYASGOLD			212		20822	106		212		99
73-349-8.0	5	Py2	PYRITE	201			301	21966	201	301		18355	100
73-349-8.0	5	Py3	PYRITE					25291	299			797	100
73-349-8.0	5	Py4	PYRITE				100	26621		300		3403	100
73-349-8.0	5	Py5	PYRITE				506	25382	101	202		3337	100
73-349-8.0	5	Py6	PYRITE				100	34943	301	201		3514	100
73-349-8.0	5	Py7	PYRITE	100				23311	100			2789	100
73-349-8.0	5	Py8	PYRITE	101	101		304	22310	101	304		1724	100
73-349-8.0	5	Py9	PYRITE		200			25508	100	500		3701	99

PRINCE LYELL

Sample	Ring	Comments	Label	Co ppm	Ni ppm	Cu ppm	Zn ppm	As ppm	Se ppm	Ag ppm	Au ppm	Pb ppm	
115003	I	1		710	210	50		720					92
115003	I	2		90	10	210		430					84
115003	I	3		5300	80	310		740					88

Sample	Ring	Comments	Label	Co ppm	Ni ppm	Cu ppm	Zn ppm	As ppm	Se ppm	Ag ppm	Au ppm	Pb ppm	PDI*
115003	I	4		13470				720					100
115003	I	5		4920	1950	110		1080					76
115003	I	6		10		290		530					82
115003	I	7		950	320	190		710					85
115003	I	8		940	100	80	190	360					89
115003	I	9		320	170	210	360	760					87
115003	I	10		60	390		370	730					91
115003	I	11		1210		260		790					89
115003	I	12		1470	1580			870					75
115003	I	13		1410	850	970	330	1050					67
115003	I	14		2460	1250	150	400	610					71
115003	I	15		5870	850			540					84
115003	I	16		3860	1810		130	590					70
115003	I	17		4250	1910	200		780					69
115003	I	18		180	300		20	440					88
115003	I	19				30		750					98
115003	I	20		1580	1400	140		550					66
115003	Ia	21		4060	610	80		440	1070				97
115003	Ia	22		8350	10	120		1380					97
115003	Ia	23			150	6960	340	730	330				42
115003	Ia	24		12340	900	100		1430	620				95
115003	Ia	25		320		280		590	620				97
115003	Ia	26		11920	220	500	70	660	160				89
115003	Ia	27		1680	30		40	650					99
115003	Ia	28		210	60		140	680	590				100
115003	Ia	29		1270	460		90	720	140				94
115003	Ia	30		3650	260		210	540	500				98
115003	Ia	31		10	210	40	70	740	460				98
115003	Ia	32		2460	2400	80		770	430				84
115003	Ia	33		440				510	430				100
636126.8	II	34		750	1070		30	580	160	160			84
636126.8	II	35		4420	430	40		590					89
624096.9	Ia	36		150				900	510				100
624096.9	II	37			420	120	180	360					74
624096.9	II	38			30			400		260			87
624096.9	II	39		290	40	90	70	720	420	40			98
624096.9	II	40		1030	340		190	540					90
624096.9	II	41		60	160			460	40				95
624096.9	II	42			180			400	590	20			99
624096.9	II	43			130		150	540					95
624096.9	II	44			400	360	300	2550		130			91
624096.9	II	45			100			2780		140			98
624096.9	II	46			230		110	390	120				95
624096.9	II	47		160	20	120		590	900				99
624096.9	II	48			260	40		370	160				94
624096.9	II	49				150	190	560		60			89
624096.9	II	50			20	40	220	530	780	190			98
624096.9	II	51			140	150		590	30	170			85
624096.9	II	52		40	140			460	230				98
624096.9	II	53			170	90		450	220				95
599377.3	III	54		2750	410	10	10	490					88
599377.3	III	55		29880	120	100		510	260				98
599377.3	III	56		20950		170	30	480					96
599377.3	III	57		1600	80	120	110	950					94
599377.3	III	58		2270	3370	40		400		40			43
599377.3	III	59		70		120	30	580		10			92
599377.3	III	60		900	50	10	30	450	300				99
599377.3	III	61		2260	110		80	400	40				97
599377.3	III	62		2690	140		120	530	20	110			94
599377.3	III	63		5680		150		480		210			89
599377.3	III	64		6020	300	70		420	330	20			96
599377.3	III	65		9240	310	60	50	510	150	30			95
599377.3	III	66		10320	330	80	70	590		30			92
599377.3	III	67		9810	100		60	460					98
599377.3	III	68		7800		10	60	560					100
599377.3	III	69		9350	240			450					95
599377.3	III	70		5580	60	20	30	470	560	60			99
599377.3	III	71		2260	100			370	120				98
599377.3	III	72		3250	160	10	10	470		30			94
599377.3	III	73		7510	170			820	100	50			97
599377.3	III	74		540	300			430		40			87
599377.3	III	75		50	40			510	340				100
599377.3	III	76			30		40	410	230				100
599377.3	III	77			40	40		430		90			91
599377.3	III	78		3550	60		100	480	140				99
599377.3	III	79					80	520	80	40			99
599377.3	III	80			70			500	220				99
599377.3	III	81		2230	80			450					97
599377.3	III	82					30	470		210			92

Sample	Ring	Comments	Label	Co ppm	Ni ppm	Cu ppm	Zn ppm	As ppm	Se ppm	Ag ppm	Au ppm	Pb ppm	PDI*
599377.3	III	83		6490	920		50	960	660				96
599377.3	III	84		6010	830		40	850	470	40			95
599377.3	III	85		4670	500	30		740	160	120			92
599377.3	III	86		8280	310			1180	370				98
599377.3	III	87		5910	290	70		1100	130				96
599377.3	III	88		7940	470	10	20	920	100	20			95
599377.3	III	89		7370	470	50		880	170	70			94
599377.3	III	90		4490	860	30		620					83
599377.3	III	91		5210	900	100	160	500	150				87
599377.3	III	92		7020	1040		10	370					79
599377.3	III	93		5250	1210		100	430	200	120			85
599377.3	III	94		2700	830		90	540	60	210			82
599377.3	III	95		2120	830	40		500		90			76
599377.3	III	96		1120	3920	140	70	480					40
599377.3	III	97		1580	50		60	320	180				99
599377.3	III	98		790		40	50	510	180				99
599377.3	III	99		1140	60		80	400	220	190			96
599377.3	III	100			60	10	30	300		30			93
599377.3	III	101		30	40	100	10	350		60			85
599377.3	III	102			10	10		550	260				100
599377.3	III	103				10	10	450	160	30			99
599377.3	III	104			40	40	40	520	90	280			92
599377.3	III	105			70	70	100	430	210	10			97
599377.3	III	106		130	40	40		440	140	60			97
599377.3	III	107		80		30	60	460	10				98
599377.3	III	108		40	20	10		520	180	50			99
599377.3	III	109		910	140	40	40	450	170				96
599377.3	III	110		530	110			450	40	240			90
599377.3	III	111		10	100	40	80	480	30				94
599377.3	III	112		1570	430	90	40	430					81
599377.3	III	113		3320	780		40	460	90	100			85
599377.3	III	114		6550	100		80	610		90			96
599377.3	III	115		7090		60		670	120	50			98
599377.3	III	116		2180	80	10	70	500					97
599377.3	III	117		280			50	420		150			94
599377.3	III	118		24070	10			530	290				100
599377.3	III	119		17270		40	20	880					99
599377.3	III	120		24150	80	10		990		90			98
599377.3	III	121					140	420	90	220			95
599377.3	III	122		120	20	60	20	450	530	80			98
599377.3	III	123		20				470					100
599377.3	III	124		2770	170	60	50	350					90
599377.3	III	125		3400	70		120	1110					99
599377.3	III	126		4400		70	70	650	390				99
624096.9	III	127					80	450	340				100
624096.9	IV	128			10		90	540				890	100
624096.9	IV	129			70	10	120	540				1260	97
624096.9	IV	130		80	50	70	410	3670	300			1190	99
624096.9	IV	131			110	90	120	630		90		1110	90
624096.9	IV	132			100	80	920	510				1130	92
624096.9	IV	133			40		140	490	150			1130	99
624096.9	IV	134		10	250		140	490				1090	92
624096.9	IV	135		100	120	150	440	600	20	50		1080	89
624096.9	IV	136			110	170	260	430	170			1430	93
624096.9	IV	137		170	40		50	1450				1370	99
624096.9	IV	138			110	80	60	3170	280			2300	99
624096.9	IV	139			40	120	150	1370	70			1460	97
624096.9	IV	141			110		60	500		100		640	93
624096.9	IV	142		260	130	140	100	2270	270	150		1150	97
624096.9	IV	143			290	40	70	570	30	70		1020	89
624096.9	IV	144		30	220		60	460		160		1470	87
624096.9	IV	145			80	30		480	120			1010	97
624096.9	IV	146			220	10		520		50		780	90
624096.9	IV	147				740	70	3960	260	10		1000	94
624096.9	IV	148		20	80	130		2250		160		1190	96
624096.9	IV	149		100	80	140		1760		70		1300	95
624096.9	IV	150			140	50	30	460		80		1100	89
624096.9	IV	151			160	90	100	860		20		1290	93
624096.9	IV	152			20	770	360	480	10			790	64
115003	IV	153		1910	60	100		450	150			1150	96
115003	IV	154		4430	320	100	50	550	10			1060	90
115003	IV	155		310	10	130		510	390			460	98
115003	IV	156		460	20			530	210			1100	100
115003	IV	157				50	80	600	510	230		1040	98
115003	IV	158		4350	1200	120		530	500	40		1130	91
115003	IV	159		3200	1610	80	90	520	30	80		910	70
115003	IV	160		550	80			480		180		990	91
115003	IV	161		600	760			590				1230	82
115003	IV	162		1880	1520	160		610	250	120		860	82

Sample	Ring	Comments	Label	Co ppm	Ni ppm	Cu ppm	Zn ppm	As ppm	Se ppm	Ag ppm	Au ppm	Pb ppm	PDI*
115003	IV	163		5580	880	90		570	260	180		1470	89
115003	IV	164			120	40	20	630				1220	94
582255.6	IV	166		730	140			500	350	350		1790	95
582255.6	IV	167		670	30	130	50	490	40	40		1440	92
582255.6	IV	168		3980	20	30	50	910				1370	99
599377.3	IV	170		9910	290	20	30	410	250	70		1080	96
599377.3	IV	171		7810	980	50	60	540				940	83
599377.3	IV	172		4110	100	60	20	390				1390	94
599377.3	IV	173		3550	130	70	110	430	140	120		1100	94
599377.3	IV	174		29280	30	100	30	340	140			1290	98
599377.3	IV	175		9180		120	30	440	80	50		1290	96
599377.3	IV	176		80	70	140		460	190	50		1440	94
599377.3	IV	177		160	30	310		490				1330	81
599377.3	IV	178		8080	80			470				1450	98
599377.3	IV	179		7130	110	50		570		30		940	96
599377.3	IV	180			50	80		520	210			1260	97
599377.3	IV	181		3710	40			420	40			1450	99
599377.3	IV	182			10	60	20	530	40			1060	97
599377.3	IV	183				190		440		10		1250	86
599377.3	IV	184		4560	10	100	70	450	180	40		1100	97
599377.3	IV	185		5250	80	110		460	60	70		980	93
599377.3	IV	186		620				560	130			1360	100
599377.3	IV	187			90	10		410				1010	95
599377.3	IV	188		1360	30	80		440		10		1370	94
599377.3	IV	189		6760	80	170	70	690	140	270		1220	93
599377.3	IV	190			10	150		390		210		1140	81
599377.3	IV	191			60	80		420	120			1210	96
599377.3	IV	192		4450	130	40		490				1200	95
599377.3	IV	193		14610	180	140	80	440	120			1400	95
599377.3	IV	194		5700	10	60		490	90	30		1150	97
599377.3	IV	195		5870		20		510		20		1100	99
599377.3	IV	196		2090	150	140	60	470		50		980	87
599377.3	IV	197		12620	100	80	20	480	170	70		1300	97
599377.3	IV	198		340	130	40		390				1350	92
599377.3	IV	199		2120	110	50	10	450				1240	94
599377.3	IV	200		1960	100			410	30	70		1460	95
599377.3	IV	201		550	40	90		500	230	40		1570	97
599377.3	IV	202		160	60	30	100	420		20		1360	95
599377.3	IV	203		27620	100	120	10	400		90		1310	96
599377.3	IV	204		4720	30	70	80	730				1130	97
599377.3	IV	205		6290	140	10		500	70	40		1560	97
599377.3	IV	206		6690	80	60	40	740	220			1120	98
599377.3	IV	207		7160		10	20	620	410	70		1340	99
599377.3	IV	208		280	10	90	90	460		30		1110	92
599377.3	IV	209			80	80	100	500	340			1260	98
599377.3	IV	210		90		90	20	430	120			1160	96
599377.3	IV	211		2630	10	10	70	470				970	99
599377.3	IV	212		190		70	60	490	30	120		1260	93
599377.3	IV	213		2170	130	70	10	480		70		1250	91
599377.3	IV	214		930	20	60		570	220			1360	98
599377.3	IV	215			20	20	70	530	30	40		1540	97
639121.3	IV	220		390	350			460	200	100		1090	94
639121.3	IV	221			170	10		530	40	160		1370	91
639121.3	IV	222			260		20	500	100			1210	95
639121.3	IV	223			1510		40	440	600	40		1220	90
639121.3	IV	224			1510		40	500	670			1330	91
639121.3	IV	225		10	240	30		430	360			1380	97
639121.3	IV	226			230	120		500	610			1520	97
639121.3	IV	227			270		30	410	190			1140	96
639121.3	IV	228		10	360	1160		450	250	70		1240	73
639121.3	IV	229		30	60	60	120	980	70	150		1110	95
639121.3	IV	230			20	20	40	480		210		1210	91
639121.3	IV	231				30		470	300			1180	99
639121.3	IV	232			160	50	40	600	190			1530	96
639121.3	IV	233		420	270	30	90	540				1520	91
639121.3	IV	234		190	280		30	420	20	40		1150	90
639121.3	IV	235		360	1040	40	180	480				1210	71
639121.3	IV	236			470	10	230	470	110			1240	91
639121.3	IV	237			270		290	520	400	110		1220	97
639121.3	IV	238			640	30	620	490		30		1040	79
639121.3	IV	239			880	10	1280	570	40	120		1170	80
639121.3	IV	240		60	770	40	260	400				1070	73
639121.3	IV	241			640		100	530				1150	82
639121.3	IV	242			630		750	500		70		1200	81
639121.3	IV	243			590	30		440		20		1530	79
639121.3	IV	244			610		130	460				1140	81
639121.3	IV	245			460		70	480	50			1040	89
605100.6	IV	246				20	500	680	150	60		1520	99
605100.6	IV	247				180	2840	390	190	10		1360	95

Sample	Ring	Comments	Label	Co ppm	Ni ppm	Cu ppm	Zn ppm	As ppm	Se ppm	Ag ppm	Au ppm	Pb ppm	PDI*
605100.6	IV	248		70	10	1660	460	500	280	80		1080	71
605100.6	IV	249		30	50	60	450	370	60	70		1470	93
605100.6	IV	250			90	260	90	570	120			1340	90
605100.6	IV	251		280	100	2830	1180	500	210	10		1660	56
605100.6	IV	252		90	40	2520	330	570		90		1400	38
605100.6	IV	255			30	10	430	440				1220	98
605100.6	IV	256			130		260	490		30		1350	95
605100.6	IV	257		2380	170	70	8050	720		180		1240	93
605100.6	IV	258		3930	80	30	1880	570		60		1150	96
605100.6	IV	259					2450	870	30			1640	100
605100.6	IV	260		2470	20		50710	560	250			1560	100
605100.6	IV	261		70	40	80	1290	9610	340			1440	100
605100.6	IV	262		440	50	40	780	650	160	210		1340	95
605100.6	IV	263		220		100	1040	6180	160	170		1420	99
605100.6	IV	264		1410	40	10	4720	420	200	20		1310	99
618051.8	IV	265		15210	20	120	60	540	160	10		1060	98
618051.8	IV	266		170	10	2570	130	440	160			1430	53
618051.8	IV	267		2970	290	190	40	1940	140			1200	95
618051.8	IV	268			110		60	500				1510	96
618051.8	IV	269			20	440	70	510	30			1540	79
618051.8	IV	270		20	60	140		560	330			1260	97
618051.8	IV	271			100	100	10	590	240			1150	96
618051.8	IV	272			60	60	110	520	190	220		1180	94
618051.8	IV	273		15160	80	10	50	670				1310	99
618051.8	IV	274		14780	30	40	20	510				1120	98
618051.8	IV	275			60	1810		460	260	250		1150	66
619098.6	IV	276		80	60	80	10	2690	20			770	98
619098.6	IV	277		100	210	280	260	1900	820			470	97
619098.6	IV	278		620	40	160	60	10910		110		1440	99
619098.6	IV	279		480	10	170		8770		180		930	99
619098.6	IV	280			70	100		480	350	190		740	95
618051.8	IV	281		2280	390	130		460	970	160		910	97
618051.8	IV	282		3650	220		90	600	790			1220	99
618051.8	IV	283		40	100	370	50	790	450			960	94
618051.8	IV	284					90	590		90		780	97
598259.7	IV	286		3030	1160	230	100	460	640			1670	91
598259.7	IV	287		6850	350	140	50	740	710			1040	97
598259.7	IV	288		11150	60	690		1950	50			1140	91
115003	IV	289		870	60			670	170			1280	99
115003	IV	290		100	210			490	280			1590	98
115003	IV	291				70		1840				1120	99
115003	IV	292		120	70	2340	150	300	240	100		1960	58
115003	IV	293		1080	350	1590		640	260	230		1760	71
618051.8	IV	300		6060	400			450				1290	92
618051.8	IV	301		3960	510	30	100	450		70		1460	85
618051.8	IV	302		680	60	130	50	570				740	91
618051.8	IV	303		350	60	80	20	510		120		1460	90
618051.8	IV	304		130	110	10	50	490	150			960	98
618051.8	IV	305		290		30		540	420			1520	99
618051.8	IV	306		870	40	40		490	10	50		1380	95
618051.8	IV	307		5390	490	90		500	390	60		1280	94
618051.8	IV	308		3310	410	50		510	10			970	89
618051.8	IV	309		5780	190			660	40	40		1070	96
618051.8	IV	310		7090	330			490		30		1100	93
618051.8	IV	311		6190	300		90	510	100	10		1250	96
618051.8	IV	312		6500	420			500		30		930	91
618051.8	IV	314		830	320	90		530	170	140		1460	91
618051.8	IV	315		1830	90			400	270	50		1120	98
618051.8	IV	316		16200	30		60	430	80			970	100
618051.8	IV	317		240	60	20	160	660	20			930	98
618051.8	IV	318		2610	350		20	970	210	10		1060	97
618051.8	IV	319		4140	100	30	80	640	90			920	98
618051.8	IV	320		2850	220	20	180	1080	120			1080	97
618051.8	IV	321		15840		50	40	490				1240	99
618051.8	IV	322		1090	220	180	30	540	400			940	95
618051.8	IV	323		9390	190	170	60	500	210			1450	95
618051.8	IV	324		2000	250	900	50	500		210		960	59
618051.8	IV	325		2500	80	60		630	40	50		920	95
618051.8	IV	326		28040	40	260		540	190	50		1010	96
618051.8	IV	327		10000		150	110	780	230			1270	98
618051.8	IV	328		420	80	140		1190	270			1340	97
618051.8	IV	329		440		160	40	770		180		1330	89
618051.8	IV	330		6980	130	200	70	1270		100		1090	93
640012.1	IV	332			80	3710		460	100	160		1090	37
640012.1	IV	335		710		40		500		90		1150	95
640012.1	IV	336		870	20			510	170	80		1300	98
626037	IV	337		360		260	20	490	50	60		1760	87
626037	IV	338		1300		70	40	540	40	80		1300	95
626037	IV	339		870	730	2090	70	470	280	120		1070	63

Sample	Ring	Comments	Label	Co ppm	Ni ppm	Cu ppm	Zn ppm	As ppm	Se ppm	Ag ppm	Au ppm	Pb ppm	PDI*
626037	IV	340		330	110	2910		600	300			1290	61
626037	IV	341		1180	60	120		590	20	10		1010	93
626037	IV	342		2960	150	160	20	500	390			890	96
626037	IV	343		300	100	1090	40	510				810	55
626037	IV	344		6940	470	10	30	2550		160		1200	96
626037	IV	345		8310	430		20	2010	80			1000	97
626037	IV	346		1630	450		40	970	170	20		1010	95
626037	IV	347		4910	340		70	710	330	250		1200	95
626037	IV	348		3350	800			770	30	110		1030	66
626037	IV	349		7410	720	30		530	90	60		1320	69
626037	IV	350		130	100	2320		500		70		1120	36
626037	IV	351		1560	140	160	10	580	50	200		1150	87
626037	IV	352				1180	20	450		170		1120	49
626037	IV	353		120	20	150	30	500				1060	90
626037	IV	354		1890	70	80		960				1080	96
626037	IV	355		720	20	100	30	1060	70	100		1380	96
626037	IV	356		1460	190		30	1840	140	60		1240	98
626037	IV	357		3660	210	30		3610		100		990	98
626037	IV	358		3160	270	130		2530		200		1460	95
626037	IV	359		2120	270	160	60	2870	90			980	97
626037	IV	360		3560	110	80		890		30		1200	95
626037	IV	361		5360	10	70		560				1370	97
626037	IV	362		5010	20	30	10	1240	100	10		1080	99
626037	IV	363		1690	60	140	150	2480				1060	97
626037	IV	364		1890	70	170	120	1920	220			1040	97
626037	IV	365		1270	120		120	1660				1020	99
626037	IV	366		1820	100	70		620				1320	94
626037	IV	367		4980		120	80	470	340	110		1260	97
626037	IV	368		3550	120	110	160	590	60	330		1460	89
626037	IV	369		3990	120		60	1010	70			950	98
626037	IV	370		310	40	4860	20	650		190		1090	26
618051.8	IV	400		170	120		10	580				1110	96
618051.8	IV	401		480	170	10	50	790		50		1220	95
618051.8	IV	402		760	90	80	90	790	200			1010	97
618051.8	IV	403		1970	30	20	150	820	410	60		1260	99
618051.8	IV	404		16270	10			670	290			1360	100
618051.8	IV	405		6330	450	40	30	1770	380			1080	97
618051.8	IV	406		40	70	80	20	570	250	30		1030	97
618051.8	IV	407					10	1740		10		1390	100
618051.8	IV	408		13170	40	50	30	520	250	50		1390	98
618051.8	IV	409		14860	540	40		500	540	10		1260	97
618051.8	IV	410			100	10		1830		110		1000	98
618051.8	IV	411			50	30	50	330	260	20		1220	98
618051.8	IV	412		690	110	80	10	1070	60	110		1110	95
618051.8	IV	413		2360	530			1200	250			1240	96
618051.8	IV	414		10720	170	20		210	380	60		1100	98
618051.8	IV	415		3590	170	20	80	550	370	50		1030	98
618051.8	IV	416		3250	160	80	10	410	160			1000	95
618051.8	IV	417		4060	190	50	40	610	570	100		1350	98
618051.8	IV	418		5510	170	50	80	630	550	10		1190	98
618051.8	IV	419		2320	260	10	6	570	140	50		1030	95
618051.8	IV	420		1980	280	40	70	530	440	30		930	97
638086.9	IV	421		2360	330	800	80	800		50		1270	72
638086.9	IV	422		1470	1660	490	30	730	90	140		1470	69
638086.9	IV	423		7040	400	460	60	900	210			960	89
115002	IV	424		3230	390	90		470				1150	86
115002	IV	425			10	40	50	610	90	90		1110	97
115002	IV	426		70	130	50		510				1240	92
115002	IV	427		900	130	80	40	490	20	70		1300	90
115002	IV	428		410	40	50		660	140			1200	98
115002	IV	429		4110	150	70	150	1430				1040	97
115002	IV	430		610		1580		510		50		1310	48
115002	IV	431		1080	130	200	30	850	40			1210	91
115002	IV	432		2070	430	310	10	2700	120			1450	94
115002	IV	433		1920	400	220		920	130			1160	91
115002	IV	434			50	120		480	30	60		750	90
115002	IV	435		30	110	60	70	500	210	150		1160	95
115002	IV	436		440	460	720	60	2240	230			1360	90
115002	IV	437		4680	430	1210	80	760	10			1070	66
115002	IV	438		2680	310	720	60	5110	140	140		1080	94
115002	IV	439		7360	290	3290	50	3770	400			1220	81
598307.9	V	440		1340	180	260			260	140		1560	88
598307.9	V	441		7710	30	450				120		1320	71
598307.9	V	442		1080		140	40		230			1120	95
598307.9	V	443		13260	110	200	150		160			1150	94
598307.9	V	444		14260	120	20	90		260	80		1090	98
598307.9	V	445		13250	210				60	160		1200	94
626067.1	V	446		780	360	230	80					1020	36
582279.4	V	447		1500	850	180			560			1300	91

Sample	Ring	Comments	Label	Co ppm	Ni ppm	Cu ppm	Zn ppm	As ppm	Se ppm	Ag ppm	Au ppm	Pb ppm	PDI*
582279.4	V	448		2170	4710	90			530	40		1010	70
582279.4	V	449		4830	430	130	10		140			1170	87
115002	V	450		2560	20	50			210	120		1260	96
115002	V	451		70	100	20	10		300	150		1110	96
115002	V	452		6020	150	30			270	10		980	97
115002	V	453		1080	50	80			100	20		1150	92
115002	V	454		630	10	40			220			1400	98
115002	V	455		740	90	40	10		80	140		1130	87
115002	V	458				50			190			1590	98
115002	V	459		290	540	20	40			10		1100	35
115002	V	460		60	110	90	120		200			1240	94
115002	V	461			120		70		250			1140	98
115002	V	462		100	110		60		80			1340	95
115002	V	463			90	30			100			1290	94
115002	V	465		40	50	30						1700	76
115002	V	466		30	320	30	50			150		1100	31
115002	V	467		920	10	260			330	10		1170	93
115002	V	468		10910	180	190	50		160	160		1100	90
115002	V	469		1160	230	250	60		200			1160	86
115002	V	471		1300	50	40	60		80	110		830	90
115002	V	472		15420	90	50	140		290			1000	98
115002	V	473		12610	190		30			50		1020	94
115002	V	474		100	220		110			120		1240	47
115002	V	475		570	670	150			150			1670	78

ROSEBERY SAMPLE	DESCRIPTION	RING	GRAIN	Co	Ni	Cu	Zn	As	Se	Ag	Au	Pb	
R3397-50	Dissem. py	1	1	270		30		310				25	96
		2	1			220		1730		60.0		320	95
		3	1	190		130		360		7.0		85	88
		4	1	850		90		510		16.0		300	94
		5	1	180		280		2230		45.0		420	95
R3397-108.5	Stringer cp-py	2	1			65	15	670					96
		3	1	150		110	15	1120	33				97
		4	1			110		1490					97
		5	1	980		120		1110					96
		8	1			150	1780		14				68
R3397-117	Stringer cp-py-sl	1	1			660	100	1660	10	11.0		540	87
		3	1			850	1490	52		16.0		15	25
		11	1			160				50.0		3970	68
		13	1			210	25	540				70	87
R3397-124.5	Massive py-sl-gn	1	1			160	130	150		41.0		250	70
		2	1			820	110	61		38.0		2180	31
		3	1			270	20	170		10.0		160	62
		4	1			130	25	91		10.0		100	64
		5	1	55		120		170				130	79
		5	2			380	15	240				140	62
R3397-129	Semi-mass sl-gn-p	1	1			180	1450	590		22.0	35	75	86
		2	1			120	110	120				150	73
		7	1	130		160	90			17.0		9340	85
		9	1			60	170	920				690	98
R3397-141	Massive barite	4	1			19700	180	480				40	6
		5	1			1030	60	1510				440	79
		6	1			5740	65	650				1460	24
		7	1		130	3510	30	550				120	28
		9	1		230	140	25	640					86
R3397-165.75	Massive barite	2	1		95	40	65	53			20		52
		9	1		65	120	3730	820		52.0		3450	94
		11	1		330	45	520	37		8.0		540	48
		12	1			2520	3210	200		300.0		140	24
		13	1		640	30	55	15				35	12
R4603-83.1	Massive py-sl-gn	2	1			130		1700		10.0		1600	97
		2	2			260	70	1590		12.0		2720	94
		3	1			520	40	2910		12.0	50	2160	92
		3	2			40	80	1600		7.0		560	99
		5	1			100	20	1280		8.0		920	97
		5	2			40		790		7.0			98
		6	1			70	520	330		17.0		220	92
		7	1			190		2210		13.0		680	97
		7	2			160		1630				3130	96
		9	1			120		1390		15.0		7450	97
R4550-38.9	Massive sl-py-gn	1	1			180	8090			25.0		20300	94
		2	1			1150	1670	1060		125.0		3420	72
		3	1			2640	450	3290		375.0		2700	75
		4	1			1340	680	2470		63.0		1270	82
		5	1			2130	1090	720		30.0		860	48
		6	1			430	3200	11600	11	28.0		4700	99
R4583-191.6	Massive sl-gn-py	1	1			90	2650	7830	9			2690	100

Sample	Ring	Comments	Label	Co ppm	Ni ppm	Cu ppm	Zn ppm	As ppm	Se ppm	Ag ppm	Au ppm	Pb ppm	PDI*
		2	1				300	830				250	100
		3	1				390	525		7.0		2665	100
		4	1			30	320	1490		10.0	20	720	98
R4548-32.7	Massive barite	1	1			210	50	8770		13.0		330	99
		2	1		90	260	110	9050	15	14.0		225	99
		2	2			140	170	6430	10			320	99
		4	1			530	1040	3610	7			200	95
		5	1				20	25				195	100
		6	1			170	30	1630				245	96

RENISON

Sample	Ring	%S	%Fe	Co ppm	Ni ppm	Cu ppm	Zn ppm	As ppm	Se ppm	Ag ppm	Au ppm	Pb ppm	
111085	R1-Core	53.46	46.54		118		145				174	757	18
	R1-mid	53.46	46.54	23	278		349						22
	R1-Rim	53.46	46.54		36		172			40	181		4
	R2-Core	53.46	46.54			526	106			36			2
	R2-Rim	53.46	46.54			1091	133			41		384	4
	R3-Core	53.46	46.54		34		151			59		146	39
	R3-Rim	53.46	46.54		35	36	181			45	131		5
111161	R2-Core	53.46	46.54	225	33	91	114			39			26
	R2-Rim	53.46	46.54	25	36	131	156				122		5
	R3-Rim	53.46	46.54		34	92	159					148	22
	R3-Core	53.46	46.54	113	33	98	207			55		297	32
	R1-Core	53.46	46.54	75		135	139				268		4
	R1-Rim	53.46	46.54	275	33	80	144					248	45

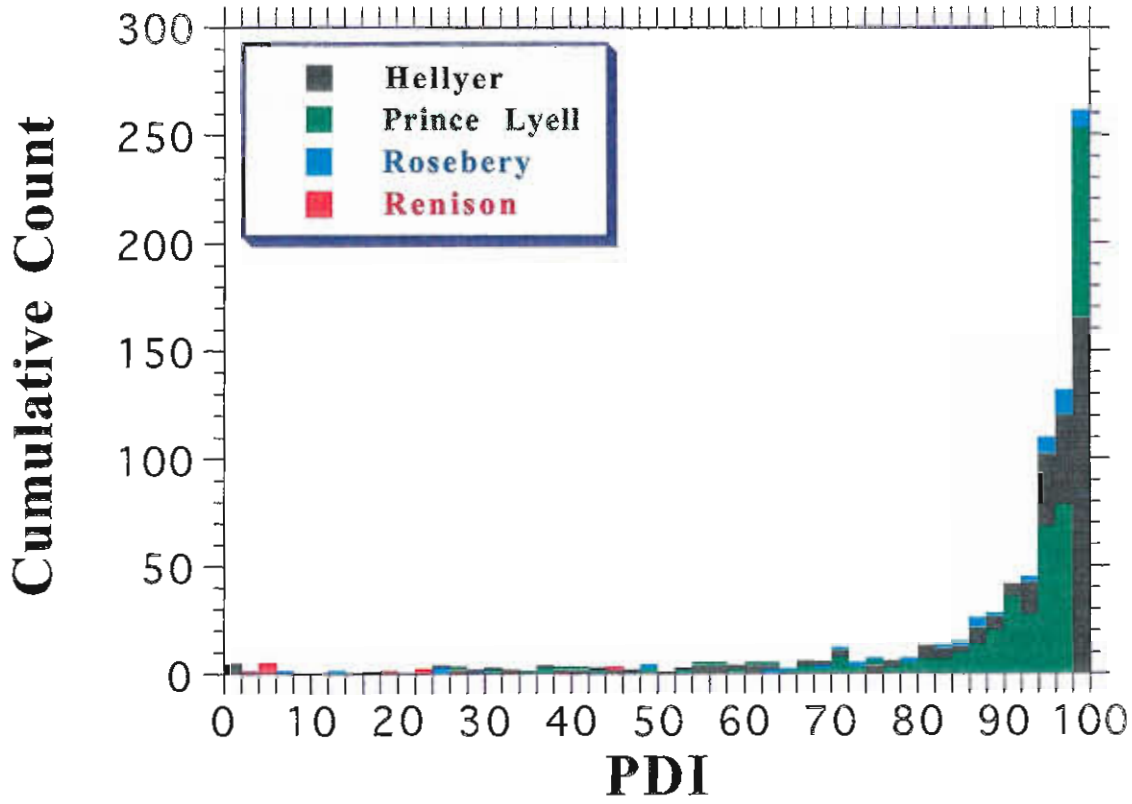
Cumulative Count
300
250
200
150
100
50
0
Hellyer
Prince Lyell
Rosebery
Renison
0 10 20 30 40 50 60 70 80 90 100
PDI

Geophysical data as a control on geological sections

Ron Berry and Michael Roach
Centre for Ore Deposit and Exploration Studies, University of Tasmania

Introduction

Project P291A includes a section on the use of geophysical modelling to test the structural interpretations produced in P291. The proposal was to use the modern high resolution magnetic data combined with the regional gravity to test if the general lithological distribution proposed in the section is reasonable. The original program included geophysical modelling along two sections. This was not continued to all sections because of the lack of constraints on geophysical properties. It was hoped that this situation could be improved in P291A if data sets on magnetic and density data were available from the sponsor companies. Unfortunately we were unable to negotiate the availability of this data.

The program involves seven sections across the Mt Read Volcanics which are suitable for the application of 2D geophysical interpretation. Of the five sections drawn in the project P291 only one was exactly E–W. The remaining sections were redrawn to fit the normal flight lines of the geophysics so that high resolution airborne magnetic data was a direct match to the structural interpretation. The northern section was redrawn north and south of the Mt Cripps Fault as part of the consideration of the effect of the Mt Cripps Fault on the regional structure and stratigraphy. A new section was also included in this report for the Professor Range–Tyndall Range line. New versions were drawn of the sections south of Queenstown and the section from Zeehan to Lake Selina. This gives seven lines on which to compare the geophysical data with the geological interpretation. High resolution airborne magnetic data have been provided by the sponsors in 2 km corridors over parts of these sections (Fig. 1)

These are:

Line	Range
5396000mN Hellyer	373000mE–377000mE
5392000mN Que River	373000mE–388000mE
These two section are also covered by Aberfoyle data flown oblique to section	
5374000mN Rosebery	376500mE–381400mE and 383000mE–389000mE
5363000mN Dundas	360000mE–381000mE
5350000mN Professor Range	372000mE–380500mE
5336000mN Strahan	None
5326000mN Jukes	None

This data was supplied in a wide range of formats which have now all been successfully translated. The initial processing is reported below.

Spectral analysis

The corrected magnetic data for the flight line closest to each geological section was plotted in profile form and correlated with the interpreted geology. Spectral analysis was conducted on each line to quantitatively assess the frequency content of the magnetic data as an adjunct to visual inspection of each profile. The aim of spectral analysis is to assess the relative importance to the overall magnetic response of magnetic sources at different depths and in particular to assess the contribution of near-surface sources. Entire magnetic lines for each section, and selected portions of each line corresponding to particular surface lithologies were analysed. Examples of typical

magnetic profiles and corresponding power spectra are shown in Figures 2, 3, 4 and 5 and are discussed below.

Line 30420 is located near Rosebery at approximately 5374000mN AMG. Along line sample spacing for this profile was 12–15 m. The total magnetic intensity profile for this line (Fig. 2) is smooth and contains little or no high frequency information, as confirmed by the smooth nature of the power spectrum (Fig. 3). There is no evidence for near surface, depth-limited magnetic sources on this section.

Line 20221 comes from the Boco area at approximately 5392000mN AMG and crosses the magnetic sandstone package north of the Pinnacles. Along line sample spacing for this profile was 6.5m. The total magnetic intensity profile (Fig. 4) includes both low and medium frequency moderate amplitude anomalies (up to 100 nT). The form of the composite magnetic anomalies on this line is compatible with a steeply west dipping sequence of bedded magnetic material. The power spectrum (Fig. 5) indicates the presence of frequencies up to approximately 8 cycles per kilometre but the form of the spectrum suggests that there are a number of different frequency components and that no single frequency and corresponding source depth predominates.

Continuity

The structures shown on the sections are based on projection from geology near the section line. They do not include objects with limited extent perpendicular to the section. The magnetic data may include such sources. The high resolution datasets are currently being processed to produce grids and stacked profiles to clearly assess the along strike continuity of each magnetic anomaly and the angle between the magnetic anomaly and the flight line. For example, in the data from the Rosebery line (Fig. 6) there is a small ramp at about 377000mE which matches the edge of the White Spur Formation. Within the next 1.5–2 km of flight line the field is flat except for two local anomalies, one of which lies on the central flight line along the structural section. The major anomaly at 379000mE to 380000mE matches the start of the Mt Black Volcanics. The anomalies are asymmetric especially in the northern lines. The central lines have a weak anomaly at this position.

2D modelling

The final section of this program is to generate profile data suitable for two dimensional forward modeling of the magnetic and gravity anomalies. The high resolution data is available for most of three lines (5396000mN, 53920000mN and 5363000mN) with shorter segments on two others. In some cases, data from three or more surveys will have to be integrated to produce these profiles. For sections without sufficient detailed data it will be necessary to use the older 1981 MRT data to generate profiles. Work is currently in progress to generate these profiles.

Summary

Modern airborne magnetic data is has been provided by the sponsors for three of the lines and for parts of two others. The first pass through the data found no evidence of significant contribution from shallow, depth limited sources or evidence for a strong bias to very deep sources. The data is now being inspected for continuity of anomalies perpendicular to the sections as required by the assumptions of 2D modeling. Profiles will then be generated to allow testing of the structural interpretations proposed in P291 and P291A.

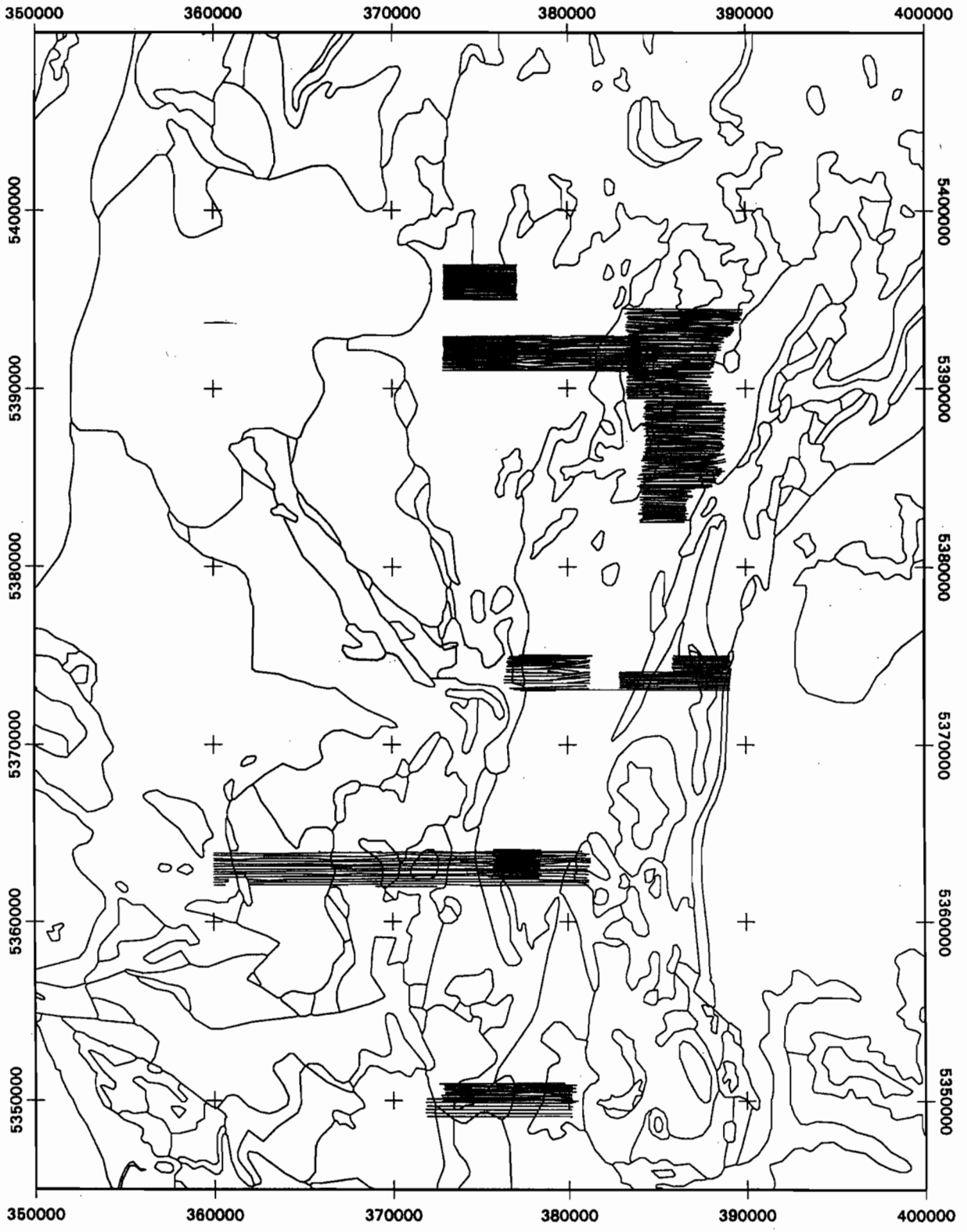

Fig. 1. High resolution magnetic data supplied by sponsors. Aberfoyle data for sections 5392000mN and 5396000mN have not been plotted.

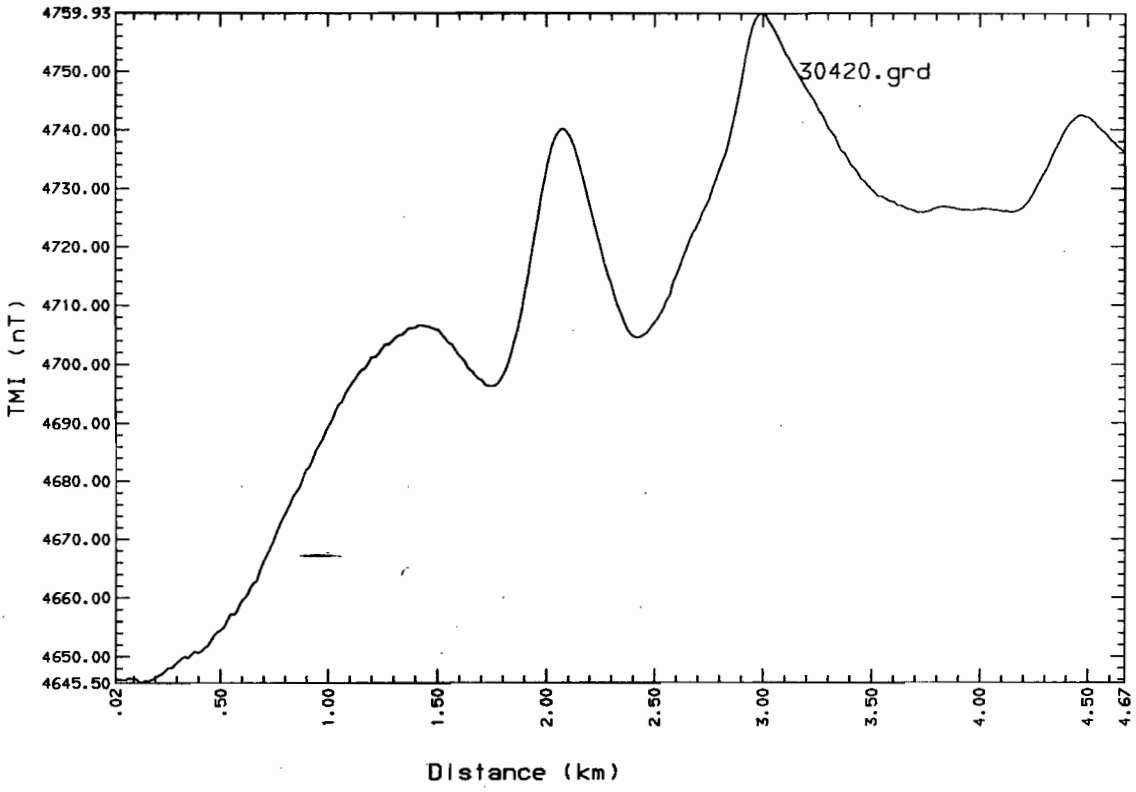

Fig. 2. Rosebery area (5374000mN), line 30420. Total magnetic intensity.

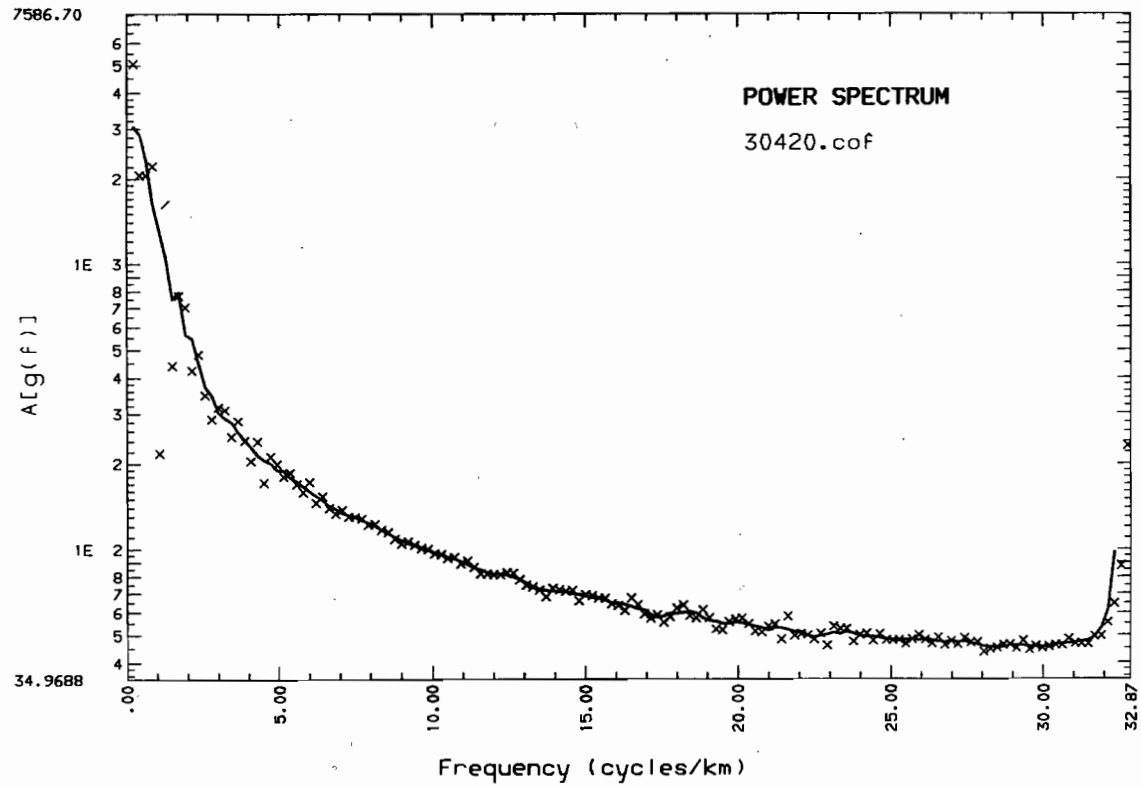

Fig. 3. Power spectrum for line 30420.

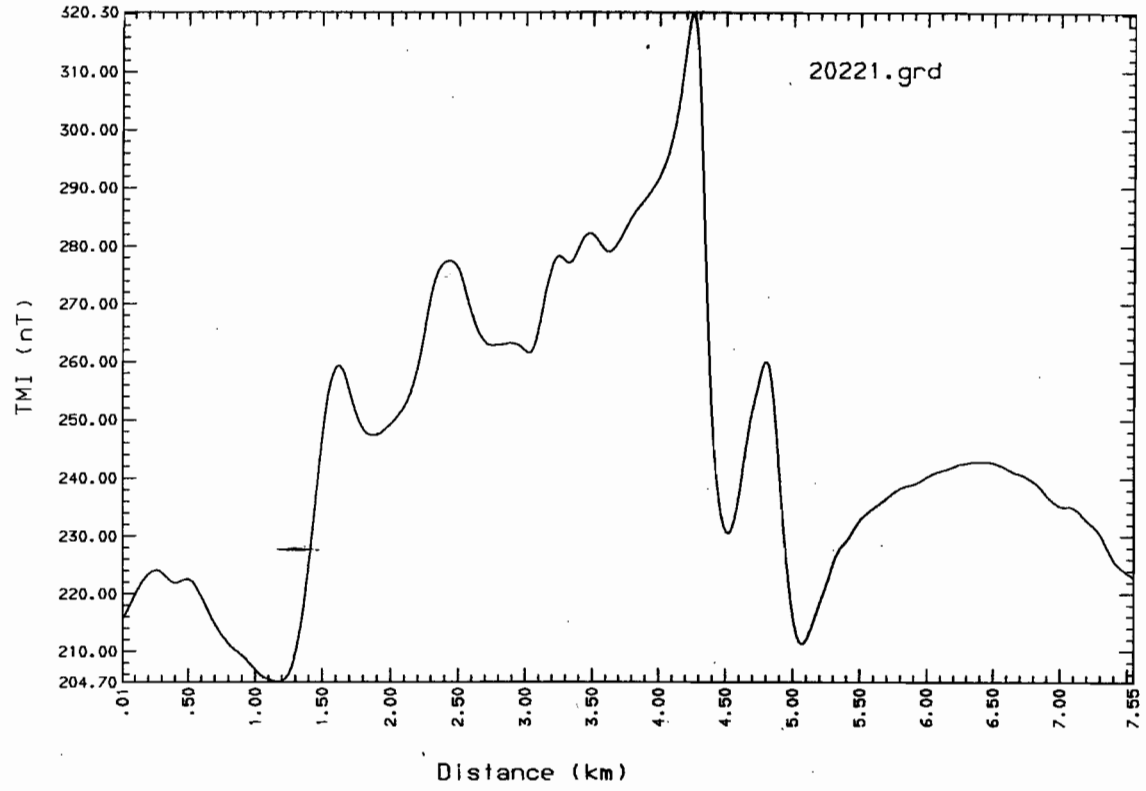

Fig. 4.Boco area (5392000mN), line 20221. Total magnetic intensity.

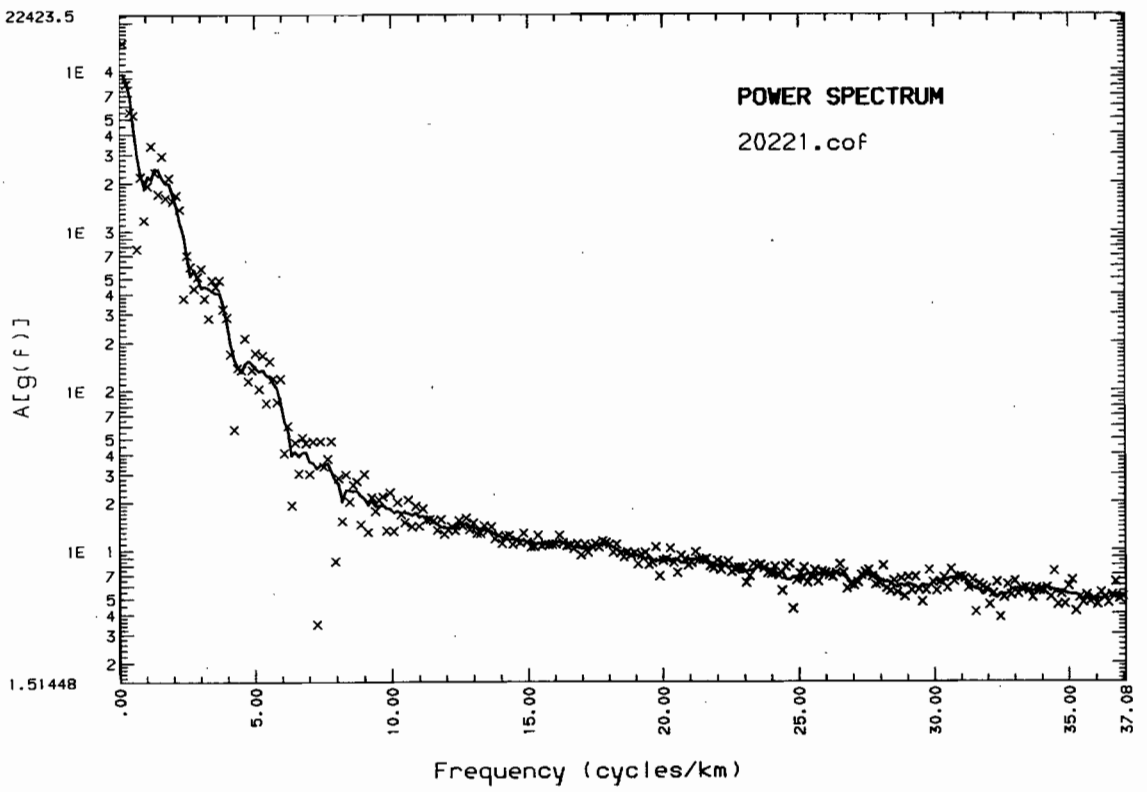

Fig. 5. Power spectrum for line 20221.

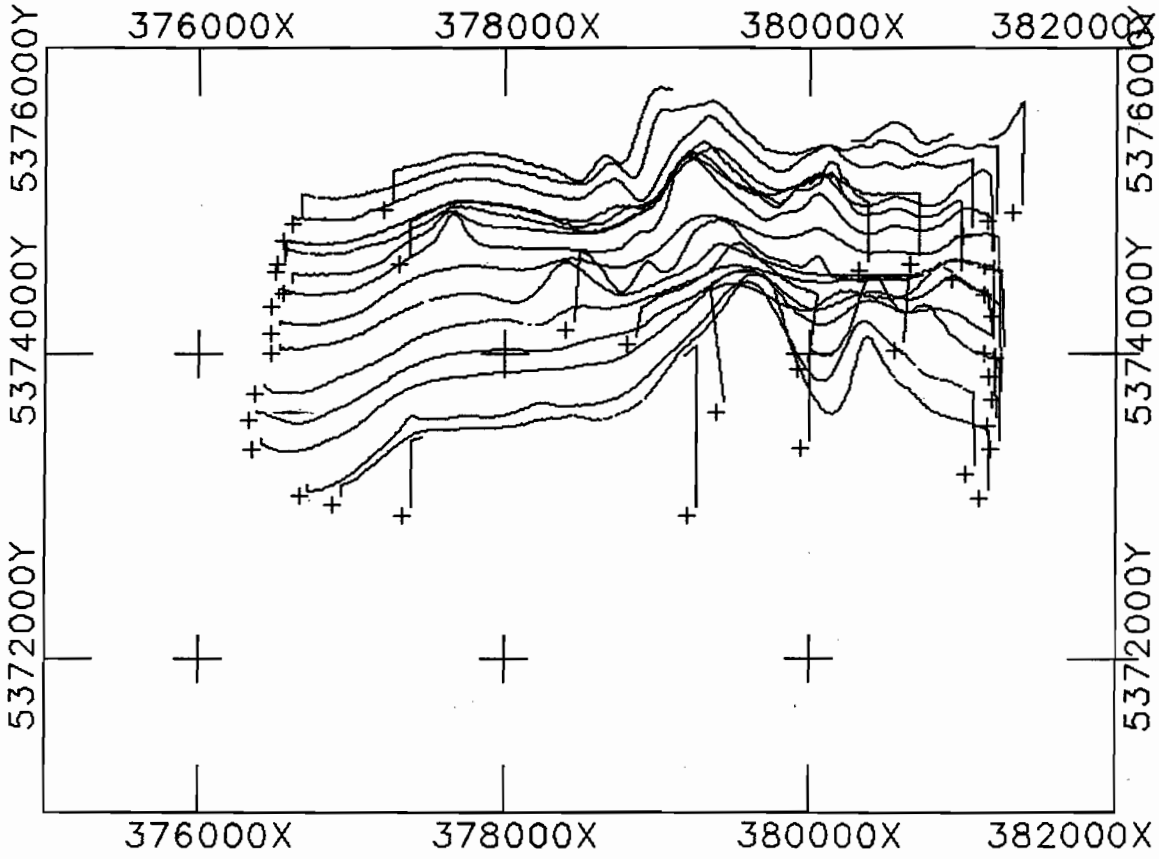

Fig. 6. Stacked profiles of total magnetic intensity in the Rosebery area.